Physical Processes in Protoplanetary Disks

Philip J. Armitage

Abstract This review, based on lectures given at the 45th Saas-Fee Advanced Course "From Protoplanetary Disks to Planet Formation", introduces physical processes in protoplanetary disks relevant to accretion and the initial stages of planet formation. After reprising the elementary theory of disk structure and evolution, I discuss the gas-phase physics of angular momentum transport through turbulence and disk winds, and how this may be related to episodic accretion observed in Young Stellar Objects. Turning to solids, I review the evolution of single particles under aerodynamic forces, and describe the conditions necessary for the development of collective gas-particle instabilities. Observations show that disks are not always radially smooth axisymmetric structures, and I discuss how gas and particle processes can interact to form observable large-scale structure (at ice lines, vortices and in zonal flows). I conclude with disk dispersal.

1 Preamble

The objective of this review is to introduce the physical processes in protoplanetary disks that are relevant to protostellar accretion and the initial stages of planet formation. Protoplanetary disks, as well as being interesting objects of study in their own right, are also simultaneously an outcome of star formation and initial conditions for planet formation. As such, we need to understand the evolution of both the dominant gaseous component and the trace of solid material that is critical for planet formation. Much interesting complexity occurs due to interactions between the two.

The review is organized around three motivating questions; how do protoplanetary gas disks evolve over time, how are solids transported and concentrated within the gas, and how do gas-phase and solid processes interact to form structure within

Philip J. Armitage
JILA, University of Colorado & NIST, Boulder, Colorado, CO 80309-0440, USA, e-mail: pja@jilau1.colorado.edu

disks? Protoplanetary disks are long-lived entities, and I begin in §2 by outlining their equilibrium structure. Disk evolution is described in §3 and §4, first following the classical approach in which the origin of angular momentum transport is unspecified, and subsequently in a more modern presentation where angular momentum transport and loss processes are ascribed to specific fluid instabilities. §5 discusses candidate theoretical explanations, some of them directly related to angular momentum transport processes, for episodic accretion outbursts. In §6 the focus switches to solids, and I review how single solid particles settle, drift, diffuse and concentrate relative to the gas. §7 then describes how these processes can give rise to structure within the disk on various scales, either at transient "particle traps" or at persistent locations such as ice lines where the disk structure varies rapidly. Finally, §8 reviews what is known about the processes, foremost amongst which is photoevaporation, that can disperse protoplanetary disks.

The lectures, even distended as in this review, could not touch upon all of the physics that an aspiring researcher in the field might require. In an effort to cover as much as possible — and to accommodate the diverse backgrounds of participants (and readers) — the material is presented with varying degrees of detail and rigor. For most topics I begin with a self-contained discussion of essential material that would often be assumed as background in papers or talks. I then discuss the underlying physics of more recent results, and give entry points to the relevant literature. The gray boxes in the text identify open issues that interest me.

One caution is in order. Quantities are generally defined and labeled following conventions in the literature, to make it easier for the reader who needs to fill in missing details or to explore further. Given the broad scope of the review there is considerable overloading of notation, with the same symbols being used to represent unrelated quantities in different sections. Take care!

2 Disk structure

The lifetime of protoplanetary disks is observed to be of the order of several Myr [138, 147], which equates to millions of dynamical times in the inner disk and thousands of dynamical times in the outer disk at 100 AU. To a first approximation we can treat the disk as evolving slowly through a sequence of axisymmetric static structures as mass accretes on to the star and is lost through disk winds, and our first task is to discuss the physics that determines those structures. Quantities that we are interested in include the density $\rho(r,z)$, the gas and dust temperatures $T(r,z)$ and $T_d(r,z)$, the chemical composition, and the ionization fraction. The importance of these for observations and for planet formation is self-explanatory, with the possible exception of the ionization fraction which determines how strongly magnetic fields couple to the gas. The density of solid particles ("dust") ρ_d is also important, but we will defer saying much about that until we have discussed turbulence, radial drift, and the aerodynamic coupling of solids and gas.

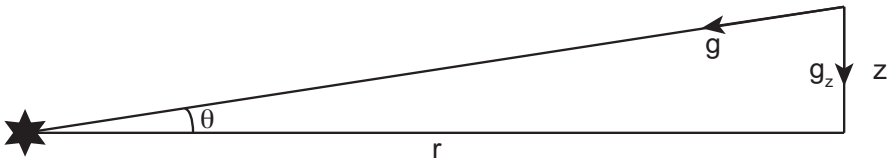

Fig. 1 The geometry for calculating the vertical hydrostatic equilibrium of a non-self-gravitating protoplanetary disk. The balancing forces are the vertical component of stellar gravity and the vertical pressure gradient.

2.1 Vertical and radial structure

2.1.1 Vertical structure

The vertical profile of gas density in protoplanetary disks is determined by the condition of hydrostatic equilibrium. The simplest case to consider is an optically thick disk that is heated by stellar irradiation, has negligible mass compared to the mass of the star, and is supported by gas pressure. We can then approximate the optically thick interior of the disk as isothermal, with constant sound speed c_s and pressure $P = \rho c_s^2$. The sound speed is related to the temperature via $c_s^2 = k_B T/\mu m_H$, where k_B is Boltzmann's constant, m_H is the mass of a hydrogen atom, and where under normal disk conditions the mean molecular weight $\mu \simeq 2.3$. In cylindrical co-ordinates, the condition for vertical hydrostatic equilibrium (Figure 1) is,

$$\frac{\mathrm{d}P}{\mathrm{d}z} = -\rho g_z = -\frac{GM_*}{r^2+z^2}\sin\theta\rho, \tag{1}$$

where M_* is the stellar mass. For $z \ll r$,

$$g_z = \frac{GM_*}{(r^2+z^2)^{3/2}} z \simeq \Omega_{\rm K}^2 z, \tag{2}$$

where $\Omega_{\rm K} \equiv \sqrt{GM_*/r^3}$ is the Keplerian orbital velocity (here defined at the mid-plane, later in §2.1.2 we will need to distinguish between the mid-plane and other locations). Equation (1) then becomes,

$$c_s^2 \frac{\mathrm{d}\rho}{\mathrm{d}z} = -\Omega_{\rm K}^2 \rho z, \tag{3}$$

which integrates to give,

$$\rho(z) = \rho_0 \exp\left[-z^2/2h^2\right], \tag{4}$$

where ρ_0 is the mid-plane density and we have defined the *vertical scale height* $h \equiv c_s/\Omega_{\rm K}$. Because the effective gravity increases with height (and vanishes at the mid-plane) this standard disk profile is gaussian, rather than exponential as in a thin isothermal planetary atmosphere. A consequence is that the scale over which the

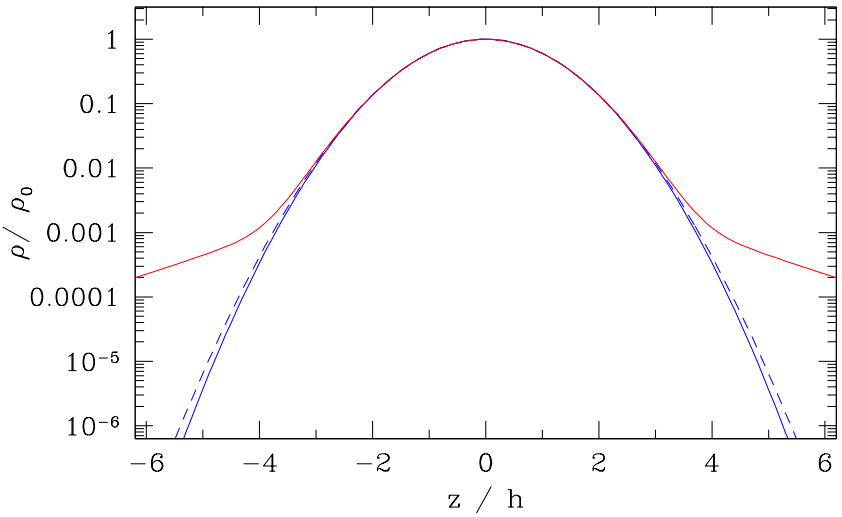

Fig. 2 Simple models for the vertical density profile of an isothermal disk, in units of the disk scale height h. The solid blue line shows the gaussian density profile valid for $z \ll r$, the dashed blue line shows the exact solution relaxing this assumption (the two are essentially identical for this disk, with $h/r = 0.05$). The red dashed curve shows a fit to numerical simulations that include a magnetic pressure component [150].

density drops by a factor of e gets smaller with z; loosely speaking disks become more "two dimensional" away from the mid-plane. Defining the surface density $\Sigma = \int \rho \mathrm{d}z$, the central density is,

$$\rho_0 = \frac{1}{\sqrt{2\pi}} \frac{\Sigma}{h}. \tag{5}$$

Up to straightforward variations due to differing conventions (e.g. some authors define $h = \sqrt{2} c_s / \Omega_\mathrm{K}$) these formulae define the vertical structure of the most basic disk model (isothermal, with a gaussian density profile). For many purposes, especially if one is mostly worried about conditions within a few h of the mid-plane, it may be a perfectly adequate description.

The most obvious cause of gross departures from a gaussian density profile is a non-isothermal temperature profile. If the disk is accreting, gravitational potential energy that is thermalized in the optically thick interior will need a vertical temperature gradient $\mathrm{d}T/\mathrm{d}z < 0$ in order to be transported to the disk photosphere and radiated. We will return to this effect in §2.2 and §3, after assessing the other assumptions inherent in equation (4). We first note that the simplification to $z \ll r$ is convenient but not necessary, and that we can integrate equation (1) without this assumption to give,

$$\rho = \rho_0 \exp\left[\frac{r^2}{h^2}\left(\left(1+z^2/r^2\right)^{-1/2}-1\right)\right]. \tag{6}$$

Protoplanetary disks *are* geometrically thin, however, with $h/r \approx 0.05$ being fairly typical. In this regime, as is shown in Figure 2, departures from a gaussian are negligibly small. We only really need to worry about the full expression for vertical gravity when considering disk winds, which flow beyond $z \sim r$.

What about the contribution of the disk itself to the vertical component of gravity? Approximating the disk as an infinite sheet with (constant) surface density Σ, Gauss' theorem tells us that the gravitational acceleration above the sheet is independent of height,

$$g_z = 2\pi G\Sigma. \tag{7}$$

Comparing this acceleration with the vertical component of the star's gravity at $z = h$, we find that the disk dominates if,

$$\Sigma > \frac{M}{2\pi}\frac{h}{r^3}. \tag{8}$$

Very roughly we can write the disk mass $M_{\rm disk} \sim \pi r^2 \Sigma$, which allows us to write the condition for the disk's own gravity to matter as,

$$\frac{M_{\rm disk}}{M_*} > \frac{1}{2}\left(\frac{h}{r}\right). \tag{9}$$

For $h/r = 0.05$, a disk mass of a few percent of the stellar mass makes a non-negligible change to the vertical structure, and such masses are not unreasonably large. As we will see in §4, however, when disk masses $M_{\rm disk}/M_* \sim h/r$ are encountered we tend to have bigger fish to fry, as this is also the approximate condition for the onset of disk self-gravity, the formation of spiral arms, and substantial departures from axisymmetry.

Magnetic pressure $P_B = B^2/8\pi$ is likely to impact the vertical density profile, at least for $z \gg h$ (here and subsequently, we use units such that B is measured in Gauss). No simple principle for predicting the strength or vertical variation of the magnetic field is known, so we turn to numerical simulations for guidance. Hirose & Turner [150] completed radiation magnetohydrodynamic (MHD) simulations of the protoplanetary disk at 1 AU, taking the surface density $\Sigma = 10^3$ g cm^{-2} and adopting as stellar parameters $M_* = 0.5\ M_\odot$, $T_{\rm eff} = 4000$ K, and $R_* = 2\ R_\odot$. Their simulations included Ohmic diffusion but ignored both ambipolar diffusion and the Hall effect (see §4 for further discussion of these processes). They found that the model disk was gas pressure dominated near the mid-plane, but that the atmosphere (or corona) was magnetically dominated. An empirical fit to their density profile is [332],

$$\rho = \frac{\rho_0}{1+\varepsilon}\left[\exp\left(-z^2/2h^2\right) + \varepsilon\exp\left(-|z|/kh\right)\right], \tag{10}$$

with $\varepsilon \simeq 1.25 \times 10^{-2}$ and $k \simeq 1.5$. This fit is shown in Figure 2. Magnetic pressure beats out gas pressure for $|z| > 4h$, leading to a low density exponential atmosphere

that is much more extended than a standard isothermal disk. Even if the atmosphere itself gives way to a disk wind at still higher altitudes (as suggested by other simulations), these results suggest that observational probes of conditions near the disk surface may be sampling regions where the magnetic field dominates.

The impact of magnetic pressure on the vertical structure of protoplanetary disks may be larger than the preceding discussion implies. Simulations of the inner disk ($r \sim 1$ AU) that include the Hall effect [195] result in the generation of strong azimuthal magnetic fields whose magnetic pressure may exceed that of the gas within one scale height, or even at the mid-plane. This implies that there could be regions of the disk where the conventional estimate of the scale height based on the temperature is significantly in error. Observational constraints on such models would be valuable, as would a better analytic understanding of what determines the vertical profile of B in disks.

2.1.2 Radial structure

The radial run of the surface density cannot be predicted from considerations of static disk structure; it is either an observational question [9] or one to address using time-dependent models (§3)[1]. Instead, we consider the azimuthal velocity v_ϕ. If the disk is static (and even if it is slowly evolving) the azimuthal component of the momentum equation,

$$\frac{\partial \mathbf{v}}{\partial t} + (\mathbf{v}\cdot\nabla)\,\mathbf{v} = -\frac{1}{\rho}\nabla P - \nabla\Phi \tag{11}$$

can be written in the mid-plane as,

$$\frac{v_\phi^2}{r} = \frac{GM_*}{r^2} + \frac{1}{\rho}\frac{\mathrm{d}P}{\mathrm{d}r}. \tag{12}$$

Here P is the pressure and all quantities are mid-plane values. Let's start with an explicit example of the consequences of this force balance in protoplanetary disks. Consider a disk with $\Sigma \propto r^{-1}$ and central temperature $T_c \propto r^{-1/2}$. We then have $c_s \propto r^{-1/4}$, $\rho \propto r^{-9/4}$ and $P \propto r^{-11/4}$. Substituting into equation (12) yields,

$$v_\phi = v_\mathrm{K}\left[1 - \frac{11}{4}\left(\frac{h}{r}\right)^2\right]^{1/2}. \tag{13}$$

[1] The *minimum mass Solar Nebula* (MMSN) [347, 142], an approximate lower bound for the amount of disk gas needed to form the planets in the Solar System, can be useful as a reference model despite its tenuous connection to actual conditions in the disk at the time of planet formation. The MMSN has a gas surface density profile $\Sigma(r) = 1.7\times10^3 (r/AU)^{-3/2}$ g cm^{-2}.

From this we deduce,

- The deviation from strict Keplerian rotation, $v_{\rm K} = \sqrt{GM_*/r}$ is of the order of $(h/r)^2$.
- Its magnitude is *small*. For a disk with $h/r = 0.03$ at 1 AU, the difference between the disk azimuthal velocity and the Keplerian value is about 0.25%, or, in absolute terms $|v_\phi - v_{\rm K}| \simeq 70$ m s^{-1}.

When we come to discuss the evolution of particles within disks (§6), it will turn out that this seemingly small effect is of paramount importance. Particles do not experience the radial pressure gradient that is the cause of the mismatch in speeds, and as a result develop a differential velocity with respect to the gas that leads to aerodynamic drag and (usually) inspiral. Because this process is so important it is worth studying not just the magnitude of the effect but also its vertical dependence. To do so, we follow Takeuchi & Lin [322] and consider an axisymmetric vertically isothermal disk supported against gravity by gas pressure. The vertical density profile is then gaussian (equation 4) in equilibrium (equation 11) we have,

$$r\Omega_{\rm g}^2 = \frac{GM_*}{(r^2+z^2)^{3/2}} r + \frac{1}{\rho}\frac{\partial P}{\partial r}. \tag{14}$$

We distinguish between the gas angular velocity, $\Omega_{\rm g}(r,z)$, the Keplerian angular velocity $\Omega_{\rm K}(r,z) = GM_*/(r^2+z^2)^{3/2}$, and its mid-plane value $\Omega_{\rm K,mid}$. The disk is fully specified by the local power-law profiles of surface density and temperature,

$$\Sigma \propto r^{-\gamma} \tag{15}$$

$$T_c \propto r^{-\beta}, \tag{16}$$

with $\gamma = 1$ and $\beta = 1/2$ being typically assumed values. Evaluating $\partial P/\partial r$ using equation (4) with $h = h(r)$ allows us to determine the equilibrium gas angular velocity in terms of the mid-plane Keplerian value,

$$\Omega_{\rm g} \simeq \Omega_{\rm K,mid}\left[1 - \frac{1}{4}\left(\frac{h}{r}\right)^2\left(\beta + 2\gamma + 3 + \beta\frac{z^2}{h^2}\right)\right]. \tag{17}$$

Provided that the temperature is a locally decreasing function of radius ($\beta > 0$), the sense of the vertical shear is that the gas rotates slower at higher z. Like the sub-Keplerian mid-plane velocities, the magnitude of the shear is only of the order of $(h/r)^2$, but this small effect may nevertheless be detectable with ALMA data [297].

For particle dynamics, what matters is the difference between the gas velocity and the local Keplerian speed. To order z^2/r^2, the vertical dependence of the Keplerian velocity is,

$$\Omega_{\rm K} \simeq \Omega_{\rm K,mid}\left(1 - \frac{3}{4}\frac{z^2}{r^2}\right). \tag{18}$$

This function decreases faster with height than $\Omega_{\rm g}$, so the difference between them, plotted in Figure 3, switches sign for sufficiently large z,

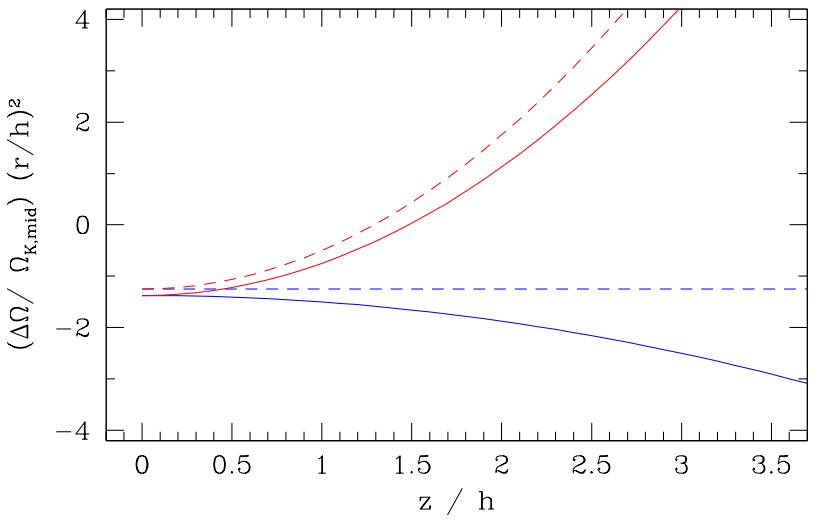

Fig. 3 The variation in angular velocity with height in the disk. In blue, the angular velocity of gas relative to the mid-plane Keplerian value, $(\Omega_{\rm g} - \Omega_{\rm K,mid})/\Omega_{\rm K,mid} \times (r/h)^2$. In red, the difference between the Keplerian angular velocity and the *local* gas angular velocity, $(\Omega_g - \Omega_{\rm K})/\Omega_{\rm K,mid} \times (r/h)^2$. The assumed disk has $\Sigma \propto r^{-1}$ and $T_c \propto r^{-1/2}$ (solid curves) or radially constant T_c (dashed curves).

$$\Omega_{\rm g} - \Omega_{\rm K} \simeq -\frac{1}{4}\left(\frac{h}{r}\right)^2 \left[\beta + 2\gamma + 3 + (\beta - 3)\,\frac{z^2}{h^2}\right] \Omega_{\rm K,mid}. \tag{19}$$

Particles that orbit the star at the local Keplerian speed move slower than the gas near the mid-plane (and thus experience a "headwind"), but faster at high altitude. For typical parameters, the changeover occurs at about $z \approx 1.5h$.

The orbital velocity will also deviate from the point mass Keplerian form if the disk mass is sufficiently high. The gravitational potential of a disk is *not* that of a point mass (and does not have a simple form for realistic disk surface density profiles), but for an approximation we assume that it is. Then the modified Keplerian velocity depends only upon the enclosed disk mass,

$$v'_{\rm K} \simeq v_{\rm K}\left(1 + \frac{M_{\rm disk}}{M_*}\right)^{1/2}. \tag{20}$$

For disk masses $M_{\rm disk} \sim 10^{-2} M_*$ the effect on the rotation curve is of comparable magnitude (but opposite sign) to the effect of the radial pressure gradient.

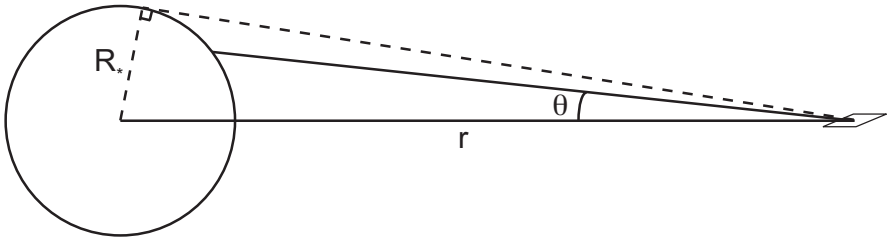

Fig. 4 The setup for calculating the radial temperature distribution of an optically thick, razor-thin disk. We consider a ray passing that makes an angle θ to the line joining the area element to the center of the star. Different rays with the same θ are labeled with the azimuthal angle ϕ; $\phi = 0$ corresponds to the "twelve o'clock" position on the stellar surface.

The simplicity of the calculation of the deviations from Keplerian rotation due to pressure gradients in the disk depends on the disk being axisymmetric. How axisymmetric (and planar) are real disks? In most cases we don't know observationally, and it's obvious that a disk formed from the collapse of a turbulent molecular cloud core might well start out significantly eccentric and warped. The rate of decay of eccentric or warp perturbations remains a subject of active research [45]. It's thus worth remembering, especially when interpreting precise kinematic observations, that un-modeled warps or eccentricities as small as $e \sim (h/r)^2$ could be significant.

2.2 Thermal physics

We seek to determine the temperature of gas and dust as $f(r,z)$. Our first task is to calculate the interior temperature of a disk heated solely by starlight. This is straightforward. At most radii of interest the dust opacity is high enough for the disk to be optically thick to both stellar radiation and to its own re-emitted radiation, which hence has a thermal spectrum. It is then a geometric problem to work out how much stellar radiation annulus of the disk intercepts, and what equilibrium T results. We will then consider the temperatures of gas and dust in the surface layers of disks. These problems are trickier. The surface layers are both optically thin and of low density, so we have to account explicitly for the heating and cooling processes and allow for the possibility that the dust and gas are too weakly coupled to maintain the same temperature. We defer until §3 the question of how accretion heating modifies these solutions.

A disk whose temperature is set by stellar irradiation is described as "passive". The model problem is a flat razor-thin disk that absorbs all incoming stellar radiation and re-emits it locally as a blackbody. We seek the temperature of the blackbody disk emission as $f(r)$. Modeling the star as a sphere of radius R_*, and constant brightness

I_*, we define spherical polar coordinates such that the axis of the coordinate system points to the center of the star (figure 4). The stellar flux passing through a surface at distance r is,

$$F = \int I_* \sin\theta \cos\phi d\Omega, \tag{21}$$

where $d\Omega$ represents the element of solid angle. We count the flux coming from the top half of the star only (and later equate that to radiation from only the top surface of the disk), so the integral has limits,

$$\begin{aligned} -\pi/2 < \phi \leq \pi/2 \\ 0 < \theta < \sin^{-1}\left(\frac{R_*}{r}\right). \end{aligned} \tag{22}$$

Substituting $d\Omega = \sin\theta d\theta d\phi$, the integral evaluates to,

$$F = I_* \left[\sin^{-1}\left(\frac{R_*}{r}\right) - \left(\frac{R_*}{r}\right)\sqrt{1-\left(\frac{R_*}{r}\right)^2} \right]. \tag{23}$$

A star with effective temperature T_* has brightness $I_* = (1/\pi)\sigma T_*^4$, with σ the Stefan-Boltzmann constant. Equating F to the one-sided disk emission $\sigma T_{\rm disk}^4$ the temperature profile is,

$$\left(\frac{T_{\rm disk}}{T_*}\right)^4 = \frac{1}{\pi}\left[\sin^{-1}\left(\frac{R_*}{r}\right) - \left(\frac{R_*}{r}\right)\sqrt{1-\left(\frac{R_*}{r}\right)^2} \right]. \tag{24}$$

The exact result is unnecessarily complicated. To simplify, we expand the right hand side in a Taylor series for $(R_*/r) \ll 1$ (i.e. far from the stellar surface) to obtain,

$$T_{\rm disk} \propto r^{-3/4}, \tag{25}$$

as the power-law temperature profile of a thin, flat, passive disk. This implies a sound speed profile, $c_s \propto r^{-3/8}$, and a disk thickness $(h/r) \propto r^{1/8}$. We therefore predict that the disk becomes geometrically thicker ("flares") at larger radii. We can also integrate equation (24) exactly over r, with the result that the luminosity from both side of the disk sums to $L_{\rm disk}/L_* = 1/4$.

A more detailed calculation of the dust emission from passive disks requires consideration of two additional physical effects [171]. First, as we just noted, the disk thickness as measured by the gas scale height flares to larger radii. If dust is well-mixed with the gas — which may or may not be a reasonable assumption — a flared disk intercepts more stellar radiation in its outer regions than a flat one, which will tend to make it flare even more strongly. We therefore need to solve for the self-consistent *shape* of the disk that simultaneously satisfies hydrostatic and thermal equilibrium at every radius. This is conceptually easy, and the slightly messy geometry required to generalize the flat disk calculation is clearly described

by Kenyon & Hartmann [171]. Second, small dust grains that are directly exposed to stellar irradiation (i.e. those where the optical depth to stellar radiation along a line toward the star $\tau < 1$) emit as a dilute blackbody with a temperature higher than if they were true blackbody emitters [171]. The reason for this is that small dust grains, of radius s, have an emissivity $\varepsilon = 1$ only for wavelengths $\lambda \leq 2\pi s$. At longer wavelengths, their emissivity declines. The details depend upon the composition and structure of the dust grains, but roughly the emissivity (and opacity κ) scale inversely with the wavelength. In terms of temperature,

$$\varepsilon = \left(\frac{T}{T_*}\right)^{\beta} \tag{26}$$

with $\beta = 1$. A dust particle exposed to the stellar radiation field is then in radiative equilibrium at temperature $T_{\rm s}$ when absorption and emission are in balance,

$$\frac{L_*}{4\pi r^2}\pi s^2 = \sigma T_{\rm s}^4 \varepsilon\,(T_{\rm s})\,4\pi s^2. \tag{27}$$

The resulting temperature,

$$T_{\rm s} = \frac{1}{\varepsilon^{1/4}}\left(\frac{R_*}{2r}\right)^{1/2} T_*, \tag{28}$$

exceeds the expected blackbody temperature by a substantial factor if $\varepsilon \ll 1$.

An illustrative analytic model that incorporates these effects was developed by Chiang & Goldreich [75]. They considered a disk with a surface density profile $\Sigma = 10^3 (r/1\,{\rm AU})^{-3/2}$ g cm^{-2} around a star with $M_* = 0.5\,M_\odot$, $T_* = 4000$ K and $R_* = 2.5\,R_\odot$. Within about 100 AU, their solution has half of the bolometric luminosity of the disk emitted as a blackbody at the interior temperature,

$$T_{\rm i} \approx 150\left(\frac{r}{1\ {\rm AU}}\right)^{-3/7}\ {\rm K}, \tag{29}$$

with equal luminosity at each radius emerging from a hot surface dust layer at,

$$T_{\rm s} \approx 550\left(\frac{r}{1\ {\rm AU}}\right)^{-2/5}\ {\rm K}. \tag{30}$$

The Chiang & Goldreich solution is a two-layer approximation to dust continuum radiative transfer for a passive, hydrostatic disk. Approximations in the same spirit have been developed that incorporate heating due to accretion [122], but the full problem requires numerical treatment. Several codes are available for its efficient solution [55, 100, 294, 315].

If our main interest is in the physical conditions at the disk mid-plane within the normal planet forming region (i.e. excluding very large orbital distances where the disk is becoming optically thin), or in the continuum Spectral Energy Distribution (SED), models for the dust temperature largely suffice. Dust dominates both the

absorption of starlight and thermal emission of reprocessed radiation and accretion heating, and in the mid-plane the gas and dust temperatures are normally closely equal (to within $\sim 10\%$ for an optical extinction $A_V > 0.1$ [168]). The gas temperature near the surface of the disk is, however, of critical importance for a number of applications,

- Interpretation of sub-mm data, where the observable emission is rotational transitions of molecules such as CO and HCO^+. These observations frequently probe the outer regions of disks, at depths where the molecules are not (of course!) photo-dissociated but where the gas is warm and not in equilibrium with the dust.
- Interpretation of near-IR and far-IR data, often from the inner disk, where we are seeing ro-vibrational transitions of molecules along with fine-structure cooling lines such as [CII] and [OI].
- Chemistry. It's cold at the disk mid-plane, and chemical reactions are sluggish. Although the densities are much lower in the disk atmosphere, the increased temperatures and exposure to higher energy stellar photons make the upper regions of the disk important for chemistry [144].

The properties of gas near the surface of disks are very closely tied to the incident flux of ultraviolet radiation from the star. Stellar UV radiation ionizes and dissociates atoms and molecules, and heats the gas by ejecting electrons from dust grains (grain photoelectric heating). Depending upon the temperature and density, the heating is balanced by cooling from rotational transitions of molecules (especially CO) and atomic fine structure lines. Also important is energy exchange due to inelastic collisions between gas molecules and dust particles (thermal accommodation) — if this process is too efficient the gas temperature will revert to match the dust which is absorbing and emitting the bulk of the star's bolometric luminosity.

Photoelectric heating [94] is typically the dominant process for dusty gas exposed to an ultraviolet radiation field. The work function of graphite grains (the minimum energy required to free an electron from them) is around 5 eV, so 10 eV FUV photons can eject electrons from uncharged grains with 5 eV of kinetic energy that ultimately heats the gas. Ejection occurs with a probability of the order of 0.1, so the overall efficiency (the fraction of the incident FUV energy that goes into heating the gas rather than the dust) can be rather high, around 5%.

A detailed evaluation of the photoelectric heating rate is involved, and resistant to a fully first-principles calculation. Weingartner & Draine [348] give a detailed description. Here, we sketch the main principles following Kamp & van Zadelhoff [169], who developed models for the gas temperature in A star disks. We consider a stellar radiation spectrum F_ν impinging on grains of graphite (work function $w = 4.4$ eV [348]) and silicate ($w = 8.0$ ev). For micron-sized grains the work function, which is a property of the bulk material, is equivalent to the ionization potential — the energy difference between infinity and the highest occupied energy level in the solid. Additionally, the probability for absorption when a photon strikes a grain is $Q_{\rm abs} \approx 1$. Most absorbed photons, however, do *not* eject electrons, rather their energy goes entirely into heating the dust grain. The yield of emitted electrons is some

function of photon energy $Y(h\nu)$, and they have some spectrum of kinetic energy E, roughly described by [94] $f(E,h\nu) \propto (h\nu - w)^{-1}$. If the grains are charged (e.g. by prior emission of photoelectrons) then the kinetic energy $(E - eU)$ available to heat the gas is that left over once the electron has escaped the electrostatic potential eU of the grain. The heating rate is then [169],

$$\Gamma_{pe} = 4 n_H \sigma \int_{E_{\min}}^{E_{\max}} \left(\int_{\nu_{\rm th}}^{\nu_{\max}} Q_{\rm abs} Y(h\nu) f(E,h\nu) F_\nu \mathrm{d}\nu \right) (E - eU)\, \mathrm{d}E, \qquad (31)$$

where n_H is the number density of hydrogen atoms, σ is the geometric cross-section per hydrogen nucleus, and the lower limits express the minimum frequency $\nu_{\rm th}$ of a photon that can overcome the work function and the minimum energy of a photoelectron that can escape from a charged grain. An assessment of the photoelectric heating rate then requires knowledge of the functions Y and f, specification of the radiation field F_ν, and calculation of the typical charge on grains of different sizes [96, 348]. The physics is conceptually identical but quantitatively distinct when the grains in question are *extremely small* (e.g. Polycyclic Aromatic Hydrocarbons, PAHs) [35, 348].

The rate of energy exchange from inelastic gas-grain collisions can be calculated with a collision rate argument. Consider grains with geometric cross-section $\sigma_d = \pi \langle s^2 \rangle$ and number density n_d, colliding with hydrogen atoms with number density n_H. The thermal speed of the hydrogen atoms is $v_{\rm th} = (8 k_B T_g / \pi m_H)^{1/2}$ and the average kinetic energy of the molecules on striking the surface is $2 k_B T_g$. The cooling rate per unit volume due to gas-grain collisions can then be written in the form [64],

$$\Lambda_{g-d} = n_d n_g \sigma_d \left(\frac{8 k_B T_g}{\pi m_H} \right)^{1/2} \alpha_T \left(2 k_B T_g - 2 k_B T_d \right), \qquad (32)$$

where T_g and T_d are the temperatures of the gas and dust respectively. The subtleties of the calculation are reflected in the "accommodation co-efficient" α_T, which is typically $\alpha_T \approx 0.3$ for silicate and carbon grains. For a specified volumetric heating rate (and assumptions as to the gas to dust ratio and properties of the grains), this expression can be used to estimate the density below which the thermal properties of gas and dust decouple.

In addition to cooling that occurs indirectly, as a consequence of gas-grain collisions, gas in the upper layers of disks also cools radiatively. In the molecular layer of the disk, the dominant coolant is typically CO, as this is the most abundant molecule that is not homonuclear (diatomic molecules, such as H_2, have no permanent electric dipole moment and hence radiate inefficiently). At higher temperatures — only attained in the very rarefied uppermost regions of the disk atmosphere — cooling by Lyα emission becomes important. Qualitatively, there are then three distinct layers in the disk:

- A cool mid-plane region, where dust and gas have the same temperature and dust cooling is dominant.

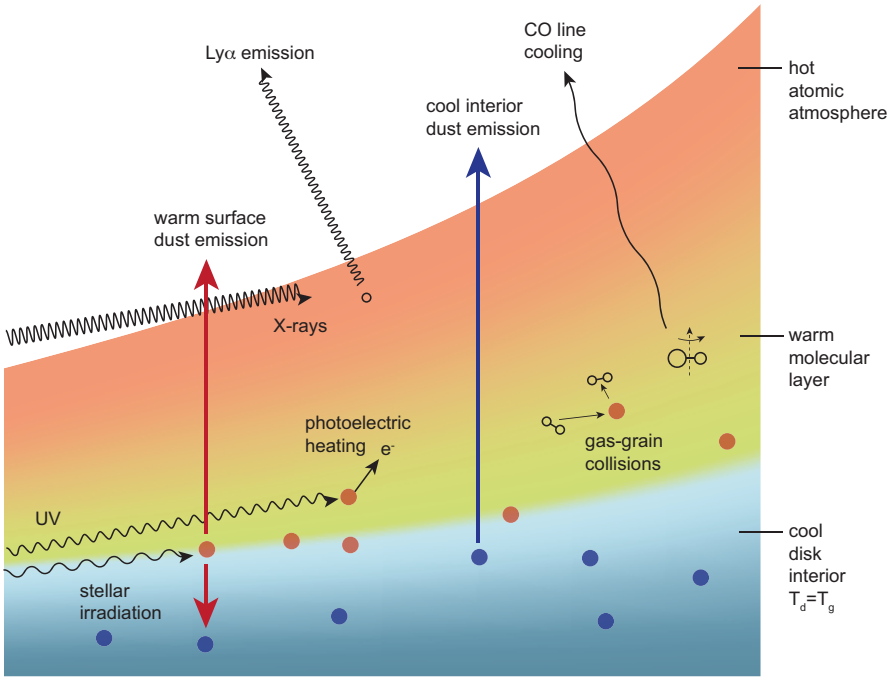

Fig. 5 Illustration of some of the physical processes determining the temperature and emission properties of irradiated protoplanetary disks.

- A warm surface layer, in which both dust and gas have temperatures that exceed the mid-plane value. The gas in the warm layer can be substantially hotter than the dust ($T \sim 10^3$ K at 1 AU), and cools both by dust-gas collisions and by CO rotational-vibrational transitions.
- A hot, low-density atmosphere, where Lyα radiation and other atomic lines (e.g. O[I]) cool the gas.

The disk structure that results from these heating and cooling processes is illustrated in Figure 5.

2.3 Ionization structure

The degree of ionization of the gas in protoplanetary disks is important because it is key to understanding how gas couples to magnetic fields, and thence to understanding the role of magnetic fields in the formation of disks, in the sustenance of turbulence within them, and in the generation of jets and magnetohydrodynamic (MHD) winds. At the most basic level, we care about the ratio of the number density of free electrons n_e to the number density of neutrals,

$$x_e \equiv \frac{n_e}{n_n}, \tag{33}$$

though we should remember that dust grains can also bear charges and carry currents. We will consider separately the thermodynamic equilibrium process of *thermal* (or collisional) ionization, which typically dominates above $T \sim 10^3$ K, and *non-thermal* ionization due to photons or particles that have an energy well in excess of the typical thermal energy in the gas.

In anticipation of results that will be derived in §4, we note that very low and seemingly negligible levels of ionization — $x_e \ll 10^{-10}$ – often suffice to couple magnetic fields to the fluid. We need to worry about small effects when considering ionization.

2.3.1 Thermal ionization

Thermal ionization of the alkali metals is important in the innermost regions of the disk, usually well inside 1 AU. In thermal equilibrium the ionization state of a single species with ionization potential χ is obeys the Saha equation [299],

$$\frac{n^{\rm ion} n_e}{n} = \frac{2U^{\rm ion}}{U}\left(\frac{2\pi m_e k_B T}{h^2}\right)^{3/2} \exp[-\chi/k_B T]. \tag{34}$$

Here, $n^{\rm ion}$ and n are the number densities of the ionized and neutral species, and n_e ($= n^{\rm ion}$) is the electron number density. The partition functions for the ions and neutrals are $U^{\rm ion}$ and U, and the electron mass is m_e. The temperature dependence is not quite just the normal exponential Boltzmann factor, because the ionized state is favored on entropy grounds over the neutral state.

In protoplanetary disks thermal ionization becomes significant when the temperature becomes high enough to start ionizing alkali metals. For potassium, the ionization potential $\chi = 4.34$ eV. We write the abundance of potassium relative to all other neutral species as $f = n_K/n_n$, and define the ionization fraction x,

$$x \equiv \frac{n_e}{n_n}. \tag{35}$$

While potassium remains weakly ionized, the Saha equation gives,

$$x \simeq 10^{-12}\left(\frac{f}{10^{-7}}\right)^{1/2}\left(\frac{n_n}{10^{15}\ {\rm cm}^{-3}}\right)^{-1/2}\left(\frac{T}{10^3\ {\rm K}}\right)^{3/4}\frac{\exp[-2.52\times10^4/T]}{1.14\times10^{-11}} \tag{36}$$

where the final numerical factor in the denominator is the value of the exponent at 10^3 K. The ionization fraction at different temperatures is shown in Figure 6. Ionization fractions large enough to be interesting for studies of magnetic field coupling are reached at temperatures of $T \sim 10^3$ K although the numbers remain extremely small – of the order of $x \sim 10^{-12}$ for these parameters.

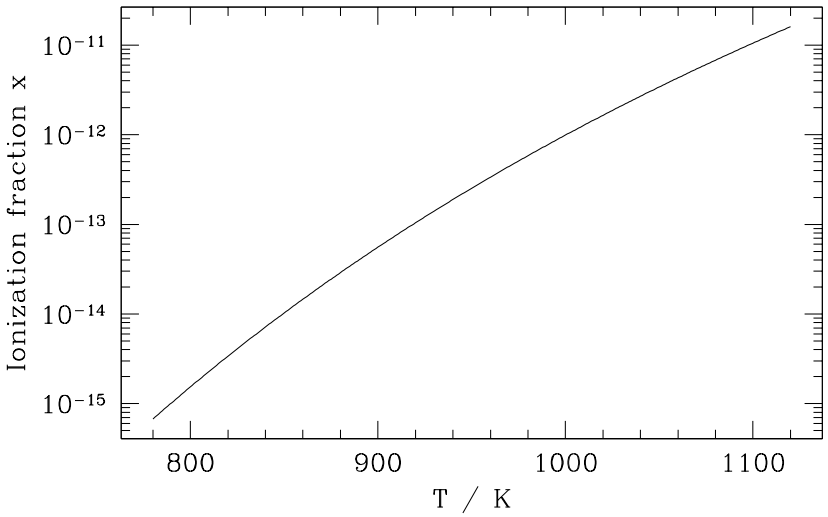

Fig. 6 The thermal ionization fraction as a function of temperature predicted by the Saha equation for the inner disk. Here we assume that potassium, with ionization potential $\chi = 4.34$ eV and fractional abundance $f = 10^{-7}$, is the only element of interest for the ionization. The number density of neutrals is taken to be $n_n = 10^{15}$ cm^{-3}.

2.3.2 Non-thermal ionization

Outside the region close to the star where thermal ionization is possible, any remnant levels of ionization are controlled by non-thermal processes. Considerations of thermodynamic equilibrium are not relevant, and we need to explicitly balance the rate of ionization by high-energy particles or photons against the rate of recombination within the disk gas.

There is no shortage of potentially important sources of ionization. Ordering them roughly in order of their penetrating power, ideas that have been suggested include,

- Ultraviolet photons (from the star, or from other stars in a cluster)
- Stellar X-rays
- Cosmic rays
- Energetic protons from a stellar corona [333]
- Particles produced from radioactive decay of nuclides within the disk [316]
- Electric discharges. [240]

We will limit our discussion to the first three of these processes.

The coronae of T Tauri stars are powerful sources of keV X-rays [273]. Typical luminosities are $L_X \simeq 10^{28} - 10^{31}$ erg s^{-1}, in X-rays with temperatures $k_B T_X$ of a few keV. The physics of the interaction of these X-rays with the disk gas involves

Compton scattering and absorption by photo-ionization, which has a cross-section $\sigma \sim 10^{-22}$ cm^2 for keV energies, decreasing with photon energy roughly as $E_{\rm phot}^{-3}$. Given an input stellar spectrum and assumptions as to where the X-rays originate, the scattering and absorption physics can be calculated using radiative transfer codes to deduce the ionization rate within the disk [101].

Depending upon the level of detail needed for a particular application, the results of numerical radiative transfer calculations can be approximated analytically. For a relatively hard stellar spectrum ($k_B T_X = 5$ keV), the ionization rate fairly deep within the disk scales with radius r and vertical column from the disk surface Σ as $r^{-2}\exp[-\Sigma/8\ {\rm g\ cm^{-2}}]$ [334]. A more detailed fit is given by Bai & Goodman (2009) [29]. For an X-ray luminosity scaled to $L_{X,29} = L_X/10^{29}$ erg s^{-1} they represent the numerical results with two components,

$$\frac{\zeta_X}{L_{X,29}}\left(\frac{r}{1\ {\rm AU}}\right)^{-2.2} = \zeta_1 \exp[-(\Sigma/\Sigma_1)^{\alpha}] + \zeta_2 \exp[-(\Sigma/\Sigma_2)^{\beta}] + ... \qquad (37)$$

where Σ is the vertical column density from the top of the disk and symmetric terms in the column density from the bottom of the disk are implied. For $k_B T_X =$ 3 keV and Solar composition gas the fit parameters are $\zeta_1 = 6\times10^{-12}$ s^{-1}, $\zeta_2 = 10^{-15}$ s^{-1}, $\Sigma_1 = 3.4\times10^{-3}$ g cm^{-2}, $\Sigma_2 = 1.59$ g cm^{-2}, $\alpha = 0.4$ and $\beta = 0.65$. For $k_B T_X = 5$ keV the fit parameters are $\zeta_1 = 4\times10^{-12}$ s^{-1}, $\zeta_2 = 2\times10^{-15}$ s^{-1}, $\Sigma_1 = 6.8\times10^{-3}$ g cm^{-2}, $\Sigma_2 = 2.27$ g cm^{-2}, $\alpha = 0.5$ and $\beta = 0.7$.

Figure 7 shows the estimates for $\zeta(\Sigma)$ for a stellar X-ray luminosity of $L_X = 10^{30}$ erg s^{-1} incident on the disk at 1 AU. If one is mainly interested in regions of the disk more than ≈ 10 g cm^{-2} away from the surfaces the single exponential fit given by Turner & Sano (2008) [334] may suffice. The more complex fitting function given by equation (37) captures the much higher rates of ionization due to X-rays higher up in the disk atmosphere.

Cosmic rays are another potential source of disk ionization. A standard description of the interstellar cosmic ray flux gives them an unattenuated ionization rate of $\zeta_{CR} \sim 10^{-17} - 10^{-16}$ s^{-1} and an exponential stopping length of 96 g cm^{-2} (substantially greater than even high energy stellar X-rays)[2]. With these parameters, X-rays would remain the primary source of ionization in the upper ≈ 50 g cm^{-2} of the disk, but cosmic rays would dominate in the region between about 50 and 500 g cm^{-2}. It is unclear, however, whether the unattenuated interstellar medium flux of cosmic rays typically reaches the surfaces of protoplanatary disks. The magnetic fields embedded in the *Solar* wind form a partial barrier to incoming cosmic ray particles, whose effect is seen in a modulation of the observed flux with the Solar cycle. T Tauri stars could have much stronger stellar winds that exclude cosmic rays efficiently. Indeed, chemical modeling of molecular line data suggests that cosmic rays are substantially excluded (to a level $\zeta_{CR} \sim 10^{-19}$) from the disk around the nearby star TW Hya [83], though how pervasive this phenomenon is remains unknown. If

[2] Umebayashi & Nakano noted that if cosmic rays have an approximately isotropic angular distribution at the disk surface, geometric effects lead to a faster than exponential attenuation deep in the disk [336].

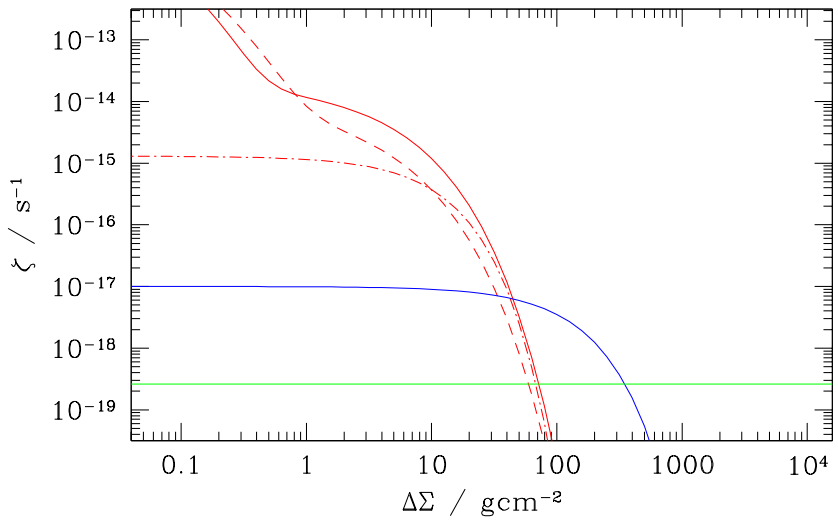

Fig. 7 Estimates of the non-thermal ionization rate due to X-rays (red curves), unshielded cosmic rays (blue) and radioactive decay of short-lived nuclides (blue), plotted as a function of the vertical column density from the disk surface. The solid red curve shows the Bai & Goodman (2009) result for an X-ray temperature $k_B T_X = 5$ keV, the dashed curve their result for $k_B T_X = 3$ keV. The dot-dashed red curve shows a simpler formula proposed by Turner & Sano (2008). All of the X-ray results have been normalized to a flux of $L_X = 10^{30}$ erg s^{-1} and a radius of 1 AU.

cosmic rays are not present, the only guaranteed source of ionization at columns more than ≈ 100 g cm^{-2} away from the disk surfaces is radioactive decay.

If our main interest is in conditions at $r \sim 1$ AU the surface density in gas is typically $\Sigma \sim 10^3$ gcm^{-2} and X-rays, which are our main concern, will not reach the mid-plane. The situation is different further out. At 100 AU typical surface densities are much lower — 1 g cm^{-2} might be reasonable — and X-rays will sustain a non-zero rate of ionizations throughout that column. On these scales ultraviolet photons can also be important. Stellar FUV radiation will ionize carbon and sulphur atoms near the disk surface, yielding a relatively high electron fraction $x_e \sim 10^{-5}$. The ionized skin that results is shallow, penetrating to a vertical column of just $0.01 - 0.1$ g cm^{-2}, but enough to be significant in the tenuous outer disk [266].

Whether cosmic rays are excluded from most or all T Tauri disks is an important question which may be addressed observationally in the near future. Theoretically one should also remember that the amount of *power* involved in non-thermal ionization is rather small when compared to that liberated by accretion [156]. Any internal disk process that could convert a small fraction

of the accretion energy into non-thermal particles would likely matter for the ionization state.

As with ionization, the rate of recombination within the disk can be calculated from complex numerical models that track reactions (often numbering in the thousands) between dozens of different species. The following discussion, which borrows heavily from the description given by Ilgner & Nelson (2006) [152] and Fromang (2013) [113], is intended only to outline some of the important principles. At the broadest level of discussion we need to consider gas-phase recombination reactions (involving molecular and gas-phase metal ions) along with recombination on the surface of dust grains.

The principles of gas-phase recombination can be illustrated by considering the possible reactions between electrons and generic molecules m and metal atoms M [252, 152]. The basic reactions are then,

- Ionization,
$$\mathrm{m} \rightarrow \mathrm{m}^+ + \mathrm{e}^-, \tag{38}$$
with rate ζ. A specific example is $\mathrm{H}_2 \rightarrow \mathrm{H}_2^+ + \mathrm{e}^-$.
- Recombination with molecular ions,
$$\mathrm{m}^+ + \mathrm{e}^- \rightarrow \mathrm{m}, \tag{39}$$
with rate $\alpha = 3 \times 10^{-6} T^{-1/2}$ cm^3 s^{-1}. An example is the dissociative recombination reaction $\mathrm{HCO}^+ + \mathrm{e}^- \rightarrow \mathrm{CO} + \mathrm{H}$.
- Recombination with gas-phase metal ions,
$$\mathrm{M}^+ + \mathrm{e}^- \rightarrow \mathrm{M} + h\nu, \tag{40}$$
with rate $\gamma = 3 \times 10^{-11} T^{-1/2}$ cm^3 s^{-1}. An example is $\mathrm{Mg}^+ + \mathrm{e}^- \rightarrow \mathrm{Mg} + h\nu$.
- Charge exchange reactions,
$$\mathrm{m}^+ + \mathrm{M} \rightarrow \mathrm{m} + \mathrm{M}^+, \tag{41}$$
with rate $\beta = 3 \times 10^{-9}$ cm^3 s^{-1}. An example is $\mathrm{HCO}^+ + \mathrm{Mg} \rightarrow \mathrm{Mg}^+ + \mathrm{HCO}$.

From such a set of reactions we form differential equations describing the time evolution of the number density of species involved. For the molecular abundance n_m, for example, we have,

$$\frac{\mathrm{d}n_\mathrm{m}}{\mathrm{d}t} = -\zeta n_\mathrm{m} + \alpha n_e n_{\mathrm{m}^+} + \beta n_\mathrm{M} n_{\mathrm{m}^+} = 0, \tag{42}$$

where the second equality follows from assuming that the system has reached equilibrium. The resulting system of algebraic equations has simple limiting solutions. For example, if there are no significant reactions involving metals then the above equation, together with the condition of charge neutrality ($n_{\mathrm{m}^+} = n_e$), gives an elec-

tron fraction $x_e = n_e/n_{\rm m}$,

$$x_e = \sqrt{\frac{\zeta}{\alpha n_{\rm m}}}. \tag{43}$$

In the more general case, the network yields a cubic equation which can be solved for the electron fraction as a function of the gas-phase metal abundance [152]. Typically the presence of metal atoms and ions is important for the ionization level.

Recombination can also occur on the surfaces of dusty or icy grains. The simplest reactions we might consider are,

$$\begin{aligned} {\rm e}^- + {\rm gr} &\rightarrow {\rm gr}^- \\ {\rm m}^+ + {\rm gr}^- &\rightarrow {\rm gr} + {\rm m}. \end{aligned} \tag{44}$$

If the first of these reactions is rate-limiting, then we can write a modified version of the ordinary differential equation (equation 42) that includes grain processes. Ignoring metals for simplicity,

$$\frac{{\rm d}n_{\rm m}}{{\rm d}t} = -\zeta n_{\rm m} + \alpha n_e n_{\rm m^+} + \sigma v_e n_{\rm gr} n_{\rm e^-}, \tag{45}$$

where σ is the cross-section of grains to adhesive collisions with free electrons and v_e is the electron thermal velocity. In the limit where *only* grains contribute to recombination we then find,

$$x_e = \frac{\zeta}{\sigma v_e n_{\rm gr}}. \tag{46}$$

If the grains are mono-disperse with radius s, then $x_e \propto 1/\sigma n_{\rm gr} \propto s$, and recombination on grain surfaces will be more important for small grain sizes. We also note that the dependence on the ionization rate ζ is linear, rather than the square root dependence found in the gas-phase case. As for metals, grain populations with commonly assumed size distributions are found to matter for the ionization level.

The above discussion of recombination leaves a great deal unsaid. For grains, an important additional consideration is related to the typical charge state, which needs to be calculated [96]. A good comparison of different networks for the calculation of the ionization state is given by Ilgner & Nelson (2006) [152], while Bai & Goodman (2009) [29] provide a clear discussion of the important processes.

The accuracy needed from calculations of ionization equilibrium is strongly problem-dependent (and in some cases, such as if we don't know if cosmic rays are present for a particular system, high accuracy may be illusory). The reader who encounters a problem involving the ionization level is advised to consider whether a simple analytic approximation is adequate, or whether solution of a full chemical network is required. Both new analytic models (that include dust), and flexible freely-available codes for computing detailed solutions, would be valuable.

3 Disk evolution

The population of protoplanetary disks is observed to evolve, but why this should happen remains hard to fully explain. For a geometrically thin, low-mass disk, the deviation from a point-mass Keplerian rotation curve is small (c.f. equation 13) and the specific angular momentum,

$$l(r) = r^2\Omega_{\rm K} = \sqrt{GM_* r} \propto r^{1/2}, \tag{47}$$

is an increasing function of orbital radius. To accrete, gas in the disk must lose angular momentum, and the central theoretical problem in disk evolution is to understand this process.

Within any shearing fluid, momentum is transported in the cross-stream direction because the random motion of molecules leads to collisions between particles that have different velocities. The classical approach to disk evolution [219, 276] treats the disk as a vertically thin axisymmetric sheet of viscous fluid, and leads to a fairly simple equation for the time evolution of the disk surface density $\Sigma(r,t)$. There appears to be a fatal flaw to this approach, because the molecular viscosity of the gas is much too small to lead to any significant rate of disk evolution. But it's not as bad as it seems. The classical disk evolution equation involves few assumptions beyond the immutable laws of mass and angular momentum conservation, and as we shall see is therefore approximately valid if the "viscosity" is re-interpreted as the outcome of a turbulent process. We will have (much) more to say about the possible origin of disk turbulence in §4.

Redistribution of angular momentum within the gas disk is not the only route to evolution. An almost equally long-studied suggestion [57] is that gas accretes because a magnetohydrodynamic (MHD) wind *removes* angular momentum entirely from the disk. Winds and viscosity have frequently between seen as orthogonal and competing hypotheses for disk evolution, but there is evidence suggesting that both processes are simultaneously important in regions of protoplanetary disks.

3.1 The classical equations

The evolution of a flat, circular and geometrically thin ($(h/r) \ll 1$) viscous disk follows from the equations of mass and angular momentum conservation [276]. Given a surface density $\Sigma(r,t)$, radial velocity $v_r(r,t)$ and angular velocity $\Omega(r)$, the continuity equation in cylindrical co-ordinates yields,

$$r\frac{\partial \Sigma}{\partial t} + \frac{\partial}{\partial r}\left(r\Sigma v_r\right) = 0. \tag{48}$$

Angular momentum conservation gives,

$$r\frac{\partial}{\partial t}\left(r^2\Omega\Sigma\right)+\frac{\partial}{\partial r}\left(r^2\Omega\cdot r\Sigma v_r\right)=\frac{1}{2\pi}\frac{\partial G}{\partial r}, \tag{49}$$

where $\Omega(r)$ is time-independent but need not be the point mass Keplerian angular velocity. The rate of change of disk angular momentum is given by the change in surface density due to radial flows and by the *difference* in the torque exerted on the annulus by stresses at the inner and outer edges. For a viscous fluid the torque G has the form,

$$G=2\pi r\cdot\nu\Sigma r\frac{\mathrm{d}\Omega}{\mathrm{d}r}\cdot r \tag{50}$$

where ν is the kinematic viscosity. The torque is the product of the circumference, the viscous force per unit length, and the lever arm r, and scales with the gradient of the angular velocity.

To obtain the surface density evolution equation in its usual form we first eliminate v_r by substituting for $\partial\Sigma/\partial t$ in equation (49) from equation (48). This gives an expression for $r\Sigma v_r$, which we substitute back into equation (48) to yield,

$$\frac{\partial\Sigma}{\partial t}=-\frac{1}{r}\frac{\partial}{\partial r}\left[\frac{1}{\left(r^2\Omega\right)'}\frac{\partial}{\partial r}\left(\nu\Sigma r^3\Omega'\right)\right], \tag{51}$$

where the primes denote differentiation with respect to radius. Specialize to a point mass Keplerian potential ($\Omega\propto r^{-3/2}$) we then find that viscous redistribution of angular momentum within a thin disk obeys an equation,

$$\frac{\partial\Sigma}{\partial t}=\frac{3}{r}\frac{\partial}{\partial r}\left[r^{1/2}\frac{\partial}{\partial r}\left(\nu\Sigma r^{1/2}\right)\right]. \tag{52}$$

This equation is a diffusive partial differential equation for the evolution of the gas, which has a radial velocity,

$$v_r=-\frac{3}{\Sigma r^{1/2}}\frac{\partial}{\partial r}\left(\nu\Sigma r^{1/2}\right). \tag{53}$$

The equation is linear if the viscosity ν is independent of Σ.

Some useful rules of thumb for the rate of evolution implied by equation (52) can be deduced with a change of variables. Defining,

$$X\equiv 2r^{1/2} \tag{54}$$

$$f\equiv\frac{3}{2}\Sigma X, \tag{55}$$

and taking the viscosity ν to be constant, we get a simpler looking diffusion equation,

$$\frac{\partial f}{\partial t}=D\frac{\partial^2 f}{\partial X^2} \tag{56}$$

with a diffusion coefficient D,

$$D=\frac{12\nu}{X^2}. \tag{57}$$

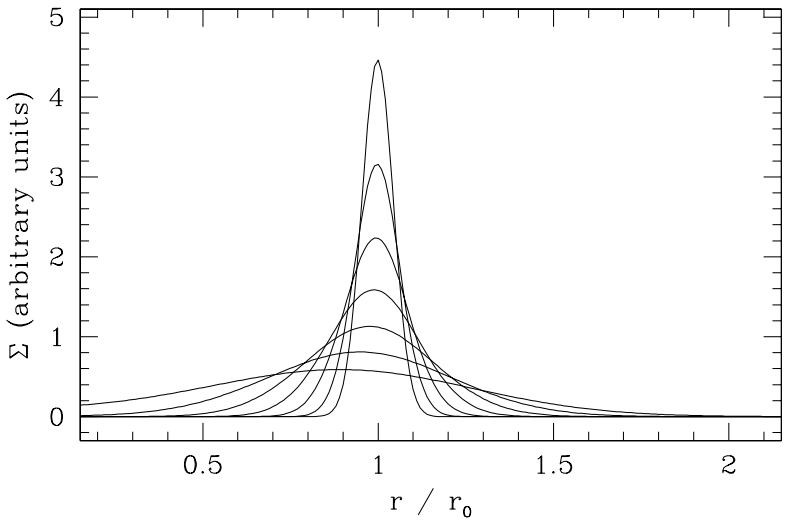

Fig. 8 The time-dependent solution to the disk evolution equation with $\nu =$ constant, showing the spreading of a ring of gas initially orbiting at $r = r_0$. From top down the curves show the surface density as a function of the scaled time variable $\tau = 12\nu r_0^{-2} t$, for $\tau = 0.004$, $\tau = 0.008$, $\tau = 0.016$, $\tau = 0.032$, $\tau = 0.064$, $\tau = 0.128$, and $\tau = 0.256$.

The diffusion time scale across a scale ΔX for an equation of the form of equation (56) is just $(\Delta X)^2/D$. Converting back to the physical variables, the time scale on which viscosity will smooth surface density gradients on a scale Δr is $\tau_\nu \sim (\Delta r)^2/\nu$. For a disk with characteristic size r, the surface density at all radii will evolve on a time scale,

$$\tau_\nu \approx \frac{r^2}{\nu}. \tag{58}$$

This is the *viscous time scale* of the disk.

We can gain some intuition into how equation (52) works by inspecting time-dependent analytic solutions that can be derived for special forms of the viscosity $\nu(r)$. For $\nu =$ constant a Green's function solution is possible. Suppose that at $t = 0$ the gas lies in a thin ring of mass m at radius r_0,

$$\Sigma(r, t = 0) = \frac{m}{2\pi r_0} \delta(r - r_0), \tag{59}$$

where $\delta(r - r_0)$ is a Dirac delta function. With boundary conditions that impose zero-torque at $r = 0$ and allow for free expansion toward $r = \infty$ the solution is [219],

$$\Sigma(x, \tau) = \frac{m}{\pi r_0^2} \frac{1}{\tau} x^{-1/4} \exp\left[-\frac{(1 + x^2)}{\tau}\right] I_{1/4}\left(\frac{2x}{\tau}\right), \tag{60}$$

in terms of dimensionless variables $x \equiv r/r_0$, $\tau \equiv 12\nu r_0^{-2} t$, and where $I_{1/4}$ is a modified Bessel function of the first kind. This solution is plotted in Figure 8 and illustrates generic features of viscous disk evolution. As t increases the ring spreads diffusively, with the mass flowing toward $r = 0$ while the angular momentum is carried by a negligible fraction of the mass toward $r = \infty$. This segregation of mass and angular momentum is generic to the evolution of a viscous disk, and must occur if accretion is to proceed without overall angular momentum loss.

3.1.1 Limits of validity

Protoplanetary disks are not viscous fluids in the same way that honey is a viscous fluid (or, for that matter, in the same way as the mantle of the Earth is viscous). To order of magnitude precision, the viscosity of a gas $\nu \sim v_{\rm th}\lambda$, where $v_{\rm th}$ is the thermal speed of the molecules and the mean-free path λ is,

$$\lambda \sim \frac{1}{n\sigma}. \tag{61}$$

Here n is the number density of molecules with collision cross-section σ. Taking σ to be roughly the physical size of a hydrogen molecule, $\sigma \sim \pi(10^{-8}\ {\rm cm})^2$, and conditions appropriate to 1 AU ($n \sim 10^{15}\ {\rm cm}^{-3}$, $v_{\rm th} \sim 10^5\ {\rm cm\ s}^{-1}$) we estimate,

$$\begin{aligned} \lambda &\sim 3\ {\rm cm} \\ \nu &\sim 3 \times 10^5\ {\rm cm}^2\ {\rm s}^{-1}. \end{aligned} \tag{62}$$

This is not a large viscosity. The implied viscous time according to equation (58) is of the order of 10^{13} yr, far in excess of observationally inferred time scales of protoplanetary disk evolution. If we nevertheless press on and use equation (52) to model disk evolution, we are implicitly modeling a system that is not an ordinary viscous fluid with a viscous equation. We need to understand when this is a valid approximation.

The first possibility, introduced by Shakura & Sunyaev (1973) in their paper on black hole accretion disks [303], retains the idea that angular momentum is conserved within the disk system, but supposes that turbulence rather than molecular processes is the agent of angular momentum transport. Looking back at the derivation of the disk evolution equation (52), we note that the fluid properties of molecular viscosity only enter twice, (i) in the specific expression for G (which, e.g. is linear in the rate of shear) and (ii) in the more basic assumption that angular momentum transport is determined by the *local* fluid properties. The rest of the derivation involves only conservation laws that hold irrespective of the nature of transport. Plausibly then, a disk in which angular momentum is redistributed by the action of turbulence should still be describable by a diffusive equation, provided that the turbulence is a local process. Proceeding rigorously, Balbus & Papaloizou (1999) [40] showed that MHD turbulence is in principle local in this sense, whereas angular momentum transport by self-gravity is in principle not. At the level of the basic

axisymmetric evolution equation then — before we turn to questions of what determines ν, or how boundary layers behave where the shear is reversed — we have not committed any cardinal sin in starting from the viscous disk equation.

Greater care is needed in situations where the disk flow is no longer axisymmetric. Fluids obey the Navier-Stokes equations, but there is no guarantee that a turbulent disk with a complex geometry will behave in the same way as a viscous Navier-Stokes flow with effective kinematic and bulk viscosities. In eccentric disks, for example, even the most basic properties (such as whether the eccentricity grows or decays) depend upon the nature of the angular momentum transport [248].

The disk evolution equation will also need modification if there are external sources or sinks of mass or angular momentum. If the disk gains or loses mass at a rate $\dot{\Sigma}(r,t)$, and *if that gas has the same specific angular momentum as the disk*, then the modification is trivial,

$$\frac{\partial \Sigma}{\partial t} = \frac{3}{r}\frac{\partial}{\partial r}\left[r^{1/2}\frac{\partial}{\partial r}\left(\nu\Sigma r^{1/2}\right)\right] + \dot{\Sigma}. \tag{63}$$

Disk evolution in the presence of thermally driven winds (such as photo-evaporative flows) can be described with this equation. Alternatively, we may consider a disk subject to an external torque that drives a radial flow with velocity $v_{r,ext}$. This adds an advective term,

$$\frac{\partial \Sigma}{\partial t} = \frac{3}{r}\frac{\partial}{\partial r}\left[r^{1/2}\frac{\partial}{\partial r}\left(\nu\Sigma r^{1/2}\right)\right] - \frac{1}{r}\frac{\partial}{\partial r}\left(r\Sigma v_{r,ext}\right). \tag{64}$$

The qualitative evolution of the disk — for example the tendency for the outer regions to expand to conserve angular momentum — can be changed if there is even a modest external torque on the system.

The evolution of disk populations is frequently modeled using the diffusion equation (52). In addition to the formal question of whether this is mathematically sensible, it is not entirely obvious that protoplanetary disks evolve significantly under viscous torques at all radii. In the outer regions, especially, it is possible that the initial surface density distribution is modified more by thermal or magnetic winds.

3.1.2 The α prescription

Molecular viscosity depends in a calculable way upon the density, temperature and composition of the fluid. Can anything similar be said about the "effective viscosity" present in disks? The standard approach is to write the viscosity as the product of the characteristic velocity and spatial scales in the disk,

$$\nu = \alpha c_s h, \tag{65}$$

where α is a dimensionless parameter. This ansatz (introduced in a related form in [303]) is known as the Shakura-Sunyaev α prescription.

We can view the α prescription in two ways. The "weak" version is to regard it as a re-parameterization of the viscosity that (perhaps) describes the leading order scaling expected in disks (so that α is a more slowly varying function of temperature, radius etc than ν). This is useful, and along with convention is the reason why numerical simulations of turbulent transport are invariably reported in terms of an effective α. One can also adopt a "strong" version of the prescription in which α is assumed to be a constant. This is powerful, as it allows for the development of a predictive theory of disk structure that is based on only one free parameter (for a textbook discussion see Frank, King & Raine [111], or for an application to protoplanetary disks see, e.g. [49]). However, its use must be justified on a case by case basis, as there is no reason why α should be a constant. Constant α models probably work better in highly ionized disk systems, where angular momentum transport across a broad range of radii occurs via the simplest version of magnetorotational instability [38], than in protoplanetary disks where the physical origin of angular momentum transport is more complex [16].

3.2 Boundary conditions

Solving equation (52) requires the imposition of boundary conditions. The most common, and simplest, is a zero-torque inner boundary condition, which exactly conserves the initial angular momentum content of the disk. If the star has a dynamically significant magnetic field, however, or if the disk is part of a binary system, other boundary conditions may be more appropriate.

3.2.1 Zero-torque boundary conditions

A steady-state solution to equation (52) with a zero-torque inner boundary condition is derived by starting from the angular momentum conservation equation (Equation 49). Setting the time derivative to zero and integrating we have,

$$2\pi r\Sigma v_r \cdot r^2\Omega = 2\pi r^3 \nu\Sigma \frac{\mathrm{d}\Omega}{\mathrm{d}r} + \text{constant}. \tag{66}$$

In terms of the mass accretion rate $\dot{M} = -2\pi r\Sigma v_r$ we can write this in the form,

$$-\dot{M} \cdot r^2\Omega = 2\pi r^3 \nu\Sigma \frac{\mathrm{d}\Omega}{\mathrm{d}r} + \text{constant}, \tag{67}$$

where the constant of integration, which is an angular momentum flux, is as yet undermined. To specify the constant, we note that if there is a point where $\mathrm{d}\Omega/\mathrm{d}r = 0$ the viscous stress vanishes, and the constant is just the advective flux of angular

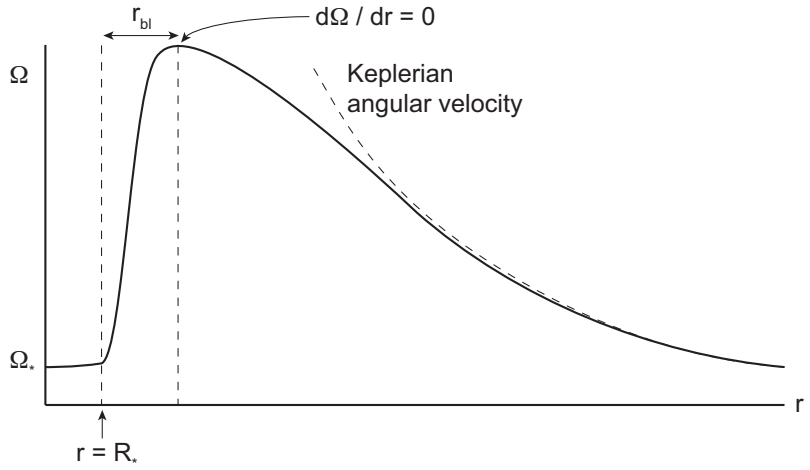

Fig. 9 A sketch of what the angular velocity profile $\Omega(r)$ must look like if the disk extends down to the surface of a slowly rotating star. By continuity there must be a point — usually close to the stellar surface — where $\mathrm{d}\Omega/\mathrm{d}r = 0$ and the viscous stress vanishes.

momentum advected,

$$\text{constant} = -\dot{M} \cdot r^2 \Omega. \tag{68}$$

The physical situation where $\mathrm{d}\Omega/\mathrm{d}r = 0$ is where the protoplanetary disk extends all the way down to the surface of a slowly rotating star. The disk and the star form a single fluid system, and the angular velocity (shown in Figure 9) must be a continuous function that connects $\Omega = 0$ in the star to $\Omega \propto r^{-3/2}$ within the disk. The viscous stress must then vanish at some radius $R_* + r_{\rm bl}$, where $r_{\rm bl}$ is the width of the *boundary layer* that separates the star from the Keplerian part of the disk. Within the boundary layer the angular velocity increases with radius, and gravity is balanced against a combination of rotation and radial pressure support. Elementary arguments [275] show that in many case the boundary layer is narrow, so that $R_* + r_{\rm bl} \simeq R_*$. We then find that,

$$\text{constant} \simeq -\dot{M} R_*^2 \sqrt{\frac{GM_*}{R_*^3}} \tag{69}$$

and the steady-state solution for the disk simplifies to,

$$\nu\Sigma = \frac{\dot{M}}{3\pi}\left(1 - \sqrt{\frac{R_*}{r}}\right). \tag{70}$$

For a specified viscosity this equation gives the steady state surface density profile of a disk with a constant accretion rate $\dot{M}$. Away from the inner boundary $\Sigma(r) \propto \nu^{-1}$, and the radial velocity (Equation 53) is $v_r = -3\nu/2r$.

In obtaining equation (70) we have derived an expression for a *Keplerian* disk via an argument that relies on the *non-Keplerian* form of $\Omega(r)$ in a boundary layer. The resulting expression for the surface density is valid in the disk at $r \gg R_*$, but would not work well close to the star *even if there is a boundary layer*. To model the boundary layer properly, we would need equations that self-consistently determine the angular velocity along with the surface density [272].

3.2.2 Magnetospheric accretion

For protoplanetary disks the stellar magnetic field can have a dominant influence on the disk close to the star [178]. The simplest magnetic geometry involves a dipolar stellar magnetic field that is aligned with the stellar rotation axis and perpendicular to the disk plane. The unperturbed field then has a vertical component at the disk surface,

$$B_z = B_* \left(\frac{r}{R_*} \right)^{-3}. \tag{71}$$

In the presence of a disk,the vertical field will thread the disk gas be distorted by differential rotation between the Keplerian disk and the star. The differential rotation twists the field lines that couple the disk to the star, generating an azimuthal field component at the disk surface B_ϕ and a magnetic torque per unit area (counting both upper and lower disk surfaces),

$$T = \frac{B_z B_\phi}{2\pi} r. \tag{72}$$

Computing the perturbed field accurately is hard (for simulation results see, e.g. [295]), but it is easy to identify the qualitative effect that it has on the disk. Defining the co-rotation radius $r_{\rm co}$ as the radius where the field lines have the same angular velocity as that of Keplerian gas in the disk,

$$r_{\rm co} = \left(\frac{G M_* P^2}{4\pi^2} \right)^{1/3}, \tag{73}$$

there are two regions of star-disk magnetic interaction:

- Interior to co-rotation ($r < r_{\rm co}$) the disk gas has a greater angular velocity than the field lines. Field lines that link the disk and the star here are dragged forward by the disk, and exert a braking torque that removes angular momentum from the disk gas.
- Outside co-rotation ($r > r_{\rm co}$) the disk gas has a smaller angular velocity than the field lines. The field lines are dragged backward by the disk, and there is a positive torque on the disk gas.

Young stars are typically rapid rotators [62], so the co-rotation radius lies in the inner disk. For $P = 7$ days, for example, the co-rotation radius around a Solar mass star is at $r_{\rm co} \simeq 15\, R_\odot$ or 0.07 AU.

The presence of a stellar magnetic torque violates the assumption of a zero-torque boundary condition, though the steady-state solution we derived previously (equation 70) will generally still apply at sufficiently large radius. The strong radial dependence of the stellar magnetic torque means that there is only a narrow window of parameters where the torque will be significant yet still allow the disk to extend to the stellar surface. More commonly, a dynamically significant stellar field will disrupt the inner disk entirely, yielding a magnetospheric regime of accretion in which the terminal phase of accretion is along stellar magnetic field lines. The disruption (or magnetospheric) radius r_m can be estimated in various ways [178], but all yield the same scaling as the spherical Alfvén radius,

$$r_m \simeq \left(\frac{k B_*^2 R_*^6}{\dot{M} \sqrt{G M_*}} \right)^{2/7}, \tag{74}$$

where B_* is the stellar surface field (defined such that $B_* R_*^3$ is the dipole moment) and k a constant of the order of unity. Taking $k = 1$ for a Solar mass star,

$$r_m \simeq 14 \left(\frac{B_*}{\mathrm{kG}} \right)^{4/7} \left(\frac{R_*}{2\, R_\odot} \right)^{12/7} \left(\frac{\dot{M}}{10^{-8}\, M_\odot\ \mathrm{yr}^{-1}} \right)^{-2/7} R_\odot. \tag{75}$$

Often, the magnetospheric radius is comparable to the co-rotation radius.

3.2.3 Accretion on to and in binaries

Boundary conditions for disk evolution also need modification in binary systems. For a coplanar disk orbiting *interior* to a prograde stellar binary companion, tidal torques from the companion remove angular momentum from the outer disk and prevent it from expanding too far [262]. The tidal truncation radius roughly corresponds to the largest simple periodic orbit in the binary potential [260], which is at about 40% of the orbital separation for a binary with mass ratio $M_2/M_1 = 0.5$. The tidal torque is a function of radius, but to a first approximation one may assume that tides impose a rigid no-expansion condition at $r = r_{\mathrm{out}}$. From equation (53),

$$\left. \frac{\partial}{\partial r} \left(\nu \Sigma r^{1/2} \right) \right|_{r = r_{\mathrm{out}}} = 0. \tag{76}$$

This type of boundary condition may also be an appropriate approximation for a circumplanetary disk truncated by stellar tides [229].

The size of the disk (and even whether it is tidally truncated at all) will be different if the disk is substantially misaligned with respect to the orbital plane of the binary [214, 237].

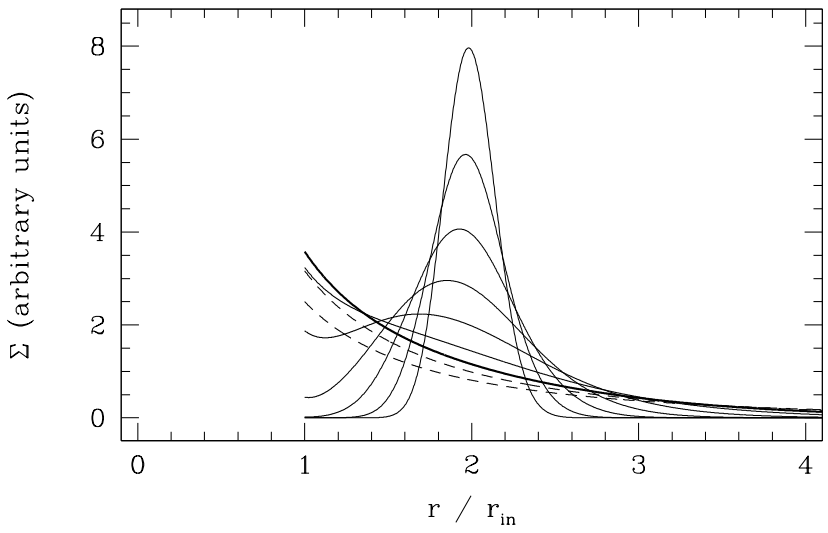

Fig. 10 The time-dependent analytic solution [277] to the disk evolution equation with a $v_r = 0$ boundary condition at $r = 1$ for the case $\nu = r$. The curves show the evolution of a ring of gas initially at $r = 2$, at times $t = 0.002$, $t = 0.004$, $t = 0.008$ etc. The bold curve is at $t = 0.128$, and dashed curves show later times. Gas initially accretes, but eventually *decretes* due to the torque being applied at the boundary.

An exterior *circumbinary* disk will also experience stellar gravitational torques, which in this case add angular momentum to the disk and slow viscous inflow. How best to model these torques is an open question, particularly in the case of extreme mass ratio binaries composed of a star and a massive planet. Pringle (1991) derived an illuminating analytic solution for circumbinary disk evolution [277], under the assumption that tidal torques *completely prevent* inflow past some radius $r = r_{\rm in}$. With this assumption the boundary condition at $r = r_{\rm in}$ is $v_r = 0$, and the task is to find a solution to equation (52) with this finite radius boundary condition. A simple solution is possible for $\nu = kr$, with k a constant. Defining scaled variables,

$$\begin{aligned} x &= r^{1/2} \\ \sigma &= \Sigma r^{3/2}, \end{aligned} \tag{77}$$

the $t > 0$ solution for an initial mass distribution,

$$\sigma(x, t = 0) = \sigma_0 \delta(x - x_1), \tag{78}$$

is [277],

$$\sigma = \frac{\sigma_0 t^{-1/2}}{4\left(3\pi k\right)^{1/2}} \left\{ \exp\left[-(x-x_1)^2/3kt\right] + \exp\left[-(x+x_1-2x_{\rm in})^2/3kt\right] \right\}. \tag{79}$$

The solution, plotted in Figure 10, can be compared to the zero-torque solution (Figure 8, though note this is for a constant viscosity). The initial evolution is similar, but at late times the torque which precludes inflow past $r_{\rm in}$ causes qualitatively different behavior. The disk switches from an accretion to a *decretion* disk, with an outward flow of mass driven by the binary torque.

Disks resembling the classical decretion disk solution may be realized under some circumstances, for example around rapidly rotating and strongly magnetized stars. Around binaries, however, it appears hard to completely shut off inflow. Numerical simulations show that angular momentum transfer to the disk co-exists with persistent inflow into a low density cavity containing the binary [20, 93]. How best to represent this complexity in a one-dimensional model is not entirely obvious.

3.3 Viscous heating

Although stellar irradiation is often the dominant source of heat for protoplanetary disks (§2.2), dissipation of gravitational potential energy associated with accretion is also important. Ignoring irradiation for the time being, we can derive the effective temperature profile of a steady-state viscous disk. In the regime where the classical equations are valid, the fluid dissipation per unit area is [276],

$$Q_+ = \frac{9}{4}\nu\Sigma\Omega^2. \tag{80}$$

Using the steady-state solution for $\nu\Sigma$ (equation 70), we equate Q_+ to the rate of local energy loss by radiation. If the disk is optically thick, the disk radiates (from both sides) at a rate $Q_- = 2\sigma T_{\rm disk}^4$, with σ being the Stefan-Boltzmann constant. This yields an effective temperature profile,

$$T_{\rm disk}^4 = \frac{3GM_*\dot{M}}{8\pi\sigma r^3}\left(1-\sqrt{\frac{R_*}{r}}\right). \tag{81}$$

Away from the inner boundary, the steady-state temperature profile for a viscous disk ($T_{\rm disk} \propto r^{-3/4}$) is steeper than for irradiation. For any accretion rate, we then expect viscous heating to be most important in the inner disk, whereas irradiation always wins out at sufficiently large radii.

The viscous disk temperature profile is **not** what we get from considering just the local dissipation of potential energy. The gradient of the potential energy per unit mass ε, is $\mathrm{d}\varepsilon/\mathrm{d}r = GM_*/r^2$. For an accretion rate $\dot{M}$, the luminosity available to be radiated from an annulus of width Δr due to local potential energy release would be,

$$L = \frac{1}{2}\frac{GM_*\dot{M}}{r^2}\Delta r, \tag{82}$$

where the factor of a half accounts for the fact that half the energy goes into increased kinetic energy, with only the remainder available to be thermalized and radiated. Equating this luminosity to the black body emission from the annulus, $2\sigma T_{\rm disk}^4 \cdot 2\pi r \Delta r$, would give a profile that is a factor three different from the asymptotic form of equation (81). The difference arises because the radial transport of angular momentum is accompanied by a radial transport of energy. The local luminosity from the disk surface at any radius then has a contribution from potential energy liberated closer in.

The optically thick regions of irradiated protoplanetary disks will be vertically isothermal. When viscous heating dominates, however, there must be a vertical temperature gradient to allow energy to be transported from the mid-plane toward the photosphere. What this gradient looks like, in detail, depends on the vertical distribution of the heating, which is not well known. However, an approximation to $T(z)$ can be derived assuming that the energy dissipation due to viscosity is strongly concentrated toward the mid-plane. We define the optical depth to the disk mid-plane,

$$\tau = \frac{1}{2}\kappa_R \Sigma, \tag{83}$$

where κ_R is the Rosseland mean opacity. The vertical density profile of the disk is $\rho(z)$. If the vertical energy transport occurs via radiative diffusion then for $\tau \gg 1$ the vertical energy flux $F(z)$ is given by the equation of radiative diffusion [299]

$$F_z(z) = -\frac{16\sigma T^3}{3\kappa_R \rho}\frac{{\rm d}T}{{\rm d}z}. \tag{84}$$

Now assume for simplicity that *all* of the dissipation occurs at $z = 0$. In that case $F_z(z) = \sigma T_{\rm disk}^4$ is constant with height. We integrate from the mid-plane to the photosphere at $z_{\rm ph}$ assuming that the opacity is also constant,

$$-\frac{16\sigma}{3\kappa_R}\int_{T_{\rm c}}^{T_{\rm disk}} T^3 dT = \sigma T_{\rm disk}^4 \int_0^{z_{\rm ph}} \rho(z')dz' \tag{85}$$

$$-\frac{16}{3\kappa_R}\left[\frac{T^4}{4}\right]_{T_{\rm c}}^{T_{\rm disk}} = T_{\rm disk}^4 \frac{\Sigma}{2}, \tag{86}$$

where the final equality relies on the fact that for $\tau \gg 1$ almost all of the disk gas lies below the photosphere. For large optical depth $T_{\rm c}^4 \gg T_{\rm disk}^4$ and the equation simplifies to,

$$\frac{T_{\rm c}^4}{T_{\rm disk}^4} \simeq \frac{3}{4}\tau. \tag{87}$$

Often *both* stellar irradiation and accretional heating contribute significantly to the thermal balance of the disk. If we define $T_{\rm disk,visc}$ to be the effective temperature that would result from viscous heating in the absence of irradiation (i.e. the quantity called $T_{\rm disk}$, with no subscript, above) and $T_{\rm irr}$ to be the irradiation-only effective temperature, then,

$$T_c^4 \simeq \frac{3}{4}\tau T_{\rm disk,visc}^4 + T_{\rm irr}^4 \tag{88}$$

is an approximation for the central temperature, again valid for $\tau \gg 1$.

These formulae can be applied to estimate the location of the snow line. In the Solar System, meteoritic evidence [238] places the transition between water vapor and water ice, which occurs at a mid-plane temperature of 150-180 K, at around 2.7 AU. This is substantially further from the Sun than would be expected if the only disk heating source was starlight. Including viscous heating, however, an accretion rate of $2 \times 10^{-8}\ M_\odot\ {\rm yr}^{-1}$ could sustain a mid-plane temperature of 170 K at 2.7 AU in a disk with $\Sigma = 400\ {\rm g\ cm}^{-2}$ and $\kappa_R = 1\ {\rm cm}^2\ {\rm g}^{-1}$. This estimate (from equation 87) is consistent with more detailed models for protoplanetary disks [49], though considerable variation in the location of the snow line is introduced by uncertainties in the vertical structure [227].

3.4 Warped disks

The classical equation for surface density evolution needs to be rethought if the disk is non-planar. Disks may be warped for several reasons; the direction of the angular momentum vector of the gas that forms the disk may not be constant, the disk may be perturbed tidally by a companion [192, 246], or warped due to interaction with the stellar magnetosphere [191].

A warp affects disk evolution through physics that is independent of its origin (for a brief review, see [245]). In a warped disk, neighboring annuli have specific angular momenta that differ in direction as well as in magnitude. If we define a unit tilt vector $\mathbf{l}(r,t)$ that is locally normal to the disk plane, the shear then has a vertical as well as a radial component [249],

$$\mathbf{S} = r\frac{{\rm d}\Omega}{{\rm d}r}\mathbf{l} + r\Omega\frac{\partial \mathbf{l}}{\partial r}. \tag{89}$$

The most important consequence of the vertical shear is that it introduces a periodic vertical displacement of radially separated fluid elements. As illustrated in Figure 11 this displacement, in turn, results in a horizontal pressure gradient that changes sign across the mid-plane and is periodic on the orbital frequency. In a Keplerian disk this forcing frequency is resonant with the epicyclic frequency.

How the disk responds to the warp-generated horizontal forcing depends on the strength of dissipation [263]. If the disk is sufficiently viscous, specifically if,

$$\alpha > \frac{h}{r}, \tag{90}$$

the additional shear is damped locally. The equation for the surface density and tilt evolution (the key aspects of which are derived in [278], though see [247] for a complete treatment) then includes terms which diffusively damp the warp at a rate

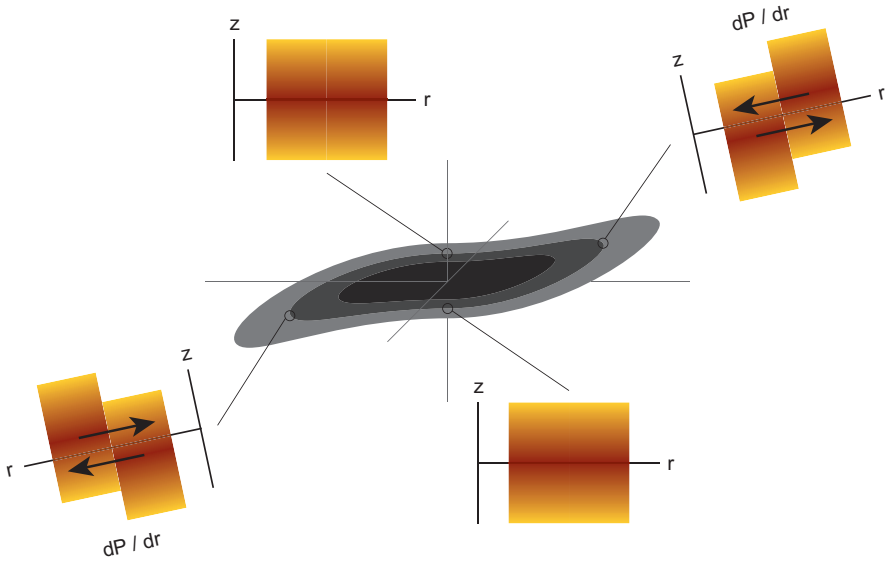

Fig. 11 Illustration (after [208, 245]) of how a warp introduces an oscillating *radial* pressure gradient within the disk. As fluid orbits in a warped disk, vertical shear displaces the mid-planes of neighboring annuli. This leads to a time-dependent radial pressure gradient $\mathrm{d}P/\mathrm{d}r(z)$. Much of the physics of warped disks is determined by how the disk responds to this warp-induced forcing.

that is related to the radial redistribution of angular momentum. Normally, warp damping is substantially faster than the viscous evolution of a planar disk. Even for a Navier-Stokes viscosity — which is fundamentally isotropic — the *effective* viscosity which damps the warp is a factor $\approx 1/2\alpha^2$ larger than its equivalent in a flat disk. Rapid evolution also occurs in the opposite limit of an almost inviscid disk with,

$$\alpha < \frac{h}{r}, \tag{91}$$

but in this case the component of angular momentum associated with the warp is communicated radially in the form of a wave. For a strictly inviscid disk the linearized fluid equations for the evolution of the tilt vector take a simple form [215],

$$\frac{\partial^2 \mathbf{l}}{\partial t^2} = \frac{1}{\Sigma r^3 \Omega} \frac{\partial}{\partial r} \left(\Sigma r^3 \Omega \frac{c_s^2}{4} \frac{\partial \mathbf{l}}{\partial r} \right). \tag{92}$$

The speed of the warp wave is $v_w \approx c_s/2$.

In most cases we expect protoplanetary disks to have $\alpha < h/r$, and warps will evolve in the wave-like regime. We expect, however, that the details of warp evolution will depend upon the nature of angular momentum transport, and

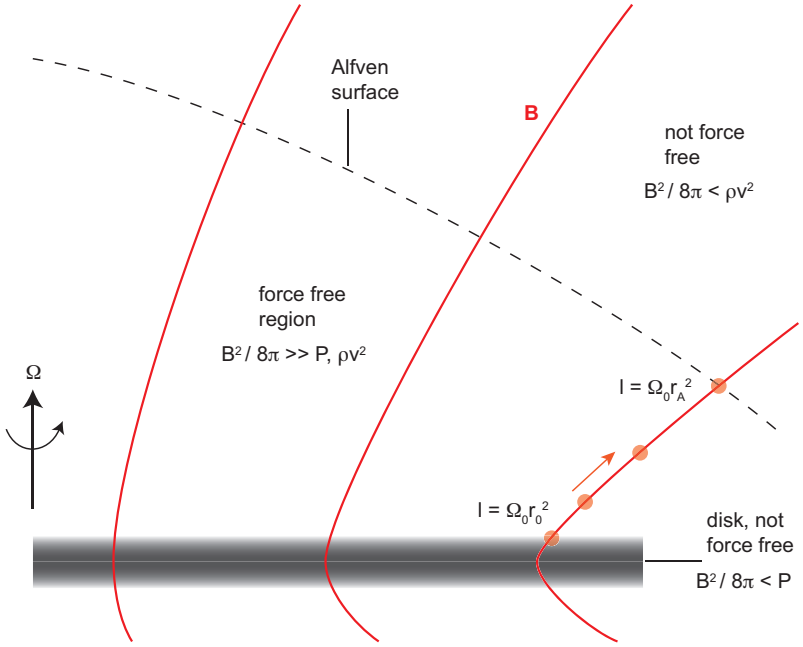

Fig. 12 Illustration, after Spruit [313], of the different regions of a disk wind solution.

nothing is known about how warps behave for the transport mechanisms (such as non-ideal MHD) most relevant to protoplanetary disks. The differences between warp evolution with realistic transport, and that with a Navier-Stokes viscosity, are of undetermined size.

3.5 Disk winds

Viscous evolution driven by redistribution of angular momentum is a consequence of turbulent (or possibly laminar) stresses that are internal to the fluid. Evolution can also be driven by external torques, the most important of which is the magnetic torque that an MHD wind exerts on the surface of the disk. An excellent pedagogical introduction to disk winds is the review by Spruit [313], while Königl & Salmeron [180] provide a more recent account that addresses the peculiarities specific to protoplanetary disks.

Winds that are driven solely by pressure gradients ("thermal winds") are of interest as a mechanism for disk dispersal (§8) but do not otherwise change the qualitative character of disk evolution. Instead, we consider here MHD winds, with the simplest case being a well-ionized disk is threaded by a large-scale ordered poloidal

magnetic field [57]. In the ideal MHD limit the fluid is tied to magnetic field lines, which can facilitate acceleration of the wind while exerting a back reaction on the disk that removes angular momentum.

Blandford-Payne winds are not the only type of MHD outflow of interest for protoplanetary disk systems. Outflows could be launched by a gradient of *toroidal* magnetic field pressure [218], perhaps during or shortly after the collapse of the cloud that forms both the star and the disk. Jets can also originate from the interaction between the stellar magnetosphere and the disk [305].

The structure of such a wind, illustrated in Figure 12, generically has three regions. Within the disk the energy density in the magnetic field, $B^2/8\pi$, is smaller than ρc_s^2, the thermal energy[3]. Due to flux conservation, however, the energy in the vertical field component, $B_z^2/8\pi$, is roughly constant with height for $z < r$, while the gas pressure typically decreases at least exponentially with a scale height $h \ll r$. This leads to a region above the disk surface where magnetic forces dominate. The magnetic force per unit volume is,

$$\frac{\mathbf{J}\times\mathbf{B}}{c} = -\nabla\left(\frac{B^2}{8\pi}\right) + \frac{\mathbf{B}\cdot\nabla\mathbf{B}}{4\pi}, \tag{93}$$

where the current,

$$\mathbf{J} = \frac{c}{4\pi}\nabla\times\mathbf{B}. \tag{94}$$

The force, in general, can be written as shown above as the sum of a magnetic pressure gradient and a force due to magnetic tension. In the disk wind region where magnetic forces dominate, the requirement that they exert a finite acceleration on the low density gas implies that the force approximately vanishes, i.e. that,

$$\mathbf{J}\times\mathbf{B} \approx 0. \tag{95}$$

The structure of the magnetic field in the magnetically dominated region is then described as being "force-free", and in the disk wind case (where B changes slowly with z) the field lines must be approximately straight to ensure that the magnetic tension term is also individually small. If the field lines support a wind, the force-free structure persists up to where the kinetic energy density in the wind, ρv^2, first exceed the magnetic energy density. This is called the Alfvén surface. Beyond the Alfvén surface, the inertia of the gas in the wind is sufficient to bend the field lines, which tend to wrap up into a spiral structure as the disk below them rotates.

Magneto-centrifugal driving can launch a wind from the surface of a cold gas disk if the magnetic field are sufficiently inclined to the disk normal. The critical inclination angle in ideal MHD can be derived via an *exact* mechanical analogy. To

[3] We can also consider situations where the magnetic pressure in the disk is stronger than the gas pressure, though it must always be weaker than ρv_ϕ^2.

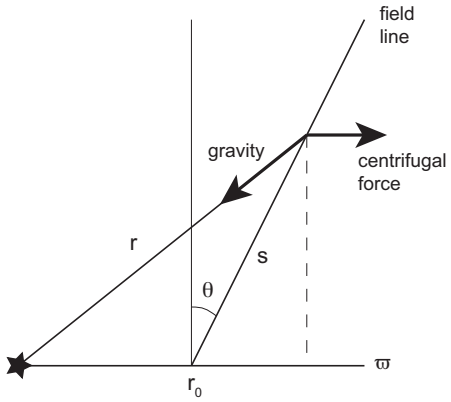

Fig. 13 Geometry for the calculation of the critical angle for magneto-centrifugal wind launching. A magnetic field line **s**, inclined at angle θ from the disk normal, enforces rigid rotation at the angular velocity of the foot point, at cylindrical radius $\varpi = r_0$ in the disk. Working in the rotating frame we consider the balance between centrifugal force and gravity.

proceed, we note that in the force-free region the magnetic field lines are (i) basically straight lines, and (ii) enforce rigid rotation out to the Alfvén surface at an angular velocity equal to that of the disk at the field line's footpoint. The geometry is shown in Figure 13. We consider a field line that intersects the disk at radius r_0, where the angular velocity is $\Omega_0 = \sqrt{GM_*/r_0^3}$, and that makes an angle θ to the disk normal. We define the spherical polar radius r, the cylindrical polar radius ϖ, and measure the distance along the field line from its intersection with the disk at $z = 0$ as s. In the frame co-rotating with Ω_0 there are no magnetic forces along the field line to affect the acceleration of a wind; the sole role of the magnetic field is to constrain the gas to move along a straight line at constant angular velocity. Following this line of argument, the acceleration of a wind can be fully described in terms of an effective potential,

$$\Phi_{\rm eff}(s) = -\frac{GM_*}{r(s)} - \frac{1}{2}\Omega_0^2 \varpi^2(s). \tag{96}$$

The first term is the gravitational potential, while the second describes the centrifugal potential in the rotating frame.

Written out explicitly, the effective potential is,

$$\Phi_{\rm eff}(s) = -\frac{GM_*}{(s^2 + 2sr_0\sin\theta + r_0^2)^{1/2}} - \frac{1}{2}\Omega_0^2 \left(r_0 + s\sin\theta\right)^2. \tag{97}$$

This function is plotted in Figure 14 for various values of the angle θ. For a vertical field line ($\theta = 0$) the effective potential is a monotonically increasing function of distance s, for modest values of θ there is a potential barrier defined by a maximum at some $s = s_{\rm max}$, while for large enough θ the potential decreases from $s = 0$. In this last case purely magneto-centrifugal forces suffice to accelerate a wind off the disk

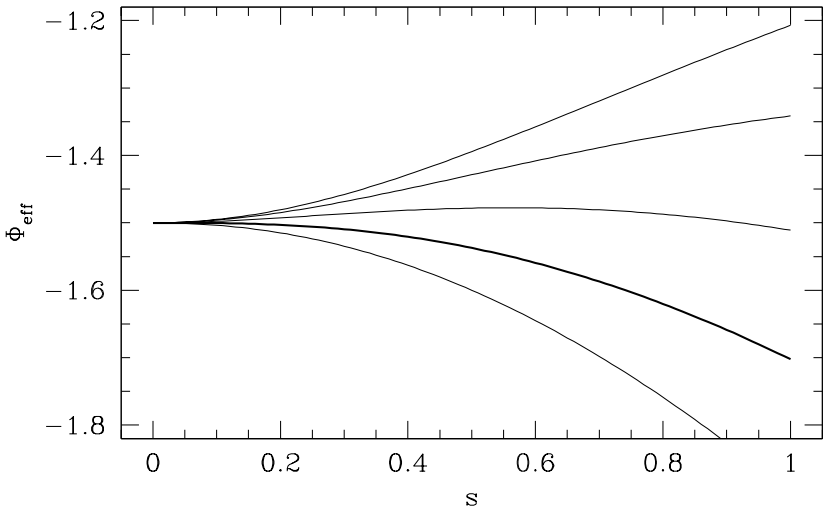

Fig. 14 The variation of the disk wind effective potential $\Phi_{\rm eff}$ (in arbitrary units) with distance s along a field line. From top downwards, the curves show field lines inclined at 0°, 10°, 20°, 30° (in bold) and 40° from the normal to the disk surface. For angles of 30° and more from the vertical, there is no potential barrier to launching a cold MHD wind directly from the disk surface.

surface, even in the absence of any thermal effects. The critical inclination angle of the field can be found by computing $\theta_{\rm crit}$, specified though the condition,

$$\left.\frac{\partial^2 \Phi_{\rm eff}}{\partial s^2}\right|_{s=0} = 0. \tag{98}$$

Evaluating this condition, we find,

$$\begin{aligned} 1 - 4\sin^2\theta_{\rm crit} &= 0 \\ \Rightarrow \theta_{\rm crit} &= 30^\circ, \end{aligned} \tag{99}$$

as the minimum inclination angle from the vertical needed for unimpeded wind launching in ideal MHD [57]. Since most of us are more familiar with mechanical rather than magnetic forces, this derivation in the rotating frame offers the easiest route to this result. But it can, of course, be derived just as well by working in the inertial frame of reference [313].

The rigid rotation of the field lines interior to the Alfvén surface means that gas being accelerated along them increases its specific angular momentum. The magnetic field, in turn, applies a torque to the disk that removes a corresponding amount of angular momentum. If a field line, anchored to the disk at radius r_0, crosses the Alfvén surface at (cylindrical) radius r_A, it follows that the angular momentum flux is,

$$\dot{L}_w = \dot{M}_w \Omega_0 r_A^2, \tag{100}$$

where $\dot{M}_w$ is the mass loss rate in the wind. Removing angular momentum at this rate from the disk results in a local accretion rate $\dot{M} = 2\dot{L}_w/\Omega_0 r_0^2$. The ratio of the disk accretion rate to the wind loss rate is,

$$\frac{\dot{M}}{\dot{M}_w} = 2\left(\frac{r_A}{r_0}\right)^2. \tag{101}$$

If r_A substantially exceeds r_0 (by a factor of a few, which is reasonable for detailed disk wind solutions) a relatively weak wind can carry away enough angular momentum to support a much larger accretion rate.

The behavior of a disk that evolves under wind angular momentum loss depends on how the wind and the poloidal magnetic field respond to the induced accretion. It is not immediately obvious that a steady accretion flow is even possible. The form of the effective potential (Figure 14) suggests that the rate of mass and angular momentum loss in the wind ought to be a strong function of the inclination of the field lines — for $\theta < 30^\circ$ there is a potential barrier to wind launching, while for $\theta \geq 30^\circ$ there is no barrier at all. How θ responds to changes in the inflow rate through the disk is of critical importance [217, 66, 250], and there is no simple analog of the diffusive disk evolution equation.

Irrespective of the (uncertain) details, viscous and wind-driven disks exhibit some qualitative difference that may enable observational tests. The classical test is the evolution of the outer disk radius, which expands in viscous models (*if* there is no mass loss, even in the form of a thermal wind) but contracts if an MHD wind dominates. Old and almost forgotten observations [312] of disk radius changes in dwarf novae (accreting white dwarfs in mass transfer binary systems) provided empirical support for viscous disk evolution *in those specific systems*. Disk winds also remove energy, and so another potential test is to look for evidence of the dissipation of accretion energy within the disk that is present in viscous models but absent for winds.

3.5.1 Magnetic field transport

The strength and radial profile of the vertical magnetic field threading the disk are important quantities for disk winds, and for turbulence driven by MHD processes. Disks form from the collapse of magnetized molecular clouds, and it is inevitable that they will inherit non-zero flux at the time of formation. The poloidal component of that flux can subsequently be advected radially with the disk gas, diffuse relative to the gas, or (if the flux has varying sign across the disk) reconnect.

A theory for the radial transport of poloidal flux within geometrically thin accretion disks was developed by Lubow, Papaloizou & Pringle (1994) [216]. They

considered a disk within which turbulence generates an effective viscosity ν and an effective magnetic diffusivity η. The disk is threaded by a vertical magnetic field $B_z(r,t)$, which is supported by a combination of currents within the disk and (potentially) a current external to the disk. Above the disk, as in Figure 12 the field is force-free. The field lines bend within the disk, such that the poloidal field has a radial component $B_{rs}(r,t)$ at the disk surface.

To proceed (following the notation in [134]), we first write the poloidal field in terms of a magnetic flux function ψ, such that $\mathbf{B} = \nabla\psi \times \mathbf{e}_\phi$, where $\mathbf{e}_\phi$ is a unit vector in the azimuthal directions. The components of the field are,

$$B_r = -\frac{1}{r}\frac{\partial\psi}{\partial z},$$
$$B_z = \frac{1}{r}\frac{\partial\psi}{\partial r}. \tag{102}$$

From the second of these relations we note that ψ is (up to a factor of 2π) just the vertical magnetic flux interior to radius r. We split ψ into two pieces, a piece $\psi_{\rm disk}$ due to currents within the disk, and a piece ψ_∞ due to external currents ("at infinity"),

$$\psi = \psi_{\rm disk} + \psi_\infty. \tag{103}$$

The external current generates a magnetic field that is uniform across the disk.

With these definitions, the evolution of the poloidal field in the simplest analysis [216, 134] obeys,

$$\frac{\partial\psi}{\partial t} + r\left(v_{\rm adv}B_z + v_{\rm diff}B_{rs}\right) = 0, \tag{104}$$

where $v_{\rm adv}$ is the advective velocity of magnetic flux and $v_{\rm diff}$ its diffusive velocity due to the turbulent resistivity within the disk. The disk component of the flux function is related to the surface radial field via an integral over the disk. Schematically,

$$\psi_{\rm disk}(r) = \int_{r_{\rm in}}^{r_{\rm out}} F(r,r')B_{rs}(r'){\rm d}r', \tag{105}$$

where F is a rather complex function that can be found in Guilet & Ogilvie (2014) [134]. The appearance of this integral reflects the inherently global nature of the problem — a current at some radius within the disk affects the poloidal magnetic field everywhere, not just locally — and makes analytic or numerical solutions for flux evolution more difficult. Nonetheless, equation (105) can be inverted to find B_{rs} from ψ, after which the more familiar equation (104) can be solved for specified transport velocities to determine the flux evolution.

Equation (104) expresses a simple competition, the inflow of gas toward the star will tend to drag in poloidal magnetic field, but this will set up a radial gradient and be opposed by diffusion. The physical insight of Lubow et al. (1994) [216] was to note that although both of these are processes involving turbulence (and, very roughly, we might guess that $\nu \sim \eta$), the scales are quite distinct. From Figure 12, we note that because the field lines bend *within the disk*, a moderately inclined

external field (with $B_{rs} \sim B_z$) above the disk only has to diffuse across a scale $\sim h$ to reconnect with its oppositely directed counterpart below the disk. Dragging in the field with the mean disk flow, however, requires angular momentum transport across a larger scale r. In terms of transport velocities, in a steady-state we have,

$$\begin{aligned} v_{\rm adv} &\sim \frac{\nu}{r}, \\ v_{\rm diff} &\sim \frac{\eta}{h}\frac{B_{\rm rs}}{B_z}, \end{aligned} \tag{106}$$

so that for $\nu \sim \eta$ and $B_{rs} \sim B_z$ diffusion beats advection by a factor $\sim (h/r)^{-1} \gg 1$. Defining the magnetic Prandtl number $P_m = \nu/\eta$ as the ratio of the turbulent viscosity to the turbulent resistivity, we would then expect that in steady-state [216],

$$\frac{B_{rs}}{B_z} \sim \frac{h}{r} P_m. \tag{107}$$

This argument is the origin of the claim that *thin disks do not drag in external magnetic fields*. It suggests that obtaining enough field line bending to launch a magneto-centrifugal wind ought to be hard, and that whatever primordial flux the disk is born with may be able to escape easily.

The physical arguments given above are robust, but a number of authors have emphasized that the calculation of the transport velocities that enter into equation (104) involves some subtleties [250, 213, 133, 134, 323]. The key point is that the viscosity and resistivity that enter into the equation for flux transport should not be computed as density-weighted vertical averages, but rather (in the case of the induction equation) as conductivity-weighted averages [133]. This makes a large difference for protoplanetary disks, where the conductivity is both generally low, and highest near the disk surface where the density is small. The derived transport velocities are, moreover, functions of the poloidal field strength, in the sense that diffusion becomes relatively less efficient as the field strength decreases. It should be noted that none of the flux transport calculations fully includes all of the MHD effects expected to be present in protoplanetary disks (see §4.4.3). It seems possible, though, that the variable efficiency of flux diffusion could simultaneously allow,

- For rapid flux loss from the relatively strongly magnetized disks formed from star formation [203], averting overly rapid wind angular momentum loss that would be inconsistent with observed disk lifetimes.
- For convergence toward a weak but non-zero net poloidal flux (possibly with a ratio of thermal to poloidal field magnetic pressure at the mid-plane $\beta \sim 10^4 - 10^7$) later in the disk lifetime [134].

As we will discuss in the next section, poloidal field strengths in roughly this range are of interest for their role in stimulating MHD instabilities within weakly ionized disks, so this is a speculative but interesting scenario.

4 Turbulence

Turbulence within protoplanetary disks is important for two independent reasons. First, if it is strong enough and has the right properties, it could account for disk evolution by redistributing angular momentum much faster than molecular viscosity. Second, turbulence has its fingers in a plethora of planet formation processes, ranging from the collision velocities of small particles [253] to the formation of planetesimals [160] and the migration rate of low-mass planets [177]. For these reasons we would like to understand disk turbulence, even if (as is possible) it is not always responsible for disk evolution.

The first order of business when considering possibly turbulent fluid systems is usually to estimate the Reynolds number, which is a dimensionless measure of the relative importance of inertial and viscous forces. For a system with characteristic size L, velocity U, and (molecular) viscosity ν, the Reynolds number is defined,

$$\mathrm{Re} = \frac{UL}{\nu}. \tag{108}$$

There is no unique or "best" definition of U and L for protoplanetary disks, but whatever choice we make gives a very large number. For example, taking $L = h$ and $U = c_s$ then our estimate of the viscosity at 1 AU (equation 62) implies $\mathrm{Re} \sim 10^{11}$. By terrestrial standards this is an enormous Reynolds number. Experiments on flow through pipes, for example — including those of Osborne Reynolds himself — show that turbulence is invariably present once $\mathrm{Re} > 10^4$ [98]. If turbulence is present within protoplanetary disks, there is no doubt that viscous forces will be negligible on large scales, and the turbulence will exhibit a broad inertial range.

Figure 15 lists some of the possible sources of turbulence within protoplanetary disks. It's a long list! We can categorize the candidates according to various criteria,

- The physics involved in generating the turbulence. The simplest possibility (which appears unlikely) is that turbulence develops spontaneously in an isothermal, purely hydrodynamical shear flow. More complete physical models invoke entropy gradients, disk self-gravity or magnetic fields as necessary elements for the origin of turbulence.
- The origin of the free energy that sustains the turbulence, which could be the radial or vertical shear, heating from the star, or velocity differences between gas and solid particles.
- The character of the instabilities proposed to initiate turbulence from an initially non-turbulent flow. *Linear* instabilities grow exponentially from arbitrarily small perturbations, while *non-linear* instabilities require a finite amplitude disturbance. Demonstrating the existence of linear instabilities is relatively easy, whereas proving that a fluid system is non-linearly stable is very hard.
- The species involved. In this section we concentrate on instabilities present in purely gaseous disks; additional instabilities are present once we consider how gas interacts aerodynamically with its embedded solid component (§6.3).

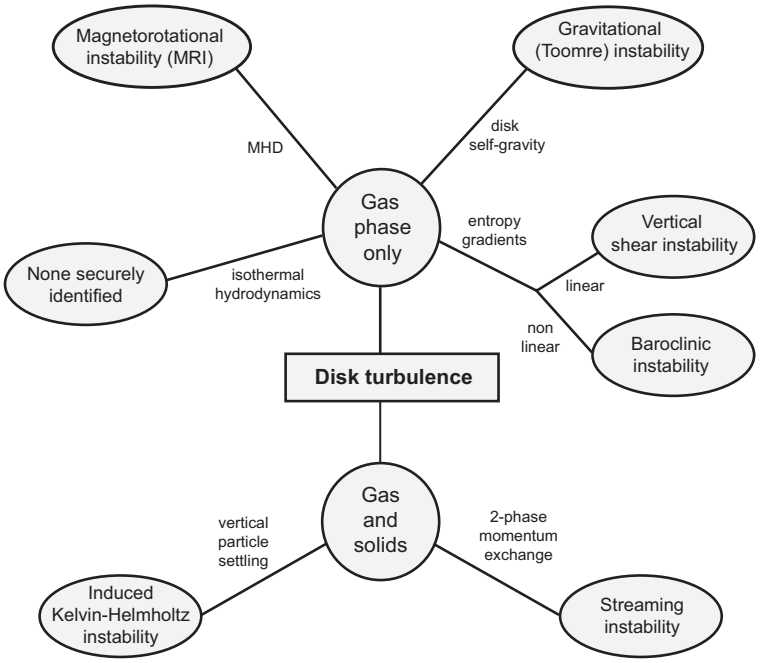

Fig. 15 A menu of the leading suspects for creating turbulence within protoplanetary disks.

Figure 16 illustrates the dominant fluid motions or forces involved in some of the most important disk instabilities.

For each candidate instability we would like to know the disk conditions under which it would be present, its growth rate, and the strength and nature of the turbulence that eventually develops. For disk evolution we are particularly interested in how efficiently the turbulence transports angular momentum (normally characterized by an effective α). In most cases the efficiency of transport can only be determined using numerical simulations, whose fluctuating velocity and magnetic fields can be analyzed to determine α via the relation [38],

$$\alpha = \left\langle \frac{\delta v_r \delta v_\phi}{c_s^2} - \frac{B_r B_\phi}{4\pi\rho c_s^2} \right\rangle_\rho , \tag{109}$$

where the angle brackets denote a density weighted average over space (and time, in some instances). The first term in this expression is the Reynolds stress from correlated fluctuations in the radial and perturbed azimuthal velocity, the second term in the Maxwell stress from MHD turbulence. We speak of the stress as being "turbulent" if the averages in the above relation are dominated by contributions from small spatial scales. It is also possible for a disk to sustain large scale stresses — for example at some radius we might have non-zero *mean* radial and azimuthal magnetic fields — which are normally described as being "laminar".

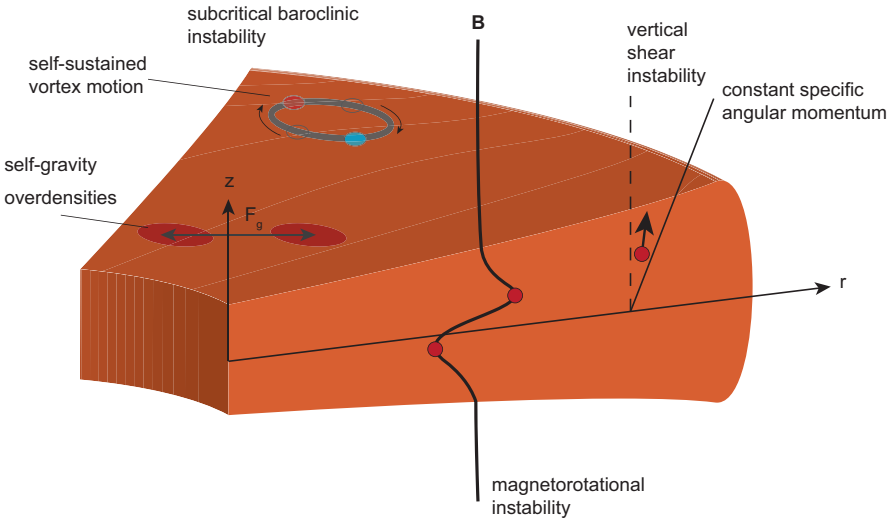

Fig. 16 A summary of the most important instabilities that can be present in protoplanetary disks. *Self-gravity* is important for sufficiently massive and cold disks. It leads to spiral arms and gravitational torques between regions of over-density. The *magnetorotational instability* occurs whenever a weak magnetic field is sufficiently coupled to differential rotation. The magnetic field acts to couple fluid elements at different radii, leading to an instability that can sustain MHD turbulence and angular momentum transport. The *vertical shear instability* feeds off the vertical shear that is set up in disks with realistic temperature profiles. It is a linear instability characterized by near-vertical growing modes. The *subcritical baroclinic instability* is a non-linear instability that operates in the presence of a sufficiently steep radial entropy gradient. It resembles radial convection, and leads to self-sustained vortices within the disk.

4.1 Hydrodynamic turbulence

The dominant motion in protoplanetary disks is Keplerian orbital motion about a central point mass. Simplifying as much as possible, we first ask whether, in the absence of magnetic fields[4], the radial shear present in a low-mass disk would be unstable to the development of turbulence. We first consider (rather unrealistically) a radially isothermal disk, where according to equation (17) there is no *vertical* shear. We then turn to the more general case where the temperature varies with radius, giving rise both to vertical shear and qualitatively distinct possibilities for instability.

[4] Ignoring magnetic fields in astrophysical accretion flows is generally a stupid thing to do, and indeed there is broad consensus that the magnetorotational instability (MRI) [38] is responsible for turbulence and angular momentum transport in most accretion disks. In protoplanetary disks, however, the low ionization fraction means that the dominance of MHD instabilities is much less obvious, and purely hydrodynamic effects could in principle be important.

4.1.1 Linear and non-linear stability

The linear stability of a shear flow with a smoothly varying $\Omega(r)$ against axisymmetric perturbations is given by Rayleigh's criterion (this is derived in most fluids textbooks, see e.g. [279]). The flow is stable if the specific angular momentum increases with radius,

$$\frac{\mathrm{d}l}{\mathrm{d}r} = \frac{\mathrm{d}}{\mathrm{d}r}\left(r^2\Omega\right) > 0 \rightarrow \text{stability}. \tag{110}$$

A Keplerian disk has $l \propto \sqrt{r}$ and is linearly stable.

There is no mathematical proof of the non-linear stability of Keplerian shear flow, but nor is there any known instability. The apparently analogous cases of pipe flow and Cartesian shear flows — which are linearly stable but undergo non-linear transitions to turbulence — are in fact sufficiently different problems as to offer no guidance [38]. There are analytic and numerical arguments against the existence of non-linear instabilities [39], which although not decisive [287] essentially rule out the hypothesis that a non-linear instability could result in *astrophysically interesting* levels of turbulence [196]. The same conclusion follows from laboratory experiments that have studied the stability of quasi-Keplerian rotation profiles in Taylor-Couette experiments [99].

Laboratory experiments, and most theoretical work, consider the stability of unstratified cylindrical shear flows. It has been suggested that new instabilities (of a distinct character, related to the existence of locations in the flow known as critical layers, for a review see [231]) arise when the vertical stratification present in disks is included [225]. Study of this possibility remains in its infancy.

4.1.2 Entropy-driven instabilities

A separate class of purely hydrodynamic instabilities (no self-gravity, no magnetic fields) are what might loosely be called "entropy-driven" instabilities, in that they rely on the existence of a non-trivial temperature structure. The prototypical entropy-driven instability is of course convection, which could occur in the vertical direction if dissipation (associated with the physical process behind angular momentum transport) sets up an unstable entropy profile. This is evidently only conceivable in the region where viscous dissipation dominates, as irradiation prefers a nearly isothermal vertical structure. Even there, convective turbulence in disks is less efficient at transporting angular momentum than it is in transporting heat [197], and this disparity creates a formidable barrier to creating consistent models in which convection is the primary source of disk turbulence. Convection may still be present in some regions of disks, perhaps especially at high accretion rates, but as a byprod-

uct of independent angular momentum transport processes (for an example in dwarf novae, see [149]).

A disk that has a radial temperature gradient necessarily has vertical shear (equation 17). The free energy associated with the vertical shear can be accessed via the vertical shear instability (VSI) analyzed by Nelson, Gressel & Umurhan (2013) [243]. The VSI is a disk application of the Goldreich-Schubert-Fricke instability [126, 112] of rotating stars, and was proposed as a source of protoplanetary disk transport by Urpin & Brandenburg [338][5]. The VSI is a linear instability with a maximum growth rate that is of the order of $h\Omega_{\rm K}$ [206], but which is strongly dependent on the radiative properties of the disk. The reason is that to access the free energy in the vertical shear requires vertical fluid displacements, which are easy in the limit that the disk is strictly vertically isothermal but strongly suppressed if it is stably stratified. The local *cooling time* of the fluid is thus a critical parameter, and the VSI will only operate in regions of the disk where radiative cooling and heating processes result in a cooling time that is the same or shorter than the dynamical time $\Omega_{\rm K}^{-1}$. This, in practice, restricts the application of the VSI to intermediate radii (Lin & Youdin suggest 5-50 AU [206]), and limits its effectiveness if the dust opacity is reduced (due to coagulation into large particles). Under the right conditions, however, numerical simulations suggest that the VSI can generate relatively small but possibly significant levels of transport, with both Nelson et al. [243] and Stoll & Kley [318] finding α of a few $\times 10^{-4}$.

The radial entropy gradient may itself be unstable. The simplest instability would be radial convection (a linear instability). For a disk with pressure profile $P(r)$, density profile $\rho(r)$, and adiabatic index γ, we define the Brunt-Väisälä frequency,

$$N_r^2 = -\frac{1}{\gamma\rho}\frac{{\rm d}P}{{\rm d}r}\frac{\rm d}{{\rm d}r}\ln\left(\frac{P}{\rho^\gamma}\right). \tag{111}$$

The Solberg-Hoïland criterion indicates that a Keplerian disk is convectively unstable if,

$$N_r^2 + \Omega_{\rm K}^2 < 0. \tag{112}$$

Protoplanetary disks never (or at least almost never) have a steep enough profile of entropy to meet this condition, so radial convection will not set in. A different instability (the subcritical baroclinic instability, SBI) is possible, however, if the weaker condition $N_r^2 < 0$ (which is just the Schwarzschild condition for non-rotating convection) is satisfied [268, 269, 199]. The SBI, which is likely related to observations of vortex formation in earlier numerical simulations [175], is a non-linear instability that can be excited by finite amplitude perturbations. (Confusingly, it is unrelated to the linear "baroclinic instability" studied in planetary atmospheres.) The SBI relies on radial buoyancy forces to sustain vortical motion via baroclinic driving. This type of effect is possible in disks in which surfaces of constant density are not parallel to surface of constant pressure. Mathematically, for a fluid with vorticity $\boldsymbol{\omega} = \nabla \times \mathbf{v}$, we can take the curl of the momentum equation to get an equation for the vortensity

[5] As we shall see, a general rule is that all disk instabilities have long histories and pre-histories.

ω/ρ,

$$\frac{\mathrm{D}}{\mathrm{D}t}\left(\frac{\omega}{\rho}\right) = \left(\frac{\omega}{\rho}\right)\cdot\nabla\mathbf{v} - \frac{1}{\rho}\nabla\left(\frac{1}{\rho}\right)\times\nabla P. \tag{113}$$

The baroclinic term, which for the SBI is responsible for generating and maintaining vorticity in the presence of dissipation, is the second term on the right hand side. The SBI, as with the VSI, is sensitive to the cooling time [199, 283], in this case because the baroclinic driving depends on the disk neither cooling too fast (which would eliminate the buoyancy effect) nor too slow (which would lead to constant temperature around the vortex). In compressible simulations, Lesur & Papaloizou (2010) [199] found that under favorable disk conditions the SBI could lead to outward transport of angular momentum with $\alpha \sim 10^{-3}$.

4.2 Self-gravity

A disk is described as *self-gravitating* if it is unstable to the growth of surface density perturbations when the gravitational force between different fluid elements in the disk is included along with the force from the central star. For a disk with sound speed c_s, surface density Σ and angular velocity Ω (assumed to be *close* to Keplerian) a linear analysis (for textbook treatments, see e.g. [14, 279]) shows that a disk becomes self-gravitating when the Toomre Q [328],

$$Q \equiv \frac{c_s\Omega}{\pi G\Sigma} < Q_{\rm crit}, \tag{114}$$

where $Q_{\rm crit} \sim 1$. We can deduce this result informally using an extension of the time scale argument that gives the thermal Jeans mass. We first note that pressure will prevent the gravitational collapse of a clump of gas, on scale Δr, if the sound-crossing time $\Delta r/c_s$ is shorter than the free-fall time $\sqrt{\Delta r^3/G\Delta r^2\Sigma}$. (We're ignoring factors of 2, π and so on.) Equating these time scales gives the minimum scale that might be vulnerable to collapse as $\Delta r \sim c_s^2/G\Sigma$. On larger scales, collapse can be averted if the free-fall time is longer than the time scale on which radial shear will separate initially neighboring fluid elements. For a Keplerian disk, this time scale is $\sim \Omega^{-1}$. If the disk is just on the edge of instability, the minimum collapse scale set by pressure support must equal the maximum collapse scale set by shear. Imposing this condition for marginal stability we obtain $c_s\Omega/G\Sigma \sim 1$, in accord with the formal result quoted above.

To glean some qualitative insight into where a disk might be self-gravitating, consider a steady-state disk that is described by an α model in which the transport arises from some process *other* than self-gravity. Collecting some previous results, the steady-state condition implies $\nu\Sigma = \dot{M}/3\pi$, the α prescription is $\nu = \alpha c_s h$, and hydrostatic equilibrium gives $h = c_s/\Omega$. Substituting into equation (114) we find,

$$Q = \frac{3\alpha c_s^3}{G\dot{M}}. \tag{115}$$

Protoplanetary disks generically get colder (and hence have lower c_s) at larger distances from the star, and this is where self-gravity is most likely to be important.

The disk mass required for self-gravity to become important can be estimated. Ignoring radial gradients of all quantities, we write the disk mass $M_{\rm disk} \sim \pi r^2 \Sigma$, and again use the hydrostatic equilibrium result $h = c_s/\Omega$. Equation (114) then gives,

$$\frac{M_{\rm disk}}{M_*} > \left(\frac{h}{r}\right), \tag{116}$$

as the condition for instability. This manipulation of a local stability criterion into some sort of global condition is ugly, and begs the question of *where* in the disk $M_{\rm disk}$ and h/r should be evaluated. We can safely conclude, nonetheless, that for a typical protoplanetary disk with $(h/r) \simeq 0.05$ a disk mass of $10^{-2}\ M_*$ will not be self-gravitating, whereas one with $0.1\ M_*$ may well be.

There are two possibles outcomes of self-gravity in a disk,

- The disk may establish a (quasi) stable state, characterized globally by trailing spiral overdensities. Gravitational torques between different annuli in the disk transport angular momentum outward, leading to accretion.
- The pressure and tidal forces, which by definition are unable to prevent the onset of gravitational collapse, may never be able to stop it once it starts. In this case the disk fragments into bound objects, which interact with (and possibly accrete) the remaining gas.

Both possibilities are of interest. Angular momentum transport due to self-gravity may be dominant, at least on large scales, at early times while the disk is still massive. Fragmentation, which was once considered a plausible mechanism for forming the Solar System's giant planets [186], remains of interest as a way to form sub-stellar objects and (perhaps) very massive planets. We will look at both in turn.

Gravity is a long-range force, and it is not at all obvious that we can deploy the machinery developed for viscous disks to study angular momentum transport in a self-gravitating disk. The transport could be largely non-local, driven for example by large-scale structures in the density field (such as bars) or by waves that transport energy and angular momentum a significant distance before dissipating [40]. There is no precise criterion for when self-gravitating transport can be described using a local theory, but numerical simulations indicate that this is a reasonable approximation for low-mass disks with $M_{\rm disk}/M_* \approx 0.1$ [209, 86, 109, 314]. Transport in more massive disks, such as might be present during the Class 0 and Class I phases of star formation, cannot be described locally (for multiple reasons, e.g. [210, 331]).

Assuming that a local description of the transport is valid, we can use a thermal balance argument to relate the efficiency of angular momentum transport to the cooling time. Adopting a one-zone model for the vertical structure, we define the thermal energy of the disk, per unit surface area, as,

$$U = \frac{c_s^2 \Sigma}{\gamma(\gamma-1)}, \tag{117}$$

where c_s is the mid-plane sound speed and γ is the adiabatic index. The cooling time (analogous to the Kelvin-Helmholtz time for a star) is then,

$$t_{\rm cool} = \frac{U}{2\sigma T_{\rm disk}^4}, \tag{118}$$

where $T_{\rm disk}$ is the effective temperature. Equating the cooling rate, $Q_- = 2\sigma T_{\rm disk}^4$, to the local viscous heating rate, $Q+ = (9/4)\nu\Sigma\Omega^2$ (equation 80), and adopting the α-prescription (equation 65), we find,

$$\alpha = \frac{4}{9\gamma(\gamma-1)}\frac{1}{\Omega t_{\rm cool}}. \tag{119}$$

This relation, which is a general property of α disks quite independent of self-gravity, just says that a rapidly cooling disk needs efficient angular momentum transport if it to generate heat fast enough to remain in thermal equilibrium.

For most sources of angular momentum transport we are no more able to determine $t_{\rm cool}$ from first principles than we are α, so the above relation does not move us forward. Self-gravitating disks, however, have the unusual property that their Toomre Q, measured in the *saturated* (non-linear) state, is roughly constant and similar to the critical value $Q_{\rm crit}$ determined from *linear* theory. This property arises, roughly speaking, because the direct dependence of the linear stability criterion on temperature (via c_s) invites a stabilizing feedback loop — a disk that cools so that $Q < Q_{\rm crit}$ is more strongly self-gravitating, and produces more heating, while one that heats so that $Q > Q_{\rm crit}$ shuts off the instability. It is therefore reasonable to assume that a self-gravitating disk that does not fragment maintains itself close to marginal stability, as conjectured by Paczynski (1978) [261].

If we assume that $Q = Q_0$ exactly (where Q_0 is some constant presumably close to $Q_{\rm crit}$) then we have enough constraints to explicitly determine the functional form of α for a self-gravitating disk. Since Q depends on the mid-plane sound speed, $c_s = \sqrt{k_B T_c/\mu m_H}$, the condition of marginal stability directly gives us $T_c(\Sigma,\Omega)$,

$$T_c = \pi^2 Q_0^2 G^2 \left(\frac{\mu m_H}{k_B}\right)\frac{\Sigma^2}{\Omega^2}. \tag{120}$$

We can use this to determine $t_{\rm cool}$, and from that α, with the aid of the vertical structure relations developed in §3.3. To keep things simple, we adopt an opacity,

$$\kappa_R = \kappa_0 T_c^2 \tag{121}$$

that is appropriate for ice grains, and assume the disk is optically thick. The opacity law, together with the relations for the optical depth, $\tau = (1/2)\Sigma\kappa_R$, and the mid-plane temperature, $T_c^4/T_{\rm disk}^4 \simeq (3/4)\tau$, then leads to,

$$\alpha = \frac{64\pi^2 Q_0^2 G^2 \sigma}{27\kappa_0}\left(\frac{\mu m_H}{k_B}\right)^2 \Omega^{-3}, \tag{122}$$

which coincidentally (for this opacity law) is only a function of Ω. It may look cumbersome — and the numerical factors are *certainly* not to be trusted — but what we have shown is that for a locally self-gravitating disk α is simply a constant times a determined function of Σ and Ω. This result allows for the evolution of low-mass self-gravitating disks to be modeled as a pseudo-viscous process [200, 78, 284].

Self-gravity is typically important in protoplanetary disks at large radii, where irradiation is usually the dominant factor determining the disk's thermal state (except at high accretion rates). The generalization of the self-regulation argument given above is obvious; if irradiation is not so strong as to stabilize the disk on its own then viscous heating from the self-gravitating "turbulence" has to make up the difference. The partially irradiated regime of self-gravitating disks has been studied using local numerical simulations [289], and the analytic generalization for the effective α that results can be found in Rafikov (2015) [285].

Ignoring irradiation again (and trusting the numerical factors that we just said were not to be trusted) we can examine the implications of equation (122) for protoplanetary disks. Taking $Q_0 = 1.5$ and $\kappa_0 = 2 \times 10^{-4}$ cm^2 g^{-1} K^{-2} [50] we find, across the region of the disk where ice grains would be the dominant opacity source, that,

$$\alpha \sim 0.3 \left(\frac{r}{50 \text{ AU}} \right)^{9/2}. \tag{123}$$

The steep radial dependence of the estimated self-gravitating α means that, unless all other sources of transport are *extremely* small, it will play no role in the inner disk. In the outer disk, on the other hand, we predict vigorous transport. The physical origin of the transport is density inhomogeneities that are caused by self-gravity, which become increasing large as α grows (explicitly, it is found [86] that the average fractional surface density perturbation $\delta\Sigma/\Sigma \propto \alpha^{1/2}$). Since even the linear threshold for gravitational instability implies that pressure forces can barely resist collapse, we expect that beyond some critical strength of turbulence a self-gravitating disk will be unable to maintain a steady-state. Rather, it will fragment into bound objects that are not (at least not immediately) subsequently sheared out or otherwise disrupted.

Our discussion up to this point might lead one to conjecture that the threshold for fragmentation could be written in terms of a critical dimensionless cooling time,

$$\beta_{\rm crit} \equiv \Omega t_{\rm cool,crit}, \tag{124}$$

or via a maximum $\alpha_{\rm crit}$ that a self-gravitating disk can sustain without fragmenting (these are almost equivalent, but defining the threshold in terms of α incorporates the varying compressibility as expressed through γ). Gammie (2001) [121], using local two dimensional numerical simulations, obtained $\beta_{\rm crit} \simeq 3$ for a two-dimensional adiabatic index $\gamma = 2$. Early global simulations [288], which were broadly consistent with Gammie's estimate, implied a maximum effective transport efficiency $\alpha_{\rm crit} \simeq 0.1$ [291].

The idea that the fragmentation threshold is uniquely determined by a single number is too simplistic. Several additional physical effects matter. First, fragmenta-

tion requires that collapsing clumps can radiate the heat generated by adiabatic compression. There is therefore a dependence not just on the magnitude of the opacity, but also on how it scales with density and temperature [166, 85]. Second, if we view fragmentation as requiring a critical over-density in a random turbulent field there should be a time scale dependence, with statistically rarer fluctuations that lead to collapse becoming probable the longer we wait [258]. (This introduces an additional implicit dependence on γ, because the statistics of turbulent density fields depend upon how compressible the gas is [104].) Finally, disks can be prompted to fragment not only if they cool too quickly, but also if they accrete mass faster than self-gravity can transport it away. Accretion-induced fragmentation appears inevitable for very massive disks, where it would lead to binary formation [183].

In addition to these physical complexities, there has been debate regarding the resolution needed for numerical convergence of simulations of fragmentation [233], and whether the simplest numerical experiments (which forgo radiation transport in lieu of local cooling prescriptions) are even well-posed problems. The numerical issues overlap, in part, with the possibility of stochastic fragmentation, and are not fully resolved. Disks may fragment for (at least) modestly longer cooling times than previously thought, though the high resolution radiation hydrodynamics simulations that might definitively resolve the physical questions have yet to be completed.

Fortunately, if our main interest is in estimating where isolated protoplanetary disks ought to fragment, the steep scaling of $\alpha(r)$ (equation 123) means that we can tolerate considerable uncertainty in $\alpha_{\rm crit}$. For a Solar mass star, fragmentation is expected beyond $r \sim 10^2$ AU [78, 284], with an uncertainty in that estimate of perhaps a factor of two. In most (but perhaps not all) cases, it is expected that the disk conditions that allow fragmentation would lead to objects with masses in the brown dwarf regime, or above [184].

4.3 Magnetohydrodynamic turbulence and transport

The Rayleigh stability criterion (equation 110) applies to a fluid disk. It does not apply to a disk containing even an arbitrarily weak magnetic field, if that field is perfectly coupled to the gas (the regime of ideal MHD). In ideal MHD, indeed, a weakly magnetized disk has entirely different stability properties from an unmagnetized one, and is unstable provided only that the angular velocity decreases outward. This is the magnetorotational instability (MRI) [37, 38], which is accepted as the dominant source of turbulence in well-ionized accretion disks (winds could still contribute to or dominate angular momentum loss). In protoplanetary disks the ideal MHD version of the MRI applies only in the thermally ionized region close to the star; across most of the disk we also need to consider both the dissipative (Ohmic diffusion, ambipolar diffusion) and the non-dissipative (the Hall effect) effects of non-ideal MHD. The Ohmic and ambipolar terms can be considered as modifying — albeit very dramatically — the ideal MHD MRI, while the Hall term introduces new effects (in part) via the Hall shear instability [187], which is a different beast

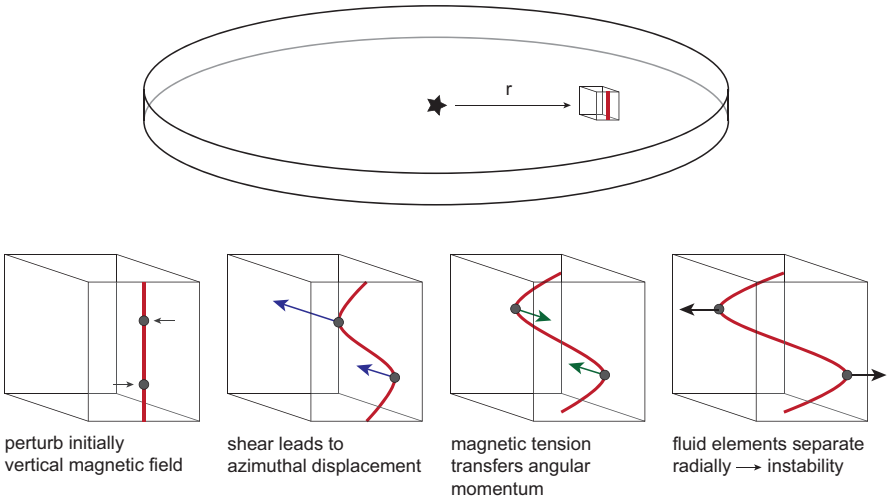

Fig. 17 Illustration showing why a weak vertical magnetic field destabilizes a Keplerian disk (the *magnetorotational instability* [38]). An initially uniform vertical field (weak enough that magnetic tension is not dominant) is perturbed radially. Due to the shear in the disk, an inner fluid element coupled to the field advances azimuthally faster than an outer one. Magnetic tension along the field line then acts to *remove* angular momentum from the inner element, and *add* angular momentum to the outer one. This causes further radial displacement, leading to an instability.

unrelated to the ideal MHD MRI. The phenomenology of disk instabilities in non-ideal MHD is rich, and appears to give rise to both turbulent and laminar angular momentum transport as well as phenomena, such as MHD disk winds, that may be observable.

4.4 The magnetorotational instability

The MRI [37] is an instability of cylindrical shear flows that contain a weak (roughly, if the field is vertical, sub-thermal) magnetic field[6]. In ideal MHD the condition for instability is simply that,

$$\frac{\mathrm{d}\Omega^2}{\mathrm{d}r} < 0. \tag{125}$$

The fact that this condition is always satisfied in disks (though not in star-disk boundary layers) accounts for the MRI's central role in modern accretion theory.

[6] The mathematics of the MRI was worked out by Velikhov [341] and Chandrasekhar [71] around 1960. Thirty years passed before Balbus & Hawley [37] recognized the importance of the instability for accretion flows.

Figure 17 illustrates what is going on to destabilize a disk that contains a magnetic field. A basically vertical field is slightly perturbed radially, so that it links fluid elements in the disk at different radii. Because of the shear in the disk, the fluid closer to the star orbits faster than the fluid further out, creating a toroidal field component out of what was initially just vertical and radial field. The tension in the magnetic field linking the two elements (which can be thought of, even mathematically, as being analogous to a stretched spring) imparts azimuthal forces to both the inner fluid (in the direction *opposite* to its orbital motion) and the outer fluid (*along* its orbital motion). The tension force thus reduces the angular momentum of the inner fluid element, and increases that of the outer element. The inner fluid then moves further inward (and the outer fluid further outward) and we have an instability.

We can derive the MRI instability condition in a very similar setup as Figure 17. Consider a disk with a power-law angular velocity profile, $\Omega \propto r^{-q}$, that is threaded by a uniform vertical magnetic field B_0. We ignore any radial or vertical variation in density (and consistent with that, ignore the vertical component of gravity) and adopt an isothermal equation of state, $P = \rho c_s^2$, with c_s a constant. Our task is to determine whether infinitesimal perturbations to this equilibrium state are stable, or whether instead they grow exponentially with time, signaling a linear instability.

To proceed (largely following [113]) we define a locally Cartesian patch of disk that corotates at radius r_0, where the angular frequency is Ω_0. The Cartesian co-ordinates (x,y,z) are related to cylindrical co-ordinates (r,ϕ,z') via,

$$\begin{aligned} x &= r - r_0, \\ y &= r_0\phi, \\ z &= z'. \end{aligned} \tag{126}$$

The local "shearing-sheet" (or in three dimensions, "shearing box") model is useful for both analytic stability studies, and for numerical simulations. In this co-rotating frame, the equations of ideal MHD pick up terms representing the fictitious Coriolis and centrifugal forces,

$$\begin{aligned} \frac{\partial \rho}{\partial t} + \nabla\cdot(\rho\mathbf{v}) &= 0, \\ \frac{\partial \mathbf{v}}{\partial t} + (\mathbf{v}\cdot\nabla)\mathbf{v} &= -\frac{1}{\rho}\nabla P + \frac{1}{4\pi\rho}(\nabla\times\mathbf{B})\times\mathbf{B} - 2\Omega_0\times\mathbf{v} + 2q\Omega_0^2 x\hat{\mathbf{x}}, \\ \frac{\partial \mathbf{B}}{\partial t} &= \nabla\times(\mathbf{v}\times\mathbf{B}). \end{aligned} \tag{127}$$

Here $\hat{\mathbf{x}}$ is a unit vector in the x-direction. As noted above, the initial equilibrium has uniform density, $\rho = \rho_0$, and a magnetic field $\mathbf{B} = (0,0,B_0)$. There are no pressure or magnetic forces, so the velocity field is determined by a balance between the Coriolis and centrifugal terms,

$$2\Omega_0\times\mathbf{v} = 2q\Omega_0^2 x\hat{\mathbf{x}}. \tag{128}$$

The equilibrium velocity field that completes the definition of the initial state is,

$$\mathbf{v} = (0, -q\Omega_0 x, 0)\,, \tag{129}$$

which has a linear shear (with $q = 3/2$ for a Keplerian disk) around the reference radius r_0.

To assess the stability of the equilibrium, we write the density, velocity and magnetic field as the sum of their equilibrium values plus a perturbation. We can recover the MRI with a particularly simple perturbation which depends on z and t only[7]. For the velocity components, for example, we write,

$$\begin{aligned} v_x &= v_x'(z,t), \\ v_y &= -q\Omega_0 x + v_y'(z,t), \\ v_z &= v_z'(z,t), \end{aligned} \tag{130}$$

and do likewise for the density and magnetic field. We substitute these expressions into the continuity, momentum and induction equations, and discard any terms that are quadratic in the primed variables, assuming them to be *small* perturbations. This would give us seven equations in total (one from the continuity equation, and three each from the other equations), but the x and y components of the momentum and induction equations are all we need to derive the MRI. The relevant linearized equations are,

$$\begin{aligned} \frac{\partial v_x'}{\partial t} &= \frac{B_0}{4\pi\rho_0}\frac{\partial B_x'}{\partial z} + 2\Omega_0 v_y', \\ \frac{\partial v_y'}{\partial t} - q\Omega_0 v_x' &= \frac{B_0}{4\pi\rho_0}\frac{\partial B_y'}{\partial z} - 2\Omega_0 v_y', \\ \frac{\partial B_x'}{\partial t} &= B_0\frac{\partial v_x'}{\partial z}, \\ \frac{\partial B_y'}{\partial t} &= B_0\frac{\partial v_y'}{\partial z} - q\Omega_0 B_x'. \end{aligned} \tag{131}$$

We convert these linearized differential equations into algebraic equations by taking the perturbations to have the form, e.g.,

$$B_x' = \bar{B}_x' e^{i(\omega t - kz)}, \tag{132}$$

where ω is the frequency of a perturbation with vertical wave-number k. The time derivatives then pull down a factor of $i\omega$, while the spatial derivatives become ik. Our four equations simplify to,

[7] An analysis that retains the x-dependence can be found in the original Balbus & Hawley (1991) paper [37], and follows an essentially identical approach. Studying the stability of non-axisymmetric perturbations (in y), however, requires a different and more involved analysis [87, 251, 326, 267].

$$
\begin{aligned}
i\omega v_x' &= -ik\frac{B_0 B_x'}{4\pi\rho_0} + 2\Omega_0 v_y', \\
i\omega v_y' &= -ik\frac{B_0 B_y'}{4\pi\rho_0} + (q-2)\Omega_0 v_x', \\
i\omega B_x' &= -ikB_0 v_x', \\
i\omega B_y' &= -ikB_0 v_y' - q\Omega_0 B_x'.
\end{aligned} \tag{133}
$$

(We've dropped the bars on the variables for clarity.) Eliminating the perturbation variables from these equations, we finally obtain the *MRI dispersion relation*,

$$\omega^4 - \omega^2\left[2k^2 v_A^2 + 2(2-q)\Omega_0^2\right] + k^2 v_A^2\left[k^2 v_A^2 - 2q\Omega_0^2\right] = 0, \tag{134}$$

where $v_A^2 = B_0^2/(4\pi\rho_0)$ is the Alfvén speed associated with the net field.

If $\omega^2 > 0$ then ω itself will be real and the perturbation $e^{i\omega t}$ will oscillate in time. Instability requires $\omega^2 < 0$, since in this case ω is imaginary and the perturbation will grow exponentially. Solving the dispersion relation we find the instability criterion is,

$$(kv_A)^2 - 2q\Omega_0^2 < 0. \tag{135}$$

Letting the field strength go to zero ($B_z \to 0$, $v_A \to 0$) we find that the condition for instability is simply that $q > 0$, i.e. that the angular velocity decrease outward. Even for an arbitrarily weak field, the result is completely different from Rayleigh's for a strictly hydrodynamic disk.

The growth rate of the instability and what it means for the magnetic field to be "weak" can also be derived from equation (134). Specializing to a Keplerian rotation law with $q = 3/2$ the dispersion relation takes the form shown in Figure 18. For a fixed magnetic field strength (and hence a fixed Alfvén speed v_A) the flow is unstable for wavenumbers $k < k_{\rm crit}$ (i.e. on large enough spatial scales), where,

$$k_{\rm crit} v_A = \sqrt{3}\Omega_0. \tag{136}$$

As the magnetic field becomes stronger, the *smallest* scale $\lambda = 2\pi/k_{\rm crit}$ which is unstable grows, until eventually it exceeds the disk's vertical extent $\approx 2h$. For stronger vertical fields no unstable MRI modes fit within the disk, and the instability is suppressed. Using $h = c_s/\Omega$, the condition that the vertical magnetic field is weak enough to admit the MRI (i.e. that $\lambda < 2h$) becomes

$$B_0^2 < \frac{12}{\pi}\rho c_s^2 \tag{137}$$

If we define the plasma β parameter as the ratio of gas to magnetic pressure,

$$\beta \equiv \frac{8\pi P}{B_0^2} \tag{138}$$

this condition can be expressed alternatively as,

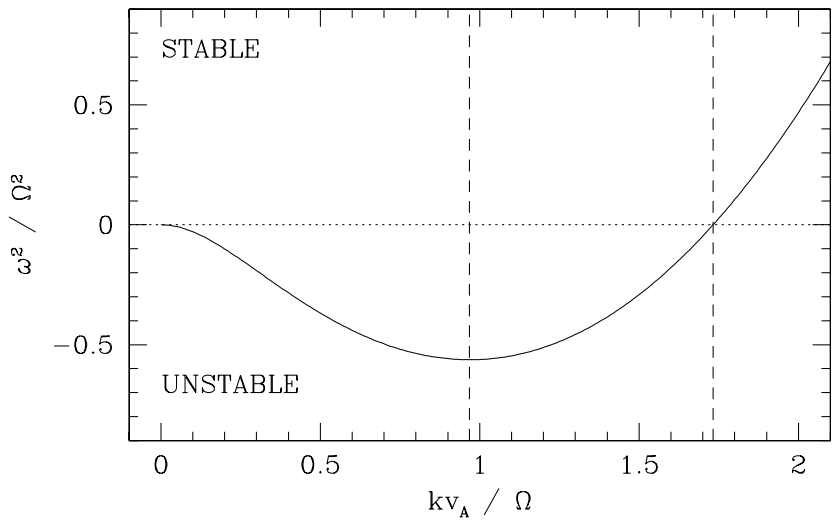

Fig. 18 The unstable branch of the MRI dispersion relation is plotted for a Keplerian rotation law. The flow is unstable ($\omega^2 < 0$) for all spatial scales smaller than $kv_A < \sqrt{3}\Omega$ (rightmost dashed vertical line). The most unstable scale (shown as the dashed vertical line at the center of the plot) is close to $kv_A \simeq \Omega$.

$$\beta > \frac{2\pi^2}{3}. \tag{139}$$

A magnetic field whose *vertical* component approaches equipartition with the thermal pressure ($\beta \sim 1$) will be too strong to admit the existence of linear MRI modes, but a wide range of weaker fields are acceptable.

The maximum growth rate is determined by setting $\mathrm{d}\omega^2/\mathrm{d}(kv_A) = 0$ for the unstable branch of the dispersion relation plotted in figure 18. The most unstable scale for a Keplerian disk is,

$$(kv_A)_{\max} = \frac{\sqrt{15}}{4}\Omega_0, \tag{140}$$

where the growth rate is,

$$|\omega_{\max}| = \frac{3}{4}\Omega_0. \tag{141}$$

This result implies an *extremely* vigorous growth of the instability, with an exponential growth time scale that is a fraction of an orbital period. This means that if a disk is unstable to the MRI it will invariably dominate the evolution.

4.4.1 Non-ideal MHD

The MRI in its ideal MHD guise is relevant to protoplanetary disks only in the thermally ionized region close to the star (§2.3.1), where $T > 10^3$ K. The very weakly ionized gas further out is imperfectly coupled to the magnetic field, and this both modifies the properties of the MRI and leads to new MHD instabilities. We will begin by sketching the derivation of the non-ideal MHD equations (following Balbus [36], who justifies several of the approximations that we will make), and then estimate the magnitude of the extra terms that arise in protoplanetary disks.

The physics of how magnetic fields affect weakly-ionized fluids is easy to visualize. We consider a gas that is almost entirely neutral, with only a small admixture of ions and electrons (analogous considerations apply if the charge carriers are dust particles, but we will not go there). Magnetic fields exert Lorentz forces on the charged species, but not on the neutrals. Collisions between the neutrals and either the ions or the electrons lead to momentum exchange whenever the neutral fluid has a velocity differential with respect to the charged fluids.

We begin by considering the momentum equation. For the neutrals we have,

$$\rho \frac{\partial \mathbf{v}}{\partial t} + \rho(\mathbf{v}\cdot\nabla)\mathbf{v} = -\nabla P - \rho\nabla\Phi - p_{nI} - p_{ne}. \tag{142}$$

Here ρ, $\mathbf{v}$ and P (without subscripts) refer to the neutral fluid, and p_{nI} and p_{ne} are the rate of momentum exchange due to collisions between the neutrals and the ions / electrons respectively. Identical equations apply to the charged species, but for the addition of Lorentz forces,

$$\begin{aligned}
\rho_e \frac{\partial \mathbf{v}_e}{\partial t} + \rho_e(\mathbf{v}_e\cdot\nabla)\mathbf{v}_e &= -\nabla P_e - \rho_e\nabla\Phi - en_e\left(\mathbf{E} + \frac{\mathbf{v}_e\times\mathbf{B}}{c}\right) - p_{en}, \\
\rho_I \frac{\partial \mathbf{v}_I}{\partial t} + \rho_I(\mathbf{v}_I\cdot\nabla)\mathbf{v}_I &= -\nabla P_I - \rho_I\nabla\Phi + Zen_I\left(\mathbf{E} + \frac{\mathbf{v}_I\times\mathbf{B}}{c}\right) - p_{In}.
\end{aligned} \tag{143}$$

In these equations $\mathbf{E}$ and $\mathbf{B}$ are the electric and magnetic fields, the ions have charge Ze, where $-e$ is the charge on an electron, and of course $p_{ne} = -p_{en}$ and $p_{nI} = -p_{In}$. Having three momentum equations looks complicated, but we can make a large simplification to the system by noting that the time scale for macroscopic evolution of the fluid is generally much longer than the time scale for collisional or magnetic forces to alter a charged particle's momentum. We can then ignore *everything* in the charged species' momentum equations, except for the Lorentz and collisional terms. For the ions we have,

$$Zen_I\left(\mathbf{E} + \frac{\mathbf{v}_I\times\mathbf{B}}{c}\right) - p_{In} = 0, \tag{144}$$

with a similar equation for the electrons. Imposing charge neutrality, $n_e = Zn_I$, we eliminate the electric field between the ion and electron equations to find an expression for the sum of the momentum transfer terms,

$$p_{In} + p_{en} = \frac{en_e}{c}(\mathbf{v}_I - \mathbf{v}_e) \times \mathbf{B}. \tag{145}$$

The current density $\mathbf{J} = en_e(\mathbf{v}_I - \mathbf{v}_e)$, so we can write this as,

$$p_{In} + p_{en} = \frac{\mathbf{J} \times \mathbf{B}}{c}. \tag{146}$$

Finally, we go to Maxwell's equations, and note that the current can be written as,

$$\frac{4\pi}{c}\mathbf{J} = \nabla \times \mathbf{B} + \frac{1}{c}\frac{\partial \mathbf{E}}{\partial t}. \tag{147}$$

The second term in Maxwell's equation is the displacement current, which is $\mathcal{O}(v^2/c^2)$ and consistently ignorable in non-relativistic MHD. Doing so, we substitute equation (146) in the neutral equation of motion to obtain,

$$\rho\frac{\partial \mathbf{v}}{\partial t} + \rho(\mathbf{v}\cdot\nabla)\mathbf{v} = -\nabla P - \rho\nabla\Phi + \frac{1}{4\pi}(\nabla \times \mathbf{B}) \times \mathbf{B}. \tag{148}$$

This is identical to the *ideal* MHD momentum equation (stated without derivation as equation 127) and pleasingly simple; we have reduced the three momentum equations to an equation for a single (neutral) fluid with a magnetic force term whose dependence on $\mathbf{B}$ is independent of the make-up of the gas. All of the complexities enter only via the induction equation.

The consistent simplification of non-ideal MHD to a momentum equation for a single fluid is not always possible. Roughly speaking it works provided that the plasma's inertia is negligible compared to that of the neutral fluid, the coupling between charged and neutral species is strong, and the recombination time is short. Zweibel [364] gives an accessible account of the conditions necessary for a valid single-fluid description. Although some of the early analytic and numerical work on the MRI in weakly-ionized disks utilized a two-fluid approach [56, 141], in many protoplanetary disk situations a single fluid model is both justified [25] and substantially simpler.

Deducing the non-ideal induction equation requires us to specify the form of the momentum coupling terms. Writing these in standard notation (which is different for the two terms, somewhat obscuring the symmetry),

$$\begin{aligned} p_{ne} &= n_e \nu_{ne} m_e(\mathbf{v} - \mathbf{v}_e), \\ p_{nI} &= \rho\rho_I\gamma(\mathbf{v} - \mathbf{v}_I), \end{aligned} \tag{149}$$

where ν_{ne} is the collision frequency of an electron with the neutrals, and γ is called the drag-coefficient. The ion-neutral coupling involves longer-range interactions than the electron-neutral coupling, and is accordingly stronger [36].

We now go back to the force balance deduced from the electron momentum equation,

$$-en_e\left(\mathbf{E}+\frac{\mathbf{v}_e\times\mathbf{B}}{c}\right)-p_{en}=0, \tag{150}$$

and attempt to write the terms involving $\mathbf{v}_e$ and p_{en} entirely in terms of the current. We start with the exactly equivalent expression,

$$\mathbf{E}+\frac{1}{c}\left[\mathbf{v}+(\mathbf{v}_e-\mathbf{v}_I)+(\mathbf{v}_I-\mathbf{v})\right]\times\mathbf{B}+\frac{\nu_{ne}m_e}{e}\left[(\mathbf{v}_e-\mathbf{v}_I)+(\mathbf{v}_I-\mathbf{v})\right]=0, \tag{151}$$

and deal with the terms in turn. We have two terms that involve $(\mathbf{v}_e-\mathbf{v}_I)$, which can be replaced immediately with the current,

$$(\mathbf{v}_e-\mathbf{v}_I)=-\frac{\mathbf{J}}{en_e}. \tag{152}$$

The first term with $(\mathbf{v}_I-\mathbf{v})$ is exactly equal to $p_{In}/(\rho\rho_I\gamma)$. If, however, $|p_{In}|\gg|p_{en}|$, then equation (146) implies that, approximately,

$$(\mathbf{v}_I-\mathbf{v})\simeq\frac{\mathbf{J}\times\mathbf{B}}{c\rho\rho_I\gamma}. \tag{153}$$

Finally it can be shown (see Balbus [36] for details) that the final term with $(\mathbf{v}_I-\mathbf{v})$ can be consistently dropped. The version of Ohm's Law that we end up with is,

$$\mathbf{E}+\frac{\mathbf{v}\times\mathbf{B}}{c}-\frac{\mathbf{J}\times\mathbf{B}}{en_ec}+\frac{(\mathbf{J}\times\mathbf{B})\times\mathbf{B}}{c^2\rho\rho_I\gamma}-\frac{\nu_{ne}m_e}{e^2n_e}\mathbf{J}=0. \tag{154}$$

The non-ideal induction equation is then obtained by applying Faraday's law,

$$\nabla\times\mathbf{E}=-\frac{1}{c}\frac{\partial\mathbf{B}}{\partial t}, \tag{155}$$

to eliminate any explicit reference to the electric field. In its usual form,

$$\frac{\partial\mathbf{B}}{\partial t}=\nabla\times\left[\mathbf{v}\times\mathbf{B}-\eta\nabla\times\mathbf{B}-\frac{\mathbf{J}\times\mathbf{B}}{en_e}+\frac{(\mathbf{J}\times\mathbf{B})\times\mathbf{B}}{c\gamma\rho\rho_I}\right]. \tag{156}$$

We have defined the magnetic resistivity,

$$\eta=\frac{c^2}{4\pi\sigma} \tag{157}$$

where σ is (here) the electrical conductivity,

$$\sigma=\frac{e^2n_e}{m_e\nu_{en}}. \tag{158}$$

As before we can replace the current with the magnetic field via,

$$\mathbf{J} = \frac{c}{4\pi}\nabla \times \mathbf{B}, \tag{159}$$

so that the induction equation is solely a function of $\mathbf{B}$. The terms on the right-hand-side are referred to as the inductive, Ohmic, Hall and ambipolar terms respectively.

The non-ideal terms in the induction equation depend upon the ionization state of the gas (through n_e and ρ_I) and upon the collision rates between the neutral and charged species (via η and γ). Standard values for these quantities are [56, 95],

$$\begin{aligned} \eta &= 234 \left(\frac{n}{n_e}\right) T^{1/2} \text{ cm}^2 \text{ s}^{-1}, \\ \gamma &= 3 \times 10^{13} \text{ cm}^3 \text{ s}^{-1} \text{ g}^{-1}. \end{aligned} \tag{160}$$

We are now ready to estimate the importance of the non-ideal terms in the environment of protoplanetary disks, and to ask what effect they have both on the MRI, and on the more general question of whether there is MHD turbulence or transport in disks.

4.4.2 Ohmic, ambipolar and Hall physics in protoplanetary disks

The non-ideal terms in equation (156) all depend inversely on the electron or ion density, so the strength of all non-ideal MHD effects relative to the inductive term increases with smaller ionization fraction. The three terms also have different dependencies on density, magnetic field strength and temperature, so the *relative* ordering of the non-ideal MHD effects varies with these parameters.

The Ohmic, Hall and ambipolar terms have different dependencies on the magnetic field geometry, and in a disk setting they influence the MRI in distinct ways (most importantly, the Hall effect differs from the others in being non-dissipative). There is therefore no model-independent way to precisely demarcate when each term will affect disk evolution. As a first guess, however, we can treat the magnetic field as a scalar and simply take the ratio of the Hall to the Ohmic term and the ambipolar to the Hall term,

$$\begin{aligned} \frac{\text{H}}{\text{O}} &= \frac{cB}{4\pi e \eta n_e}, \\ \frac{\text{A}}{\text{H}} &= \frac{e n_e B}{c \gamma \rho \rho_I}. \end{aligned} \tag{161}$$

Since $\eta \propto (n/n_e)$ and $n_e \propto \rho_I$ both of these ratios depend on (B/n). Substituting for η and γ, and taking the ion mass that enters into the ambipolar term as $30 m_H$, we can estimate the magnetic field strength for which the Ohmic and Hall terms have equal magnitude, and similarly for the Hall and ambipolar terms,

$$B_{\text{O=H}} \approx 0.5 \left(\frac{n}{10^{15} \text{ cm}^{-3}}\right) \left(\frac{T}{100 \text{ K}}\right)^{1/2} \text{ G},$$

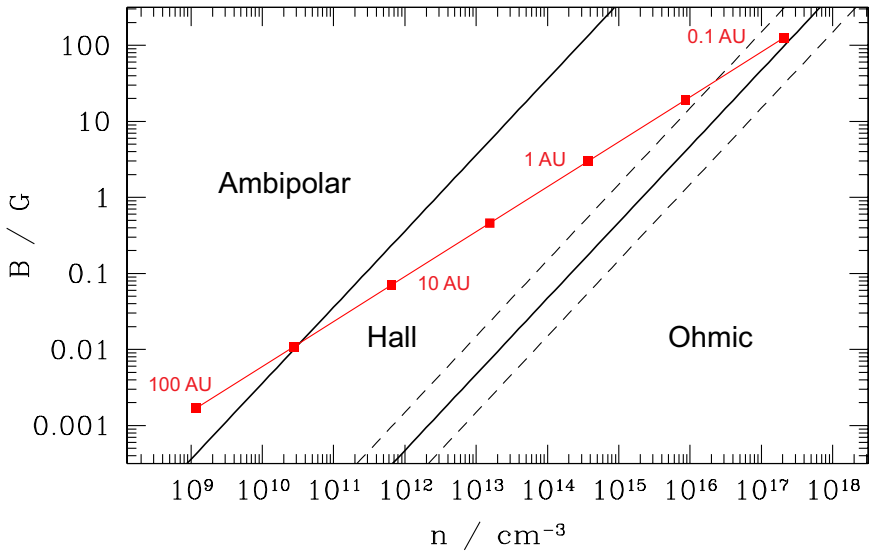

Fig. 19 Regions of the (n,B) parameter space in which different non-ideal terms are dominant. The boundary between the Ohmic and Hall regimes is plotted for $T = 100$ K (solid line) and also for temperatures of 10^3 K (upper dashed line) and 10 K (lower dashed line). The red line shows a very rough estimate of how the magnetic field in the disk might vary with density between the inner disk at 0.1 AU and the outer disk at 100 AU.

$$B_{\rm H=A} \approx 4 \times 10^{-3} \left(\frac{n}{10^{10}\ {\rm cm}^{-3}} \right)\ {\rm G}. \tag{162}$$

Figure 19 shows these dividing lines in the (n,B) plane. Ohmic diffusion is dominant at high densities / low magnetic field strengths. Ambipolar diffusion dominates for low densities / high field strengths. The Hall effect is strongest for a fairly broad range of intermediate densities.

Estimating where protoplanetary disks fall in the (n,B) plane can be done in various ways. For a Solar System-motivated estimate we can start with the disk field inferred from laboratory measurements of chondrules in the Semarkona meteorite [116], which suggest that near the snow line ($r \simeq 3$ AU) the disk field was $B \simeq 0.5$ G. (There are caveats and a large systematic uncertainty associated with this measurement, all of which we ignore for now.) Let us assume that the surface density and temperature profiles are $\Sigma \propto r^{-3/2}$ and $T \propto r^{-1/2}$ respectively, and that the magnetic field pressure is the same fraction of the thermal pressure at all radii in the disk. Taking $\Sigma \simeq 300$ g cm^{-2} and $T = 150$ K at 3 AU, the inferred scalings of mid-plane density and magnetic field strength are then,

$$\begin{aligned} n &\approx 2 \times 10^{13} \left(\frac{r}{3\ {\rm AU}} \right)^{-11/4}\ {\rm cm}^{-3}, \\ B &\approx 0.5 \left(\frac{r}{3\ {\rm AU}} \right)^{-13/8}\ {\rm G}. \end{aligned} \tag{163}$$

The track defined by these relations is plotted in Figure 19 for radii between 0.1 AU and 100 AU.

As we have emphasized, neither our approach to ranking the strength of the non-ideal terms, nor our estimate of the radial scaling of disk conditions, are anything more than crude guesses. Other approximations are equally valid (for example, one can order the terms in the (n,T) plane instead [41, 188, 16]). Nevertheless, because n and B vary by so many orders of magnitude across Figure 19 the critical inferences we can draw are quite robust. We predict that the Hall effect is the dominant non-ideal MHD process at the disk mid-plane between (conservatively) 1 AU and 10 AU. Ohmic diffusion can become important as we approach the thermally ionized region interior to 1 AU. Ambipolar diffusion dominates at sufficiently large radii, of the order of 100 AU, and in the lower density gas away from the mid-plane.

4.4.3 The dead zone

The linear stability of Keplerian disk flow in non-ideal MHD has been extensively investigated (see, e.g. [56, 159, 344, 41, 188, 91]), and the reader interested in the non-ideal analogs to the MRI dispersion relation derived as equation (134) should start there. Proceeding less formally, we follow Gammie (1996) [119] to estimate the conditions under which Ohmic dissipation (ignoring for now the Hall term) would damp the MRI. The basic idea is to compare the time scale on which the ideal MRI would generate tangled magnetic fields to that on which Ohmic diffusion would smooth them out. We first note that diffusion erases small-scale structure in the field more efficiently than large scale features, so that the appropriate comparison is between growth and damping of the largest scale MRI models. Starting from the MRI dispersion relation (equation 134), for a Keplerian disk we consider the weak-field / long wavelength limit ($kv_A/\Omega \ll 1$). The growth rate of the MRI is,

$$|\omega| \simeq \sqrt{3} k v_A. \tag{164}$$

Writing this as a function of the spatial scale $\lambda = 2\pi/k$, we have,

$$|\omega| \simeq 2\pi\sqrt{3}\frac{v_A}{\lambda}. \tag{165}$$

Up to numerical factors the MRI on a given scale then grows on the Alfvén crossing time. Equating this growth rate to the Ohmic damping rate,

$$|\omega_\eta| \sim \frac{\eta}{\lambda^2} \tag{166}$$

we conclude that Ohmic dissipation will suppress the MRI on the largest available scale $\lambda \approx h$ provided that,

$$\eta > 2\pi\sqrt{3} v_A h. \tag{167}$$

We can express this result in a different form. Analogous to the fluid Reynolds number (equation 108) the magnetic Reynolds number Re_M is defined as,

$$\mathrm{Re}_M \equiv \frac{UL}{\eta} \tag{168}$$

where U is a characteristic velocity and L a characteristic scale. Taking $U = v_A$ and $L = h$ for a disk, the condition for Ohmic dissipation to suppress the MRI becomes

$$\mathrm{Re}_M < 1 \tag{169}$$

where order unity numerical factors have been omitted.

We now convert the condition for the suppression of the MRI into a limit on the ionization fraction $x \equiv n_e/n$. We make use of the formula for the magnetic resistivity (equation 160) and assume that Maxwell stresses transport angular momentum, so that $\alpha \sim v_A^2/c_s^2$ (this follows approximately from equation 109). The magnetic Reynolds number can then be estimated to be,

$$\mathrm{Re}_M = \frac{v_A h}{\eta} = \frac{\alpha^{1/2} c_s^2}{\eta \Omega}. \tag{170}$$

Substituting for η and c_s^2, the magnetic Reynolds number in a protoplanetary disk scales as,

$$\mathrm{Re}_M \approx 1.4 \times 10^{12} x \left(\frac{\alpha}{10^{-2}}\right)^{1/2} \left(\frac{r}{1\ \mathrm{AU}}\right)^{3/2} \left(\frac{T}{300\ \mathrm{K}}\right)^{1/2} \left(\frac{M_*}{M_\odot}\right)^{-1/2}. \tag{171}$$

For the given parameters, the critical ionization fraction below which Ohmic diffusion will quench the MRI is

$$x_{\mathrm{crit}} \sim 10^{-12}. \tag{172}$$

Clearly a very small ionization fraction suffices to couple the magnetic field to the gas and allows the MRI to operate, but there are large regions of the disk where even these ionization levels are not obtained and non-ideal effects are important.

Based on this analysis Gammie [119] noted, first, that the criterion for the MRI to operate under near-ideal MHD conditions in the inner disk coincides with the requirement that the alkali metals are thermally ionized (Figure 6). The development of magnetized turbulence in the disk at radii where $T > 10^3$ K can therefore be modeled in ideal MHD. Second, he proposed that Ohmic diffusion would damp MHD turbulence in the low ionization environment near the disk mid-plane on scales of the order of 1 AU, creating a *dead zone* of sharply reduced turbulence and transport. Gammie's original model is incomplete, as it did not include either ambipolar diffusion or the Hall effect, but the basic idea motivates much of the current work on MHD instabilities in disks.

4.4.4 Turbulence and transport in non-ideal MHD

Once we consider the full set on non-ideal terms, the first question is to assess the level of turbulence and transport that is expected as a function of their strengths. This is a well-defined but already difficult theoretical question, given that interesting values of the Ohmic, ambipolar and Hall terms span a broad range (depending physically on the temperature, density, ionization fraction and magnetic field strength). To define the problem in its most idealized form, we rewrite the non-ideal induction equation (156) as,

$$\frac{\partial \mathbf{B}}{\partial t} = \nabla \times \left[\mathbf{v} \times \mathbf{B} - \eta_O \nabla \times \mathbf{B} - \eta_H \frac{\mathbf{J} \times \mathbf{B}}{B} - \eta_A \frac{(\mathbf{J} \times \mathbf{B}) \times \mathbf{B}}{B^2} \right], \tag{173}$$

where *dimensionally* η_O, η_H and η_A are all diffusivities. There are different ways to construct dimensionless numbers from the diffusivities, but one useful set is,

$$\begin{aligned} \Lambda_O &\equiv \frac{v_A^2}{\Omega \eta_O} \ \text{(Ohmic Elsasser number)}, \\ \mathrm{Ha} &\equiv \frac{v_A^2}{\Omega \eta_H} \ \text{(Hall Elsasser number)}, \\ \mathrm{Am} &\equiv \frac{v_A^2}{\Omega \eta_A} \ \text{(ambipolar Elsasser number)}. \end{aligned} \tag{174}$$

(Note that the ambipolar Elsasser number can also be written as $\mathrm{Am} \equiv \gamma \rho_I / \Omega$, which is the number of ion-neutral collisions per dynamical time Ω^{-1}.) We further specify the net vertical magnetic field (if any) via the ratio of the mid-plane gas and magnetic field pressures (equation 138),

$$\beta_z = \frac{8\pi P}{B_z^2}. \tag{175}$$

Our question can then be rephrased; what is the level of angular momentum transport and turbulence in an MHD disk at radii where the non-ideal terms are characterized by the dimensionless parameters (Λ_O, Ha, Am, β_z).

Ohmic diffusion acts as a strictly dissipative process that stabilizes disks to magnetic field instabilities on scales below some critical value. Ambipolar diffusion is in principle more complex, because it does not dissipate currents that are parallel to the magnetic field. This distinction substantially impacts the linear stability of ambipolar-dominated disks [188], but appears to matter less for the non-linear evolution, whose properties are analogous to Ohmic diffusion. For both dissipative processes, simulations show that MRI-driven turbulence is strongly damped when the relevant dimensionless parameter (either Λ_0 or Am) drops below a critical value that depends upon the initial field geometry but is $\sim 1 - 10^2$ [300, 335, 310, 32, 308]. Consistent with the dead zone idea [119], we therefore expect substantial modification of the properties of MHD turbulence both in the mid-plane around 1 AU (where

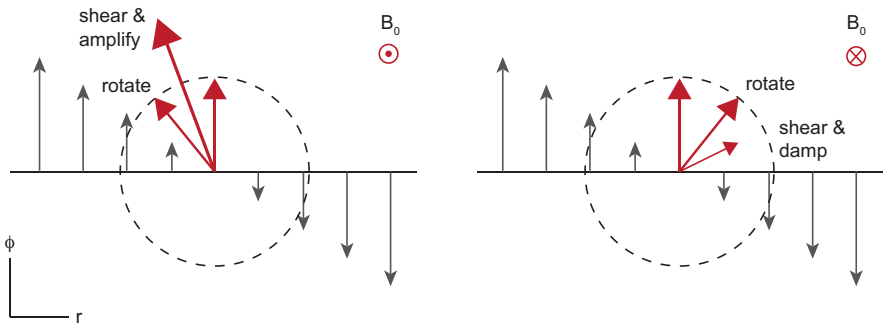

Fig. 20 An illustration (adapted from Lesur, unpublished) of the Hall shear instability [187]. In the presence of a vertical field threading the disk, the Hall effect acts to rotate an initially toroidal field component either clockwise or anti-clockwise, depending upon the *sign* of the vertical field. The rotated field vector is then either amplified or damped by the shear. This instability differs from the MRI both technically (in that there is no reference to orbital motion, any shear flow suffices) and physically (via the dependence on the direction of the vertical magnetic field as well as its strength).

Ohmic diffusion is the dominant dissipative process) and in the disk atmosphere and at large radii $\sim 10^2$ AU (where ambipolar diffusion dominates).

The MRI dispersion relation is also modified by the Hall effect [344, 41], which differs from the other non-ideal terms in that it modifies the field structure without any attendant dissipation. In this respect the Hall term most closely resembles the inductive term $\nabla \times (\mathbf{v} \times \mathbf{B})$, and its strength can usefully be characterized by the ratio of the Hall to the inductive term. Non-linear simulations of the Hall effect in disks, which were pioneered by Sano & Stone [301, 302], have only recently been able to access the strongly Hall-dominated regime relevant to protoplanetary disks [189, 195, 27, 28]. In vertically stratified disks with a net vertical field, Lesur et al. (2014) [195] find that the Hall effect has a controlling influence on disk dynamics on scales between 1 AU and 10 AU. For $\beta_z = 10^5$ a strong but *laminar* Maxwell stress (i.e. one dominated by large-scale radial and toroidal fields in equation 109) results when the net field is aligned with the rotation axis of the disk, whereas anti-alignment leads to extremely weak turbulence and transport.

The results from Hall-MHD simulations of protoplanetary disks are best interpreted not as a modification of the MRI, but rather as the signature of a distinct *Hall shear instability* [187]. In the presence of a net vertical magnetic field the Hall effect acts to *rotate* magnetic field vectors lying in the orbital plane (Figure 20), with the sense of the rotation determined by whether the new field is aligned or anti-aligned to the rotation axis. In the aligned field case, the Hall-induced rotation allows the magnetic field to be amplified by the shear, while damping occurs in the anti-aligned limit. Unlike the MRI, the Hall shear instability does not depend on the Coriolis force, and is indifferent to the sign of the angular velocity gradient. By generating a radial field directly from an azimuthal one, the Hall effect (given a

net field) supports a mean-field disk dynamo cycle [329, 195] that is qualitatively different from anything that is possible in ideal MHD.

Elementary arguments show that the Hall effect is important across a range of radii in protoplanetary disks (Figure 19). Whether existing simulations capture the full extent of non-ideal MHD behavior in disks is, however, open to question. The numerical implementation of the Hall effect in simulation codes poses significant challenges, and the presence of large-scale fields in the saturated state suggests that local simulations may not be adequate to describe the outcome. The level of turbulence that accompanies the predominantly large-scale transport by Maxwell stresses appears particularly uncertain.

Going beyond the idealized question of the effect of the non-ideal terms on turbulence and transport, our goal is to use the results described above to predict the structure and evolution of protoplanetary disks. This introduces new layers of uncertainty. To predict disk properties from first principles, we need at a minimum to know the strength of the different sources of ionization (§2.3.2), the rates of gas-phase and dust-induced recombination, and the global evolution of any net magnetic field (§3.5.1). We also need to model (or have good reasons to ignore) various non-MHD effects, including the hydrodynamic angular momentum transport processes already discussed and mass loss by photoevaporation [3] (§8). Given these uncertainties, the best that we can currently do is to highlight a number of qualitative predictions that receive support from numerical simulations:

- Net vertical magnetic fields are important for disk evolution. A vertical magnetic field enhances angular momentum transport by the MRI even in ideal MHD (roughly as $\alpha \propto \beta_z^{-1/2}$ [140]). In non-ideal MHD, local simulations by Simon et al. [308, 307] suggest that ambipolar damping of the MRI in the outer disk prevents resupply of the inner disk with gas *unless* a net field is present[8]. A net field with $\beta_z \simeq 10^4 - 10^5$ suffices, comparable to the fields expected in global models of flux evolution [134] but much weaker than the likely initial field left over from star formation. Accretion on scales of 30-100 AU occurs predominantly through a thin surface layer that is ionized by FUV photons [266, 308, 307], and is largely independent of the Hall effect [28].
- MHD winds and viscous transport can co-exist in disks. Local numerical simulations in ideal MHD by Suzuki & Inutsuka [320] showed that in the presence of net vertical field, the MRI was accompanied by mass and angular momentum loss in a disk wind. Winds are likewise seen in net field protoplanetary disk simulations at 1 AU that include Ohmic and ambipolar diffusion [33], in simulations at

[8] It is not obvious that the inner disk *is* resupplied by gas, or, to put it more formally, that the disk attains a steady-state. Out to ~ 10 AU the viscous time scale is short enough that the disk will plausibly adjust to a steady state (provided only that a steady state is possible, see §5), but no such argument works out to 100 AU. Ultimately the question of whether gas at 100 AU ever reaches the star will need to be settled by observations as well as by theory.

30-100 AU where ambipolar diffusion dominates [307], and in simulations that include all non-ideal terms [195]. Caution is required before interpreting these local simulation results as quantitative predictions, because although the effective potential for wind launching is correctly represented (equation 97) there is a known and unphysical dependence of the mass loss rate on the vertical size of the simulation domain [114]. Outflows are also seen in the (few) existing *global* net field simulations [131], however, supporting the view that weak field MHD outflows could be a generic feature of protoplanetary disk accretion. Drawing on these results, Bai [26] has proposed that MHD winds may dominate disk evolution on AU-scales, and co-exist with a mixture of viscous transport and wind loss on larger scales in the ambipolar dominated regime [307].

- Turbulence and angular momentum transport are not synonymous. In classical disk theory, the value of α determines not only the rate at which the disk evolve, but also the strength of turbulence and its effect on small solid particles. This link is doubly broken in more complete disk models. First, as already noted, angular momentum loss via winds (which need not be accompanied by turbulence) may be stronger than viscous transport at some radii. Second, even the internal component of transport may be primarily a large-scale "laminar" Maxwell stress, rather than small-scale turbulence [307, 195].
- The sign of the net field could lead to bimodality in disk properties. The Hall effect is the strongest non-ideal term interior to about 10 AU, and simulations [195, 27, 28] confirm the expectation from linear theory [344, 41, 187] that a disk with a weak field that is aligned to the rotation axis behaves quite differently from one with an anti-aligned field. Although there are possible confounding factors — for example the long-term evolution of the net field may itself differ with the sign of the field — it appears likely that the striking asymmetry seen in simulations introduces *some* observable bimodality in disk structure [311].

Figure 21 illustrates a possible disk structure implied by the above results. The figure should be regarded as a work in progress; there is plenty of work remaining before we fully understand either the physics of potential angular momentum transport and loss processes, or how to tie that knowledge together into a consistent scenario for disk structure and evolution.

Hall MHD can also affect the collapse of molecular clouds and the formation of protostellar disks [182, 330], influencing for example their initial sizes. The Hall current, along with the other non-ideal terms, can also modify the accretion properties of circumplanetary disks [170]

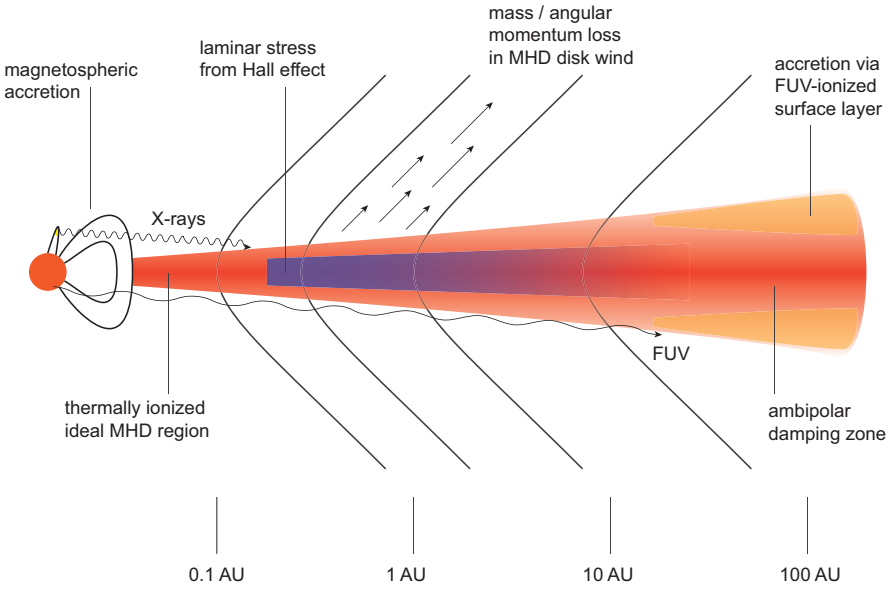

Fig. 21 A suggested structure for protoplanetary disks *if* MHD processes dominate over other sources of transport. The different regions are defined by the strength of non-ideal MHD terms (Ohmic diffusion, ambipolar diffusion and the Hall effect), and by mass and angular momentum loss in MHD disk winds. The Hall effect is predicted to behave differently if the net field threading the disk is anti-aligned to the rotation axis (here, alignment is assumed). Ionization by stellar X-rays and by FUV photons couples the stellar properties to those of the disk.

4.5 Transport in the boundary layer

The nature of transport in the boundary layer deserves a brief discussion. As discussed in §3.2.1 boundary layers are expected when the accretion rate is high enough to overwhelm the disruptive influence of the stellar magnetosphere (see equation 75 for a semi-quantitative statement of this condition). For most stars this requires high accretion rates, so the boundary layer and adjacent disk are hot enough to put us into the regime of thermal ionization and ideal MHD. In the disk, we then expect angular momentum transport via the MRI. In the boundary layer, however, we face a problem. By definition, $\mathrm{d}\Omega/\mathrm{dr} > 0$ in the boundary layer (see Figure 9), and this angular velocity profile is *stable* against the MRI (equation 125). Something else much be responsible for transport in this region.

The angular velocity profile in the boundary layer is stable against the generation of turbulence by either the Rayleigh criterion or the MRI. It turns out to be

unstable, however, to the generation of waves via a mechanism analogous to the hydrodynamic Papaloizou-Pringle instability of narrow tori [264]. Belyaev et al. [51, 52], using both analytic and numerical arguments, have shown that waves generated from the supersonic shear provide non-local transport of angular momentum (and energy) across the boundary layer. Magnetic fields are amplified by the shear [13] but do not play an essential role in boundary layer transport [52]. In protostellar systems boundary layers are present during eruptive accretion phases (see §5) when strong radiation fields are present [176]. Future work will need to combine the recent appreciation of the importance of wave angular momentum transport with radiation hydrodynamics for a full description of the boundary layer.

5 Episodic accretion

Young stellar objects (YSOs) are observed to be variable. The short time scale (lasting hours to weeks) component of that variability is complex [84], but can probably be attributed to a combination of turbulent inhomogeneities in the inner disk, stellar rotation [61], and the complex dynamics of magnetospheric accretion [2]. There is also longer time scale variability — lasting from years to (at least) many decades, that in some cases takes the form of well-defined outbursts in which the YSO brightens dramatically. The traditional classification of outbursting sources divides them into FU Orionis events [145, 139], characterized by a brightening of typically 5 magnitudes followed by a decay over decades, and EXors [146], which display repeated brightenings of several magnitudes over shorter time scales. The statistics on these uncommon long-duration outbursts (especially FU Orionis events [148]) are limited, and it is not even clear — either observationally or theoretically — whether FUOrs and EXors are variations on a theme or genuinely different phenomena [21]. Nonetheless, it is established that episodic accretion is common enough to matter for both stellar accretion and for planet formation processes occurring in the inner disk [21]. Our focus here is on the origin of these accretion outbursts.

Observations show that FU Orionis outbursts involve a large increase in the mass accretion rate through the inner disk on to the star [139]. During the outburst the inner disk will be relatively thick ($h/r \approx 0.1$), and hot enough to be thermally ionized. We therefore expect efficient angular momentum transport from the MRI, with $\alpha \approx 0.02$. Writing the viscous time scale (equation 58) in terms of these parameters,

$$t_\nu = \frac{1}{\alpha\Omega}\left(\frac{h}{r}\right)^{-2}, \tag{176}$$

we can estimate the disk radius associated with a (viscously driven) outburst of duration $t_{\rm burst}$,

$$r \simeq (GM_*)^{1/3}\,\alpha^{2/3}\left(\frac{h}{r}\right)^{4/3} t_{\rm burst}^{2/3}. \tag{177}$$

For a Solar mass star we find,

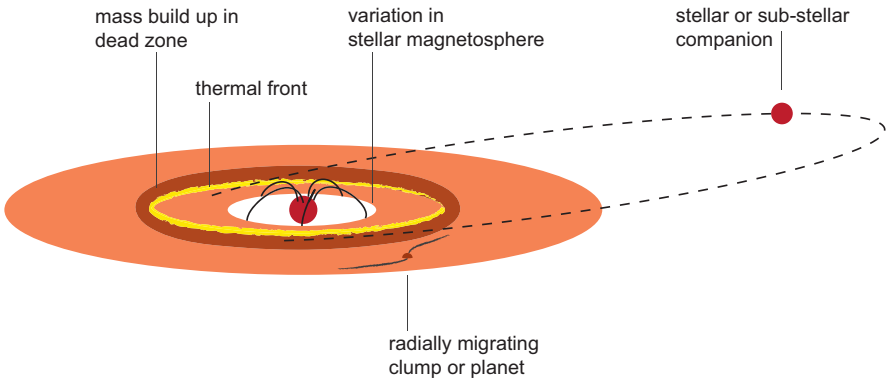

Fig. 22 An illustration of some of the processes suggested as the origin of episodic YSO accretion.

$$r \simeq 0.25 \left(\frac{\alpha}{0.02}\right)^{2/3} \left(\frac{h/r}{0.1}\right)^{4/3} \left(\frac{t_{\rm burst}}{100\ {\rm yr}}\right)^{2/3} {\rm AU}. \tag{178}$$

Disk-driven outbursts of broadly the right duration are thus likely to involve events on sub-AU scales, and could be associated physically with the magnetosphere, with the thermally ionized inner disk, or with the inner edge of the dead zone.

The physical origin of episodic accretion in YSOs has not been securely identified. Mooted ideas, illustrated in Figure 22, fall into two categories. The first category invokes secular instabilities of protoplanetary disk structure that may occur on AU and sub-AU scales. The idea is that the inner disk may be intrinsically unable to accrete at a steady rate, and instead alternates between periods of high accretion rate when gas is draining on to the star and periods of low accretion rate when gas is accumulating in the inner disk. The instability could be a classical thermal instability [50], of the type accepted as causing dwarf nova outbursts [193], or a related instability of dead zone structure [120, 18]. The second category appeal to triggers independent of the inner disk to initiate the outburst. Ideas in this class are various and include perturbations from binary companions [59], the tidal disruption of radially migrating gas clumps / giant planets [342, 242], and disk variability linked to a stellar magnetic cycle [11]. Neither category of ideas is fully compelling (in the sense of being both fully worked out and consistent with currently accepted disk physics), so our discussion here will focus on a few key concepts that are useful for understanding current and future models of episodic accretion.

5.1 Secular disk instabilities

The classical instabilities that may afflict thin accretion disks are the thermal and viscous instabilities [276]. These are quite distinct from the basic fluid dynamical instabilities (the MRI, the VSI etc) that we discussed in §4, in that they address

the stability of derived disk models rather than the fluid per se. Thus the thermal instability is an instability of the equilibrium vertical structure of the disk, while viscous instability in an instability of an (assumed) smooth radial structure under viscous evolution.

Before discussing how thermal or viscous instability might arise, we first define what these terms mean. Consider an annulus of the disk that is initially in hydrostatic and thermal equilibrium, such that the heating rate Q_+ matches the cooling rate Q_-. The heating rate per unit area depends upon the central temperature (equation 80), and can be written assuming the α-prescription as,

$$Q_+ = \frac{9}{4}\nu\Sigma\Omega^2 = \frac{9}{4}\alpha\frac{k_B T_c}{\mu m_H}\Sigma\Omega. \tag{179}$$

The cooling rate directly depends upon the effective temperature, $T_{\rm disk}$, but this can always be rewritten in terms of T_c using a calculation of the vertical thermal structure (§3.3). In the simple case when the disk is optically thick, for example, we have from equation (87) that $T_c^4/T_{\rm disk}^4 \simeq (3\tau/4)$, and hence,

$$Q_- = \frac{8\sigma}{3\tau}T_c^4. \tag{180}$$

Both α and τ may be functions of T_c. Now consider perturbing the central temperature on a time scale that is long compared to the dynamical time scale (so that hydrostatic equilibrium holds) but short compared to the viscous time scale (so that Σ remains fixed)[9]. The disk will be unstable to runaway heating if an upward perturbation to the temperature increases the heating rate more than it increases the cooling rate, i.e. if,

$$\frac{{\rm d}\log Q_+}{{\rm d}\log T_c} > \frac{{\rm d}\log Q_-}{{\rm d}\log T_c}. \tag{181}$$

The same criterion predicts runaway cooling in the event of a downward perturbation. A disk that is unstable in this sense is described as *thermally unstable*. It would heat up (or cool down) until it finds a new structure in which heating and cooling again balance.

To determine the condition for viscous stability, we start by considering a steady-state solution $\Sigma(r)$ to the diffusive disk evolution equation (52). Following Pringle [276] we write $\mu \equiv \nu\Sigma$ and consider perturbations $\mu \to \mu + \delta\mu$ on a time scale long enough that *both* hydrostatic and thermal equilibrium hold (in this limit T_c is uniquely determined and $\nu = \nu(\Sigma)$). Substituting in equation (52) the perturbation $\delta\mu$ obeys,

$$\frac{\partial}{\partial t}(\delta\mu) = \frac{\partial\mu}{\partial\Sigma}\frac{3}{r}\frac{\partial}{\partial r}\left[r^{1/2}\frac{\partial}{\partial r}\left(r^{1/2}\delta\mu\right)\right]. \tag{182}$$

The perturbation $\delta\mu$ will grow if the diffusion coefficient, which is proportional to $\partial\mu/\partial\Sigma$, is negative. This is *viscous instability*, and it occurs if,

[9] This may seem to require fine tuning, but in fact the ordering of time scales in a geometrically thin disk always allows for such a choice [276].

$$\frac{\partial}{\partial \Sigma}(\nu\Sigma) < 0. \tag{183}$$

A disk that is viscously unstable would tend to break up into rings, whose amplitude would presumably be limited by the onset of fluid instabilities that could be thought of as modifying the $\nu(\Sigma)$ relation.

5.1.1 The S-curve: a toy model

The instabilities of interest for YSO episodic accretion can broadly be considered to be thermal-type instabilities. Noting that $Q_+ \propto \alpha T_c$, and $Q_- \propto T_c^4/\tau \propto T_c^4/\kappa$ (where κ is the opacity at temperature T_c), we see that instability may occur according to equation (181) if,

- $\mathrm{d}\log Q_+/\mathrm{d}\log T_c$ is large, i.e. if α is strongly increasing with temperature.
- $\mathrm{d}\log Q_-/\mathrm{d}\log T_c$ is small, i.e. if κ is strongly increasing with temperature.

We expect α to increase rapidly with T_c at temperatures around 10^3 K, as we transition between damped non-ideal MHD turbulence at low temperature and the more vigorous ideal MHD MRI at higher temperature. We expect κ to increase most strongly at temperatures around 10^4 K, as hydrogen is becoming ionized and there is a strong contribution to the opacity from H^- scattering (in this regime κ can vary as something like T^{10} [50]). Either of these changes can result in instability.

Before detailing the specifics of possible thermal and dead zone instabilities in protoplanetary disks, it is useful to analyze a toy model that displays their essential features. We consider an optically thick disk, described by the usual classical equations [111], whose angular momentum transport efficiency α and opacity κ are both piece-wise constant functions of central temperature T_c. Specifically,

$$\begin{aligned} T_c < T_{\rm crit} &: \alpha = \alpha_{\rm low}, \kappa = \kappa_{\rm low}, \\ T_c > T_{\rm crit} &: \alpha = \alpha_{\rm high}, \kappa = \kappa_{\rm high}, \end{aligned} \tag{184}$$

with $\alpha_{\rm low} \leq \alpha_{\rm high}$ and $\kappa_{\rm low} \leq \kappa_{\rm high}$. Our goal is to calculate the explicit form of the $\dot{M}(\Sigma)$ relation in the "low" and "high" states below and above the critical temperature $T_{\rm crit}$. For a steady-state disk, at $r \gg R_*$, heated entirely by viscous dissipation, the equations we need (mostly from §3) read,

$$\begin{aligned} T_{\rm disk}^4 &= \frac{3\Omega^2}{8\pi\sigma}\dot{M}, \\ \frac{T_c^4}{T_{\rm disk}^4} &= \frac{3}{4}\tau, \\ \tau &= \frac{1}{2}\kappa\Sigma, \\ \nu\Sigma &= \frac{\dot{M}}{3\pi}, \end{aligned}$$

$$\nu = \alpha \frac{c_s^2}{\Omega} = \frac{\alpha}{\Omega} \frac{k_B T_c}{\mu m_H}. \tag{185}$$

Note that the stellar mass M_* and radius in the disk r enter these formulae only via their combination in the Keplerian angular velocity Ω. Eliminating T_c, $T_{\rm disk}$, τ and ν between these equations, we obtain a solution for $\dot{M}(\Sigma)$,

$$\dot{M} = \frac{9\pi}{4} \left(\frac{k_B^4}{\mu^4 m_H^4 \sigma} \right)^{1/3} \kappa^{1/3} \alpha^{4/3} \Omega^{-2/3} \Sigma^{5/3}, \tag{186}$$

valid on either the low or the high branch when the appropriate values for α and κ are inserted. A solution on the low branch is possible provided that $\Sigma \leq \Sigma_{\rm max}$, where $\Sigma_{\rm max}$ is defined by the condition that $T_c = T_{\rm crit}$. Similarly, a high branch solution requires $\Sigma \geq \Sigma_{\rm min}$ with $T_c = T_{\rm crit}$ at $\Sigma_{\rm min}$. The limiting surface densities are given by,

$$\begin{aligned} \Sigma_{\rm max} &= \frac{8}{3^{3/2}} \left(\frac{\mu m_H \sigma}{k_B} \right)^{1/2} \Omega^{-1/2} T_{\rm crit}^{3/2} \kappa_{\rm low}^{-1/2} \alpha_{\rm low}^{-1/2}, \\ \Sigma_{\rm min} &= \frac{8}{3^{3/2}} \left(\frac{\mu m_H \sigma}{k_B} \right)^{1/2} \Omega^{-1/2} T_{\rm crit}^{3/2} \kappa_{\rm high}^{-1/2} \alpha_{\rm high}^{-1/2}. \end{aligned} \tag{187}$$

If $\kappa_{\rm high} > \kappa_{\rm low}$ and / or $\alpha_{\rm high} > \alpha_{\rm low}$, then $\Sigma_{\rm max} > \Sigma_{\rm min}$ and there will be a range of surface densities where accretion rates corresponding to either the low or the high branch are possible.

Figure 23 shows, for a fairly arbitrary choice of the model parameters, the thermal equilibrium solutions that correspond to the low and high states of the disk annulus. One should not take the results of such a toy model very seriously, but it captures several features of more realistic models,

- The solution has stable thermal equilibrium solutions on two branches, a low state branch where $\dot{M}$ for a given surface density is small, and a high state branch where it is substantially larger. In the toy model these branches are entirely separate, but in more complete models they are linked by an *unstable* middle branch (giving the plot the appearance of an "S"-curve).
- There is a range of surface densities for which either solution is possible.
- There is a band of accretion rates for which no stable equilibrium solutions exist.
- The position of the S-curve in the $\Sigma - \dot{M}$ plane is a function of radius, with the band of forbidden accretion rates moving to higher $\dot{M}$ further from the star.

The S-curve is derived from a local analysis, and the existence of annuli whose thermal equilibrium solutions have this morphology is a necessary but not sufficient condition for a global disk outburst. That time dependent behavior of some sort is inevitable can be seen by supposing that the annulus at 0.25 AU in Figure 23 is fed with gas from outside at a rate that falls into the forbidden band. No stable thermal equilibrium solution with this accretion rate is possible. If the disk is initially on the lower branch, the rate of gas supply exceeds the transport rate through the annulus,

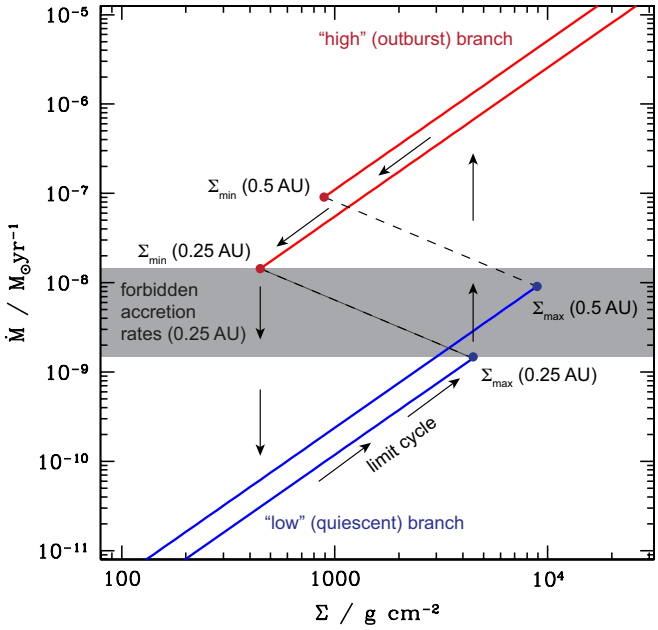

Fig. 23 Example S-curves in the accretion rate–surface density plane from the toy model described in the text. For these curves we take $\kappa_{\rm low} = \kappa_{\rm high} = 1$ cm^2 g^{-1}, $\alpha_{\rm low} = 10^{-4}$, $\alpha_{\rm high} = 10^{-2}$, and $T_{\rm crit} = 10^3$ K. The lower of the two curves is for $\Omega = 1.6 \times 10^{-6}$ s^{-1} (0.25 AU for a Solar-mass star), the upper for $\Omega = 5.6 \times 10^{-7}$ s^{-1} (0.5 AU).

and the surface density increases. This continues until Σ reaches and exceeds $\Sigma_{\rm max}$, at which point the only available solution lies on the high branch at much higher accretion rate. The annulus transitions to the high branch, where the transport rate is now larger than the supply rate, and the surface density starts to drop. The cycle is completed when Σ falls below $\Sigma_{\rm min}$, triggering a transition back to the low state.

The evolution of a disk that is potentially unstable (i.e. one that has some annuli with S-curve thermal equilibria) is critically dependent upon the *radial* flow of mass and heat, which are the key extra ingredients needed if an unstable disk is to "organize" itself and produce a long-lived outburst. To see this, imagine a disk where annuli outside r_f are already on the high branch of the S-curve, while those inside remain on the low branch. The strong radial gradient of T_c implies a similarly rapid change in ν, which leads to a large mass flux from the annuli that are already in outburst toward those that remain quiescent (equation 53). The resulting increase in surface density, along with the heat that goes with it, can push the neighboring annulus on to the high branch, initiating a propagating "thermal front" that triggers a large scale transition of the disk into an outburst state.

The quantitative modeling of global disk evolution including these thermal processes is well-developed within the classical α disk formalism [193]. For a minimal

model, all that is needed is to supplement the disk evolution equation (52) with a model for the vertical structure (conceptually as described for the toy model above) and an equation for the evolution of the central temperature. This takes the form [65, 193],

$$\frac{\partial T_c}{\partial t} = \frac{Q_+ - Q_-}{c_p \Sigma} - \frac{\mathscr{R} T_c}{\mu c_p} \frac{1}{r} \frac{\partial}{\partial r} (r v_r) - v_r \frac{\partial T_c}{\partial r} + ... \tag{188}$$

Here c_p is the specific heat capacity at constant pressure, and $\mathscr{R}$ is the gas constant. The first term on the right hand side describes the direct heating and cooling due to viscosity and radiative losses, while the second and third terms describe $P\mathrm{d}V$ work and the advective transport of heat associated with radial mass flows. In general there should be additional terms to represent the radial flow of heat due to radiative and / or turbulent diffusion (these effects are small in most thin disk situations, but become large when there is an abrupt change in T_c at a thermal front). The treatment of these additional terms is somewhat inconsistent in published models, though they can significantly impact the character of derived disk outbursts [254].

5.1.2 Classical thermal instability

In physical rather than toy models for episodic accretion α and κ are smooth rather than discontinuous functions of the temperature. A local instability, with a resulting S-curve, occurs if one or both of these functions changes sufficiently rapidly with T_c (so that equation 181 is satisfied). No simple condition specifies when a disk that has some locally unstable annuli will generate well-defined global outbursts, but loosely speaking outbursts occur provided that the branches of the S-curve (and the values of $\Sigma_{\rm max}$ and $\Sigma_{\rm min}$) are well separated.

The classical cause of disk thermal instability is the rapid increase in opacity associated with the ionization of hydrogen, at $T \simeq 10^4$ K. Around this temperature κ can rise as steeply as T^{10}, and the disk will invariably satisfy at least the condition for local thermal instability. The evolution of disks subject to a hydrogen ionization thermal instability was first investigated as a model for dwarf novae (eruptive disk systems in which a white dwarf accretes from a low-mass companion star) [136, 234], and subsequently applied to low-mass X-ray binaries. Thermal instability models provide a generally good match to observations of outbursts in these systems (which are of shorter duration that YSO outbursts, and correspondingly better characterized empirically), and are accepted as the probable physical cause. Good fits to data require models to include not only the large change in κ that is the cause of classical thermal instability, but also changes in α between the low and high branches of the S-curve. Typically $\alpha_{\rm low} \leq 10^{-2}$, whereas $\alpha_{\rm high} \sim 0.1$ [174]. MHD simulations that include radiation transport have shown that the S-curve derived from α disk models can be approximately recovered as a consequence of the MRI, and that the difference in stress between the quiescent and outburst states may be attributable to the development of vertical convection within the hot disk [149].

By eye, the light curves of FU Orionis events look quite similar to scaled versions of dwarf novae outbursts, so the success of thermal instability models in the latter

sphere makes them a strong candidate for YSO accretion outbursts. The central temperature of some outbursting FUOr disks, moreover, almost certainly does exceed the 10^4 K needed to ionize hydrogen, making it inevitable that thermal instability physics will play some role in the phenomenon. Detailed thermal instability models of FU Orionis events were constructed by Bell & Lin [50], who combined a one-dimensional (in r) treatment of the global evolution with detailed α model vertical structure calculations. They were able to find periodic solutions that describe "self-regulated" disk outbursts (i.e., requiring no external perturbation or trigger), with the disk alternating between quiescent periods (with $\dot{M} = 10^{-8} - 10^{-7}\ M_\odot\ \mathrm{yr}^{-1}$) and outburst states (with $\dot{M} \geq 10^{-5}\ M_\odot\ \mathrm{yr}^{-1}$). These properties, and the inferred outburst duration of $\sim 10^2$ yr, are in as good an agreement with observations as could reasonably be expected given the simplicity of the model.

The weakness of classical thermal instability models as an explanation for YSO accretion outbursts is that they require unnatural choices of the viscosity parameter α [12]. Thermal instability is indisputably tied to the hydrogen ionization temperature, which exceeds even the mid-plane temperatures customarily attained in protoplanetary disks. The required temperatures can be reached (if at all) only extremely close to the star, and the radial region affected by instability extends to no more than 0.1-0.2 AU. The viscous time scale on these scales is short, so matching the century-long outbursts seen in FUOrs requires a very weak viscosity — Bell & Lin [50] adopt $\alpha_{\mathrm{high}} = 10^{-3}$. This is at least an order of magnitude lower than the expected efficiency of MRI transport under ideal MHD conditions [89, 309]. Moreover, in the specific case of FU Orionis itself, radiative transfer models suggest that the region of high accretion rate during the outburst extends out to 0.5-1 AU [356], substantially larger than would be expected in the thermal instability scenario.

5.1.3 Instabilities of dead zones

A dead zone in which the MRI is suppressed by Ohmic resistivity (§4.4.3) supports a related type of instability whose high and low states are distinguished primarily by different values of α, rather than by the thermal instability's different values of κ. The origin of instability is clear within Gammie's original conception [119] of the dead zone, which has a simple two-layer structure. The surface of the disk, ionized by X-rays[10], is MRI-active and supports accretion with a local $\alpha \sim 10^{-2}$. Below a critical column density Ohmic resistivity completely damps MRI-induced turbulence (according to equation 170), and the disk is dead with $\alpha = 0$. This structure can be bistable if the surface density exceeds that of the ionized surface layer. The low accretion rate state corresponds to a cool, externally heated disk with a dead zone; the high accretion rate state to a hot thermally ionized disk at the same Σ.

Martin & Lubow [228, 230] have shown that the local physics of Ohmic dead zone instability can be analyzed in an manner closely analogous to thermal instability. The sole difference lies in the reason why the lower state ceases to exist above a

[10] Cosmic rays in the original model, though this is an unimportant distinction.

critical surface density ($\Sigma_{\rm max}$ in Figure 23). For thermal instability $\Sigma_{\rm max}$ is set by the onset of ionization at the disk mid-plane, and the attendant rise in opacity. A simple dead zone, however, *does not get hotter with increasing* Σ, because the heating (either from irradiation, or viscous dissipation in the ionized surface layer) occurs at low optical depth at a rate that is independent of the surface density. It is then not obvious how even a very thick dead zone can be heated above 10^3 K, "ignited", and induced to transition to the high state of the S-curve.

One way to trigger a jump to the high state is to postulate that some source of turbulence other than the MRI is present to heat the disk. Gammie [120] suggested that inefficient transport through the ionized surface layer would lead to the build of mass in the dead zone [119] until $Q \approx 1$ and self-gravity sets in (see §4.2). We can readily estimate the properties we might expect for an instability triggered in this manner by the onset of self-gravity at small radii. Suppose that at 1 AU the temperature in the quiescent (externally irradiated) disk state is 150 K. Then to reach $Q = 1$ requires gas to build up until $\Sigma \simeq 7 \times 10^4$ g cm^{-2}, at which point the mass interior is $M \sim \pi r^2 \Sigma \sim 0.025\, M_\odot$. This is comparable to the amount of mass accreted per major FU Orionis-like outburst. In the outburst state the disk will be moderately thick (say $h/r = 0.3$ [49]), and the viscous time scale $(1/\alpha\Omega)(h/r)^{-2}$ works out to be about 200 yr for $\alpha = 0.01$, again similar to inferred FUOr time scales. At this crude level of estimate, it therefore seems possible that a self-gravity triggered dead zone instability could be consistent both with the inferred size of the outbursting region [356] and with theoretical best guesses as to the strength of angular momentum transport in ideal MHD conditions.

Time-dependent models for outbursts arising from a dead zone instability were computed by Armitage et al. [18], and subsequently by several groups in both one-dimensional [359, 357, 228, 254] and two-dimensional models [358, 24]. The more recent studies show that a self-gravity triggered instability of an Ohmic dead zone can give rise to outbursts whose properties are broadly consistent with those of observed FUOrs. Instability persists even if there is a small residual viscosity within the dead zone [23, 230], which could arise hydrodynamically in response to the "stirring" from the overlying turbulent surface layer [105].

It is established that Gammie's dead-zone structure, as originally postulated [119], can be unstable to the development of a limit cycle in which outbursts and quiescent intervals alternate. It is much less clear whether a more realistic (we think) inner disk structure, affected by all three non-ideal terms (§4.4.4), evolves in a similar way. Ambipolar diffusion can damp turbulence in the low density surface layer, while the Hall effect (and winds) can lead to significant laminar stresses. It remains to be shown that our best theoretical models for disks on AU scales are locally unstable in the same way as a simple Ohmic dead zone, and to investigate the type of global outbursts that any instabilities might yield. The Hall effect and / or winds could in principle also lead to entirely different types of eruptive behavior.

5.2 Triggered accretion outbursts

Accretion variability, including (perhaps) the large scale outbursts of FUOrs, can also be triggered by processes largely independent of the inner disk itself. Stellar activity cycles, binaries with small periastron distances, and tidal disruption of gaseous clumps or planets may all contribute.

5.2.1 Stellar activity cycles

As discussed in §3.2.2 the inner disk is expected [178] and observed [60] to be disrupted by the stellar magnetosphere. The complex dynamics of the interaction between the field — which may be misaligned to the stellar spin axis and have non-dipolar components — and the disk [190] is likely the dominant cause of T Tauri variability on time scales comparable to the stellar rotation period (i.e. days to weeks). If the strength of the field also varies systematically due to the presence of activity cycles analogous to the Solar cycle, these could trigger longer time scale (years to decades) accretion variability. The simplest mechanism is modulation of the magnetospheric radius across corotation [79]. When the field is strong and $r_m > r_{\rm co}$ the linkage between the stellar field lines and the disks adds angular momentum to the disk, impeding accretion in the same way as gravitational torques from a binary (§3.2.3)[11]. Gas then accumulates just outside the magnetospheric radius, and can subsequently be accreted in a burst when the field weakens.

The viability of such magnetically "gated" accretion as an origin for large scale variability is limited by the short viscous time scale of the disk at $r \approx r_m$, which makes it hard to accumulate large masses of gas if the stellar fields are, as expected, of no more than kG strength. Models [11] suggest that significant decade-long variability could be associated with protostellar activity cycles, but there is no clear path to generating FU Orionis outbursts. Activity cycles are more promising as an explanation for lower amplitude, periodic EXor outbursts [88]. We note that there has been little if any work on the possible interactions between time-variable stellar magnetic fields and an inner disk that has its own net field.

5.2.2 Binaries

An eccentric binary with an AU-scale periastron distance could funnel gas into the inner disk, increasing the accretion rate and leading to an outburst if the increased surface density is high enough to trigger thermal or dead zone instability. This mechanism was proposed by Bonnell & Bastien [59], and has subsequently been studied with higher resolution simulations [270, 108]. Although there are some differences between the predicted outbursts and those observed (this is almost inevitable, as the limited sample of FUOrs is already quite diverse), it is clear that close encounters

[11] In compact object accretion, this is described as the "propellor" regime of accretion [153].

from binary or cluster companions induce episodes of substantially enhanced accretion. The obvious prediction — that FUOrs ought to be found with observable binary companions or preferentially associated with higher-density star forming regions — is neither confirmed nor ruled out given the small sample of known objects.

5.2.3 Clump tidal disruption

A final possibility is that accretion outbursts could be triggered by the tidal disruption of a bound object (a planet or gas cloud) that migrates too close to the star. The necessary condition for this to occur is given by the usual argument for the Roche limit. If we consider a planet with radius R_p and mass M_p, orbiting a star of mass M_* at radius r, the differential (tidal) gravitational force between the center of the planet and its surface is,

$$F_{\rm tidal} = \frac{GM_*}{r^2} - \frac{GM_*}{(r+R_p)^2} \simeq \frac{2GM_*}{r^3} R_p. \tag{189}$$

Equating the tidal force to the planet's own self-gravity, $F_{\rm self} = GM_p/R_p^2$, we find that tidal forces will disrupt the planet at a radius $r_{\rm tidal}$ given approximately by,

$$r_{\rm tidal} = \left(\frac{M_*}{M_p}\right)^{1/3} R_p. \tag{190}$$

An equivalent condition is that tidal disruption occurs when the mean density of the planet $\bar{\rho} < M_*/r^3$.

It is difficult to tidally disrupt a mature giant planet. A Jupiter mass planet has a radius of $R_p \simeq 1.5\ R_J$ at an age of 1 Myr [226], and will not be disrupted outside the photospheric radius of a typical young star. (Though such planets, if present in the inner disk, could alter the course of thermal or dead zone instability [82, 207].) If tidal disruption is to be relevant to episodic accretion we require, first, that the outer disk is commonly gravitationally unstable to fragmentation, and, second, that the clumps that form migrate rapidly inward (in the Type 1 regime discussed by Kley in this volume) without contracting too rapidly. Numerical evidence supports the idea that clump migration can be rapid [342, 47, 70, 235], though it is at best unclear whether contraction can be deferred sufficiently to deliver clumps that would be tidally disrupted on sub-AU scales [118]. Assuming that these pre-conditions are satisfied, however, Nayakshin & Lodato [242] studied the tidal mass loss from the close-in planets and its impact on the disk. They found that the tidal disruption of $\sim 20\ R_J$ clumps, interior to 0.1 AU, led to accretion outbursts consistent with the basic properties of FUOrs.

The primary theoretical doubts about tidal disruption as a source of outbursts concern the relative rates of inward migration and clump contraction, which are both hard to calculate at substantially better than order of magnitude level. Observa-

tionally, this process would produce outbursts in systems whose disks were young, massive, and probably still being fed by envelope infall.

Predicting the evolution of the inner disk on year-to-century time scales from first principles is extremely hard, and none of the mechanisms for episodic accretion discussed in this section has been subject to strict enough scrutiny to merit dogmatic conclusions. Each comes with its own theoretical caveats, and *no single mechanism* seems well-suited to explain the entire range of outburst behavior seen in YSOs [21]. Episodic accretion may be caused by a significant modification of a known process, a combination of known processes, or a process yet to be identified.

6 Single particle evolution

The evolution of solid particles within disks differs from that of gas because solid bodies are unaffected by pressure gradients but do experience aerodynamic forces. We discuss here how these differences affect the motion of single particles orbiting within the gas disk, and how we can describe the evolution of a "fluid" made up of small solid particles interacting aerodynamically with the gas. Issues such as the rate and outcome of particle collisions, that are central to early stage planet formation, are treated in the accompanying chapter by Kley, and elsewhere [15].

The key parameter describing the aerodynamic coupling between solid particles and gas is the *stopping time*. For a particle of mass m that is moving with velocity Δv relative to the local gas, the stopping time is defined as,

$$t_s \equiv \frac{m\Delta v}{|F_{\rm drag}|}, \tag{191}$$

where $F_{\rm drag}$ is the magnitude of the aerodynamic drag force that acts in the opposite direction to Δv. Very frequently, what matters most is how the stopping time compares to the orbital time at the location of the particle. We therefore define a dimensionless stopping time by multiplying t_s by the orbital frequency $\Omega_{\rm K}$,

$$\tau_s \equiv t_s \Omega_{\rm K}. \tag{192}$$

The dimensionless stopping time is also called the *Stokes number*.

For our immediate purposes it largely suffices to describe aerodynamic effects in terms of the stopping time, but eventually you will want to translate the results into concrete predictions for how particles of various sizes and material properties behave. This requires specifying $F_{\rm drag}$, whose form depends on the size of the particle relative to the mean free path of gas molecules, and (in the fluid regime) on the Reynolds number of the flow around the particle [349]. If the particle radius s is

small compared to the mean free path λ ($s < 9\lambda/4$) the particle experiences *Epstein drag*, with a drag force,

$$\mathbf{F}_{\rm drag} = -\frac{4\pi}{3}\rho s^2 v_{\rm th}\Delta\mathbf{v}. \tag{193}$$

Here ρ is the density of the surrounding gas, and the thermal speed of the molecules,

$$v_{\rm th} = \sqrt{\frac{8k_BT}{\pi\mu m_H}} \tag{194}$$

is roughly the same as the sound speed. Because Epstein drag is proportional to the velocity difference Δv (rather than the more familiar square of the velocity difference), the stopping time is a function of the particle properties that is independent of the velocity difference. For a spherical particle of material density ρ_m,

$$t_s = \frac{\rho_m}{\rho}\frac{s}{v_{\rm th}}. \tag{195}$$

The mean free path in protoplanetary disks is of the order of cm (larger in the outer disk), so the Epstein regime is relevant for particles that range from dust to those of small macroscopic dimensions. Drag laws appropriate for larger bodies, which fall into the Stokes regime of drag, are given by Whipple [349].

6.1 Radial drift

The most important consequence of aerodynamic forces is the phenomenon of *radial drift*. In §2.1.2 we showed that radial pressure gradients result in a gas orbital velocity that differs from the Keplerian value by 50-100 m s^{-1} (using typical disk parameters at 1 AU). Most commonly, the gas is partially supported against gravity by the pressure gradient, and so rotates more slowly than the Keplerian value. Let us consider how this velocity differential affects the evolution of solids in various limits, initially ignoring turbulence and ignoring the feedback of aerodynamic forces *on the gas*, and then including these processes.

6.1.1 Particle drift without feedback

Large bodies ($\tau_s \gg 1$) orbit at close to the Keplerian speed, and the effect of gas on their evolution can be considered as a simple "headwind" if the disk is sub-Keplerian. Suppose that the gas orbits at a speed $v_K - \Delta v$, with $\Delta v \ll v_K$. The drag force $|F_{\rm drag}| = m\Delta v\Omega_{\rm K}/\tau_s$ does work at a rate,

$$\dot{E} \simeq -|F_{\rm drag}|v_K, \tag{196}$$

that leads to a change in the orbital energy $E = -GM_*m/2a$, where a is the radius of the orbit. Noting that,

$$\dot{E} = \frac{GM_*m}{2a^2}\frac{\mathrm{d}a}{\mathrm{d}t}, \tag{197}$$

and equating the two expressions for $\dot{E}$, we find that the orbit decays at a speed $v_r = \mathrm{d}a/\mathrm{d}t$ that is given by,

$$v_r = -\frac{2}{\tau_s}\Delta v. \tag{198}$$

The radial drift of large bodies is inversely proportional to their Stokes number.

The simple headwind argument fails for small particles with $\tau_s \ll 1$, which instead are forced to orbit *at the gas speed* by the strong aerodynamic coupling. The particles do not feel the pressure gradient, so their non-Keplerian orbital motion results in a net radial force,

$$\frac{F_r}{m} = \frac{(v_K - \Delta v)^2}{a} - \frac{GM_*}{a^2} \simeq -\frac{2v_K\Delta v}{a}. \tag{199}$$

Equating this to the drag force for *radial* motion at speed v_r, $|F_{\rm drag}|/m = v_r\Omega_{\rm K}/\tau_s$, we find that radial drift for small particles occurs at the terminal drift speed,

$$v_r = -2\tau_s\Delta v. \tag{200}$$

This is the speed relative to the gas, so for a disk that is accreting there is an additional component given by the gas' radial velocity.

Intermediate-sized particles orbit at some speed between that of the gas and that given by the Keplerian velocity. To derive the general rate of radial drift [346, 322], we consider a gas disk whose orbital velocity is,

$$v_{\phi,\rm gas} = v_K\left(1-\eta\right)^{1/2}. \tag{201}$$

The parameter $\eta \propto (h/r)^2$. For example, if the disk has $\Sigma \propto r^{-1}$ and central temperature $T_c \propto r^{-1/2}$, we showed in §2.1.2 that $\eta = (11/4)(h/r)^2$. Defining the particle radial and azimuthal velocities to be v_r and v_ϕ respectively, the equations of motion are,

$$\frac{\mathrm{d}v_r}{\mathrm{d}t} = \frac{v_\phi^2}{r} - \Omega_{\rm K}^2 r - \frac{1}{t_{\rm s}}\left(v_r - v_{r,\rm gas}\right) \tag{202}$$

$$\frac{\mathrm{d}}{\mathrm{d}t}\left(rv_\phi\right) = -\frac{r}{t_{\rm s}}\left(v_\phi - v_{\phi,\rm gas}\right). \tag{203}$$

The azimuthal equation can be simplified by noting that the specific angular momentum remains close to Keplerian,

$$\frac{\mathrm{d}}{\mathrm{d}t}\left(rv_\phi\right) \simeq v_r\frac{\mathrm{d}}{\mathrm{d}r}\left(rv_K\right) = \frac{1}{2}v_r v_K. \tag{204}$$

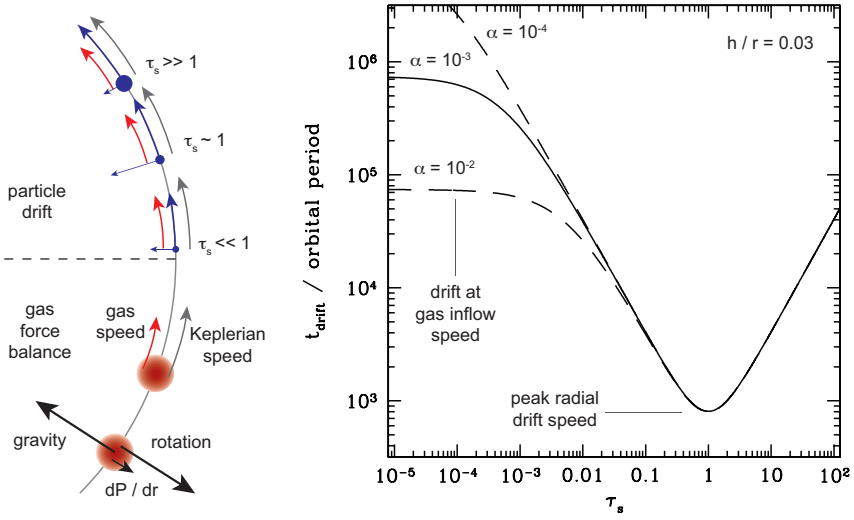

Fig. 24 Particles drift inwards in a disk wherever $\mathrm{d}P/\mathrm{d}r$, due to the combination of aerodynamic forces and sub-Keplerian gas rotation. The radial drift time scale $t_{\rm drift} = r/|v_r|$, in units of the local orbital period, is plotted as a function of the dimensionless stopping time τ_s. The fastest radial drift occurs for $\tau_s = 1$. The specific numbers shown in the plot are appropriate for a disk with $h/r = 0.03$ and α values of 10^{-2} (lowest curve on the left-hand side of the figure), 10^{-3} and 10^{-4}.

This yields,

$$v_\phi - v_{\phi,\rm gas} \simeq -\frac{1}{2}\frac{t_{\rm s} v_r v_K}{r}. \tag{205}$$

We now substitute for Ω_K in the radial equation using equation (201). Discarding higher order terms we obtain,

$$\frac{\mathrm{d}v_r}{\mathrm{d}t} = -\eta\frac{v_K^2}{r} + \frac{2v_K}{r}\left(v_\phi - v_{\phi,\rm gas}\right) - \frac{1}{t_{\rm s}}\left(v_r - v_{r,\rm gas}\right). \tag{206}$$

The $\mathrm{d}v_r/\mathrm{d}t$ term is negligible. Dropping that, we eliminate $(v_\phi - v_{\phi,\rm gas})$ between equations (205) and (206) to obtain,

$$v_r = \frac{(r/v_K)t_{\rm s}^{-1}v_{r,\rm gas} - \eta v_K}{(v_K/r)t_{\rm s} + (r/v_K)t_{\rm s}^{-1}}. \tag{207}$$

In terms of the Stokes number the final result for the particle radial velocity is,

$$v_r = \frac{\tau_{\rm s}^{-1}v_{r,\rm gas} - \eta v_K}{\tau_{\rm s} + \tau_{\rm s}^{-1}}. \tag{208}$$

The previously derived results for very small and very large particles are recovered by taking the appropriate limits.

The speed of the radial drift implied by equation (208) is shown in Figure 24. Very rapid drift is predicted for particles with $\tau_s \sim 1$. For our fiducial disk model with $\Sigma \propto r^{-1}$, $T_c \propto r^{-1/2}$ and $h/r = 0.03$, the radial drift time scale $t_{\rm drift} = r/|v_r|$ is just 10^3 orbital periods — one thousand years at 1 AU! Particles with this stopping time are very roughly meter-sized, and their rapid drift is the origin of the "meter-sized barrier" that severely constrains models of planetesimal formation [74, 160].

6.1.2 Drift with diffusion

If the disk is turbulent, small dust particles that are aerodynamically well-coupled to the gas will diffuse radially and vertically. (The same physics will apply to trace gas species, such as water or CO molecules.) Diffusion will tend to equalize the *concentration* of the dust or trace gas species relative to the dominant gaseous component in the disk. To derive an equation for the evolution of the trace species [81], we initially ignore any radial drift due to aerodynamic effects and write the concentration of the trace gas or dust (generically the "contaminant") as,

$$f = \frac{\Sigma_d}{\Sigma}, \tag{209}$$

where Σ_d is the surface density of the contaminant. If the contaminant is neither created nor destroyed within the region of the disk under consideration, continuity demands that,

$$\frac{\partial \Sigma_d}{\partial t} + \nabla \cdot \mathbf{F}_d = 0, \tag{210}$$

where $\mathbf{F}_d$, the flux, can be decomposed into two parts: an advective piece describing transport of the dust or gas with the mean disk flow, and a diffusive piece describing the tendency of turbulence to equalize the concentration of the contaminant across the disk. For $f \ll 1$ we can assume that the diffusive properties of the disk depend only on the *gas* surface density, in which case the flux can be written as,

$$\mathbf{F}_d = \Sigma_d \mathbf{v} - D\Sigma \nabla \left(\frac{\Sigma_d}{\Sigma} \right). \tag{211}$$

Here $\mathbf{v}$ is the mean velocity of gas in the disk and D is the turbulent diffusion coefficient. The diffusive term vanishes if f is constant. Combining this equation with the continuity equation for the gaseous component, we obtain an evolution equation for f in an axisymmetric disk. In cylindrical polar co-ordinates,

$$\frac{\partial f}{\partial t} = \frac{1}{r\Sigma} \frac{\partial}{\partial r} \left(Dr\Sigma \frac{\partial f}{\partial r} \right) - v_r \frac{\partial f}{\partial r}. \tag{212}$$

This result has the form of an advection-diffusion equation, with the advective component being due to the radial flow of the disk gas. It is easy to generalize this equa-

tion to account for the radial drift of larger particles that are imperfectly coupled to the gas, by adding an additional flux representing the radial drift speed [4].

Determining what is the appropriate value for the turbulent diffusion coefficient D involves many of the same uncertainties that afflict the determination of the turbulent viscosity. For trace gas species and very small dust particles the zeroth-order expectation is that $D \approx \nu$ [239], though simulations of non-ideal MHD disk turbulence show both significant deviations and anisotropy between the vertical and radial directions [362]. For larger bodies there is a well-determined analytic scaling with the Stokes number of the particles [353].

6.1.3 Particle pile-up

Solids that experience significant radial drift tend to become concentrated ("pile-up") in the inner disk [354, 351]. The basic effect is present in the simplest case where diffusion and inward drag by the mean flow are small, and feedback of the particles on the gas can be neglected. The radial drift speed is then, approximately,

$$v_r \simeq -\tau_s \eta v_K, \tag{213}$$

with $\eta \propto (h/r)^2$. For particles that are in the Epstein regime of drag, the stopping time in the mid-plane is (from equations 195 and 5),

$$t_s = \frac{\rho_m}{\rho_0}\frac{s}{v_{th}} = \sqrt{2\pi}\frac{\rho_m h}{\Sigma}\frac{s}{v_{th}}. \tag{214}$$

Since $h = c_s/\Omega$, and c_s and v_{th} differ only by a numerical factor, we obtain,

$$\tau_s = \frac{\pi}{2}\frac{\rho_m}{\Sigma}s. \tag{215}$$

Suppose now (perhaps not very realistically) that the surface density profile of solids has attained a steady-state, such that the mass flux is constant with radius. Then,

$$\dot{M}_d = -2\pi r \Sigma_d v_r = \text{constant}, \tag{216}$$

and substituting for v_r we find,

$$\frac{\Sigma_d}{\Sigma} \propto \left(\frac{h}{r}\right)^{-2} r^{-1/2}. \tag{217}$$

For a disk with constant (h/r) the steady-state concentration of solids increases closer to the star as $r^{-1/2}$. In the more realistic case of a flaring disk with mid-plane temperature profile, say, $T_c \propto r^{-1/2}$, the effect is stronger. A constant α model of

such a disk has a steady-state gas surface density profile $\Sigma \propto r^{-1}$, with the solids following $\Sigma_d \propto r^{-2}$.

6.1.4 The Nakagawa-Sekiya-Hayashi equilibrium

Up till now we have implicitly assumed that the evolution of the gas is unaffected by the evolution of the solids within it. Obviously this can never be strictly correct. If a population of solid particles are losing angular momentum to the gas through aerodynamic forces and spiraling inward, the gas must gain a corresponding amount of angular momentum. If the solid to gas ratio is only of the order of 1%, however, one might suppose that the effect of the angular momentum exchange on the gas would be small and, perhaps, ignorable. This is only partially true. First, a number of processes, including vertical particle settling [97], gas loss via photo-evaporation [327, 4] or MHD winds, and radial drift itself [351], can boost the solid to gas ratio, at least locally. Second, the equilibrium solution for radial drift in the presence of back reaction on to the gas can be unstable to the *streaming instability* [352], which can result in strong localized clumping of the solids.

The generalization of the radial drift formula (equation 208) to account for the back reaction of the drift on the gas is known as the Nakagawa-Sekiya-Hayashi (NSH) equilibrium [241]. The NSH solution is derived by considering the interaction between solids and gas in a simple disk model that ignores the effects of turbulence and vertical gravity. Both the gas, with density ρ_g, pressure P and velocity $\mathbf{v}_g$, and the solid particles, with density density ρ_p and velocity $\mathbf{v}_p$, are treated as fluids that interact with each other via aerodynamic drag. They obey continuity and momentum equations of the form [352],

$$\frac{\partial \rho_p}{\partial t} + \nabla \cdot (\rho_p \mathbf{v}_p) = 0, \tag{218}$$

$$\nabla \cdot \mathbf{v}_g = 0, \tag{219}$$

$$\frac{\partial \mathbf{v}_p}{\partial t} + \mathbf{v}_p \cdot \nabla \mathbf{v}_p = -\Omega_{\rm K}^2 \mathbf{r} - \frac{1}{t_s}(\mathbf{v}_p - \mathbf{v}_g), \tag{220}$$

$$\frac{\partial \mathbf{v}_g}{\partial t} + \mathbf{v}_g \cdot \nabla \mathbf{v}_g = -\Omega_{\rm K}^2 \mathbf{r} + \frac{1}{t_s}\frac{\rho_p}{\rho_g}(\mathbf{v}_p - \mathbf{v}_g) - \frac{\nabla P}{\rho_g}. \tag{221}$$

We have replaced the continuity equation for the gas with the condition for incompressibility, which is valid provided that velocities remain highly subsonic. The only other differences between the equations for the two species are the presence of a pressure gradient term in the gas momentum equation, and the pre-factor in the aerodynamic drag term expressing the differing inertia of the two fluids.

It is straightforward to derive the steady-state axisymmetric solution for the drift of solids and gas from the above equations [241, 352]. To illustrate the difference between the NSH and no-feedback solutions, we quote here just the result for the relative radial velocity of the solids and the gas. With our definition of η (equation 201) this takes the form,

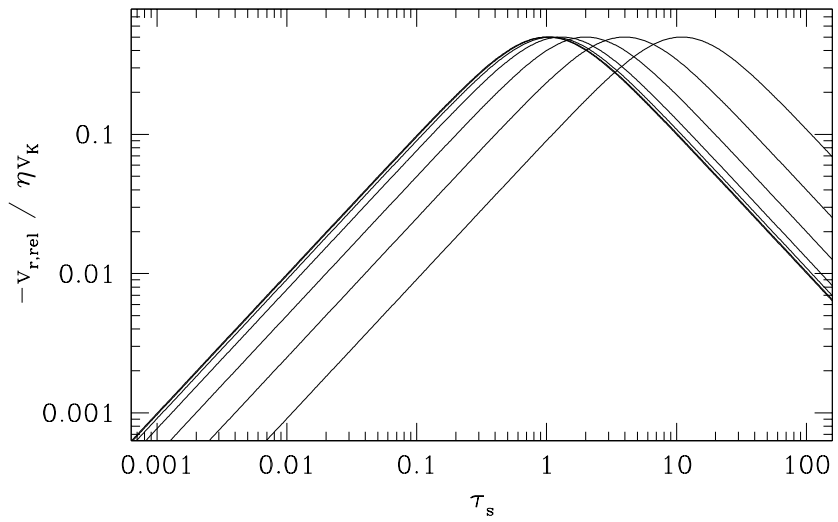

Fig. 25 The relative velocity of solids compared to gas (normalized by ηv_K, the parameter specifying departure of the gas disk from Keplerian rotation) is plotted as a function of the Stokes number τ_s. From left to right the curves show the NSH equilibrium solutions for $\rho_p/\rho_g = 10^{-2}$ (effectively identical to the no-feedback solution), 3×10^{-2}, 0.1, 0.3, 1, 3 and 10.

$$v_{r,\mathrm{rel}} = -\frac{\rho_g}{\rho} \frac{\eta \tau_s v_K}{1 + (\tau_s \rho_g/\rho)^2}, \tag{222}$$

where $\rho = \rho_g + \rho_p$. Equation (208) is recovered in the case where $\rho_p \ll \rho_g$ and feedback can be neglected (note that we have ignored any radial gas motions due to processes *other* than particle-gas coupling in this version of the NSH solution).

The predicted relative radial velocity between the solid and gas components is plotted in Figure 25 for various values of the solid to gas ratio. For $\rho_p/\rho_g = 10^{-2} - 10^{-1}$ the rate of drift at a given value of the stopping time is very similar to the no-feedback solution given by equation (208). For large values of ρ_p/ρ_g, however, the peak of the relative velocity curve (which in this limit is predominantly outward motion of the *gas*) shifts to somewhat higher values of τ_s.

6.2 Vertical settling

Aerodynamic drag also modifies the vertical distribution of solids relative to gas. We first consider the forces acting on a small particle of mass m at height z above the mid-plane of a laminar disk. The vertical component of stellar gravity exerts a force,

$$|F_{\mathrm{grav}}| = m\Omega_{\mathrm{K}}^2 z \tag{223}$$

The gas in the disk is supported against this force by the vertical pressure gradient, but solid particles are not. If started at rest a particle will accelerate until the gravitational force is balanced by drag. In the Epstein regime (given by equation 193) the resulting terminal velocity is,

$$v_{\rm settle} = \frac{\rho_m}{\rho}\frac{s}{v_{\rm th}}\Omega_{\rm K}^2 z. \tag{224}$$

Using numerical values appropriate for a 1 μm particle at $z \sim h$ at 1 AU ($\rho = 6\times10^{-10}$ g cm^{-3}, $z = 3\times10^{11}$ cm, $v_{\rm th} = 10^5$ cm s^{-1}) gives a settling speed $v_{\rm settle} \approx 0.06$ cm s^{-1}. The settling time, defined as,

$$t_{\rm settle} = \frac{z}{|v_{\rm settle}|} \tag{225}$$

is about 1.5×10^5 yr. In the absence of turbulence micron-sized particles ought to settle out of the upper layers of the disk on a time scale that is shorter than the disk lifetime.

Turbulent diffusion acts to counteract the effects of settling. If the particle fluid with density ρ_p behaves as a trace species (i.e. $\rho_p/\rho \ll 1$) then it obeys an advection-diffusion equation [97, 115],

$$\frac{\partial\rho_p}{\partial t} = D\frac{\partial}{\partial z}\left[\rho\frac{\partial}{\partial z}\left(\frac{\rho_p}{\rho}\right)\right] + \frac{\partial}{\partial z}\left(\Omega_{\rm K}^2 t_s \rho_p z\right). \tag{226}$$

Steady-state solutions to this equation can be found in the limit where the particle layer is thin enough that the *gas* density is approximately constant across the particle scale height. The dimensionless friction time τ_s is then independent of z and we find,

$$\frac{\rho_p}{\rho} = \left(\frac{\rho_p}{\rho}\right)_{z=0}\exp\left[-\frac{z^2}{2h_p^2}\right], \tag{227}$$

where h_p, the scale height of the particle concentration ρ_p/ρ, is,

$$h_p = \sqrt{\frac{D}{\Omega_{\rm K}^2 t_s}}. \tag{228}$$

If the turbulent diffusivity is comparable to the turbulent viscosity, i.e. $D \sim \nu$, the ratio of the concentration scale height to the gas scale height is just,

$$\frac{h_p}{h} \simeq \sqrt{\frac{\alpha}{\tau_s}}. \tag{229}$$

Solid particles become strongly concentrated toward the disk mid-plane whenever their dimensionless friction time substantially exceeds α. For reasonable values of α this requires substantial particle growth.

6.3 Streaming instability

Youdin & Goodman [352] demonstrated that the aerodynamically coupled system of gas and solids, described by the NSH equilibrium, is linearly unstable to the growth of perturbations. The instability, known as the *streaming instability* by (very rough) analogy with the two-stream instability of plasmas, taps the free energy present in the relative motion between the solid and gaseous fluids, which is ultimately sustained by the background gradient in the pressure. It provides the best-studied route to forming planetesimals (km or larger bodies that are largely decoupled from the gas) from smaller solids with $\tau_s \sim 1$ or less.

The pre-requisites for the existence of the streaming instability are two-way aerodynamic coupling between gas and dust within a rotating system (with shear and Coriolis force). A minimal mathematical analysis can be performed in the "terminal velocity approximation", in which the relative velocity between gas and dust is,

$$\Delta \mathbf{v} = -\frac{\nabla P}{\rho} t_s. \tag{230}$$

This approximation yields a third-order dispersion relation [352, 158], while a more complete analysis (still neglecting vertical stratification) results in a sixth-order system. The linear growth rates, plotted in Youdin & Goodman [352], are functions of τ_s and the ratio of solid to gas density, ρ_d/ρ_g. Growth is typically substantially slower than dynamical, with the most unstable modes having scales $\ll h$. For $\tau_s \sim 10^{-2}$ and $\rho_p/\rho_g \sim 0.1$, for example, the linear growth time scale is a few hundred orbits.

A simple physical (as opposed to mathematical) explanation of the streaming instability is frustratingly elusive. (Analogies to "traffic jams", or to the drag reducing properties of pelotons in bicycle races, are more relevant to the strong clustering that *results* from the streaming instability than to its existence as a linear instability.) The reader distressed by this state of affairs may seek solace in papers by Chiang & Youdin [74], and by Jacquet et al. [158], who discuss the origin of instabilities in simplified or related physical systems.

The relationship between the saturated state of the streaming instability (which is of greatest interest when the fluctuations in particle density are very strongly non-linear) and the linear growth phase is non-obvious, and requires numerical simulations. Starting with the work of Johansen & Youdin [163], several authors have quantified the outcome of the instability in protoplanetary disks (for recent examples, see e.g. [30, 161, 350]). Simplifying greatly, the streaming instability depends on the local solid to gas ratio (or metallicity, with super-Solar metallicities $Z > 10^{-2}$ being favored [165, 30]) and on the magnitude of the deviation from Keplerian velocity $\eta v_K/c_s$ (with *small* values of this parameter promoting clumping [31]). Using two-dimensional simulations Carrera et al. [67] suggest that the streaming instability can result in strong clumping for $10^{-3} < \tau_s < 3$, with the sweet spot where the lowest metallicity is required occurring for $\tau_s \approx 0.1$ at $Z \approx 0.015$.

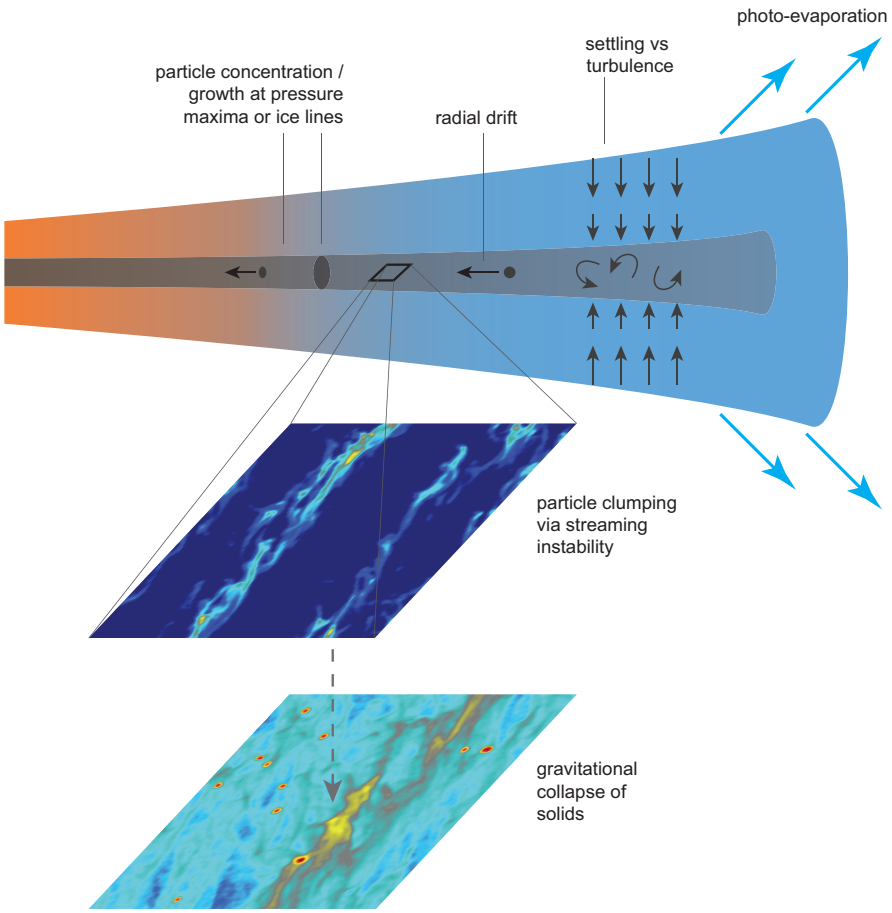

Fig. 26 Illustration of some of the processes that can lead to streaming instability in the aerodynamically coupled particle-gas system. (Simulations of the streaming instability and gravitational collapse by Jake Simon.)

The existence of a strongly inhomogenous distribution of solid particles has important implications for particle growth and planetesimal formation, irrespective of whether the over-densities are strong or very strong. There is particular interest, however, in determining whether the streaming instability can yield over-densities that exceed the Roche density (§5.2.3), given approximately by,

$$\rho_p \sim \frac{M_*}{r^3}. \tag{231}$$

Particle clumps whose density exceeds the Roche density can collapse gravitationally into planetesimals, whose properties (such as size and binarity [244]) will depend upon the statistics of the particle density field generated by the streaming in-

stability. Simulations that include self-gravity show that collapse is a likely outcome in regions of the disk where the streaming instability is strong [162, 161].

The circumstances that lead to the formation of streaming-unstable regions within protoplanetary disks, along with the outcome of the instability when it occurs, are by no means definitively established. Figure 26 illustrates the flavor of theoretical models now under investigation [160], which invoke the single particle processes discussed in this section as essential elements. Vertical settling and radial drift, operating on particles that have grown through collisions [58] to be imperfectly coupled to the gas, act to enhance the local metallicity toward the values where the streaming instability would operate. Settling and pile-up, however, may not always be sufficient, and the next section is devoted to processes that can generate structure and additional enhancement in the local metallicity within the disk.

7 Structure formation in protoplanetary disks

Up until now we have largely assumed that the gas and dust in protoplanetary disks follow axisymmetric distributions, with smooth (but very probably different [10]) radial profiles. This is an approximation, which is known to fail spectacularly in some observed systems. We have already discussed the possibility that disks may be warped (§3.4), and warps are observed in systems including HD 142527 [68]. Other observational indications of non-trivial disk structure include,

- Classification of a significant fraction of protoplanetary disks as *transitional disks* [102], based on evidence of inner cavities in (at least) the dust distribution.
- Radial structure in molecular emission linked to the presence of ice lines, for example of CO [281].
- Multiple rings of emission seen in high resolution mm / sub-mm observations of HL Tau [7].
- Pronounced non-axisymmetric ("horseshoe"-shaped) sub-mm emission in systems including IRS 48 [339].
- Spiral arms and other non-axisymmetric structures seen in scattered light images of disks [130].

An open and important question is whether these structures are a consequence of — or a precursor to — planet formation. That question cannot yet be answered, but keeping it in mind we discuss here a number of processes that can lead to the formation of directly observable (and hence necessarily large-scale) structure in one or both of the gas and dust distributions within disks. Independent of the topical observational interest, any process that can generate inhomogeneity in the solid distribution is potentially important theoretically. Forming planetesimals appears to be *hard* (at least for us, though perhaps not in Nature), but could be made easier if there are processes that locally enhance the ratio of solids relative to the gas.

7.1 Ice lines

The water snow line, together with the silicate sublimation front and various ice lines in the outer disk, are potentially critical locations for planet formation. Most often, this importance is quantified by noting that the equilibrium chemical composition of a Solar abundance gas has a substantially larger mass of condensible solids outside the snow line than inside (by about a factor of 4 in the classical Minimum Mass Solar Nebula [142], rather less than that using more modern calculations of the chemical equilibrium [211]). The likelihood that this leads to a jump in solid surface density at the snow line is then invoked as the reason why the Solar System has only terrestrial planets at smaller radii, and giants beyond.

These arguments are valid but incomplete. First, the equilibrium chemical composition is only linked directly to the solid surface density in the limit where the solid particles remain small and well-coupled to the gas. Particles that grow to be large enough that radial drift becomes significant will instead develop a surface density profile that is both different from that of the gas (§6.1.3, [354]), and dependent on the size distribution. If icy particles are typically substantially larger than silicates (as is frequently suggested) their more rapid radial drift could lead to an instantaneously *lower* surface density of solids outside the snow line than inside. Second, although it is *possible* to construct models in which an assumed jump in planetesimal surface density at the snow line contributes to efficient core formation, the compositional effect is not the whole story. The greater area of planetary feeding zones at larger radii, along with more complex effects such as Type 1 migration and pebble accretion, affect the outcome of planet formation at different radii to a similar extent. In my opinion the most important role of ice lines may instead be as a preferential site for planetesimal formation, or perhaps as a location where Type 1 migration stalls.

The pressure in the protoplanetary disk is substantially below that of the triple point of water, and hence the snow line marks a radial transition between ice and water vapor. Under mid-plane conditions, the corresponding temperature is typically $T = 150 - 180$ K. Where this isotherm lies in the disk is a function of the stellar luminosity and accretion rate — neither of which are constant over time — and of the disk opacity which may change due to coagulation. Theoretical models [194, 122, 236] suggest that $r_{\rm snow}$ moves inward from ≈ 3 AU, at such time as the accretion rate $\dot{M} \approx 10^{-7}\ M_\odot\ {\rm yr}^{-1}$, to within 1 AU when the accretion has dropped to $\dot{M} \approx 10^{-9}\ M_\odot\ {\rm yr}^{-1}$. At still lower $\dot{M}$ the inner disk becomes optically thin, and the resultant rise in temperature pushes the snow line back out to 2-3 AU.

Martin & Livio [227] showed that the above estimates, calculated within the framework of relatively simple disk models that include viscous heating and irradiation, are significantly modified if the true disk structure instead resembles Gammie's [119] layered model with a mid-plane dead zone. The calculation of snow line evolution may require further revision if winds — which

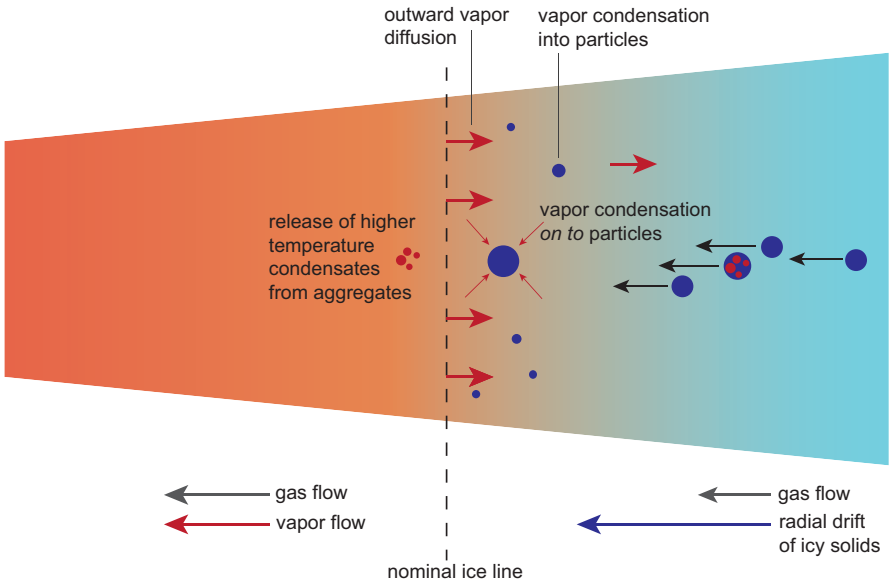

Fig. 27 Illustration of some of the physical processes occurring near ice lines in the protoplanetary disk. Icy materials drifting radially inward sublimate when they reach the ice line, releasing any higher temperature materials that were embedded into aggregates [76]. The resulting vapor flows toward the star at the same speed as the rest of the gas, but also diffuses outward down the steep gradient in concentration [317]. It may then recondense, either into new particles or on to pre-existing particles [296]. Some combination of these effects may feedback upon the gas physics via changes to either the opacity or, in models where MHD processes dominate angular momentum transport, the ionization state [185].

potentially change both the surface density profile and the fraction of potential energy that goes into disk heating — are important on AU-scales.

Figure 27 illustrates some of the key physical processes occurring near ice lines. *Where* ice lines occur can be calculated by use of the Clausius-Clapeyron relation, which gives the saturated vapor pressure $P_{\rm eq}$ at temperature T in terms of the latent heat L of the phase transition,

$$P_{\rm eq} = C_L e^{-L/\mathscr{R}T}. \tag{232}$$

Here $\mathscr{R}$ is the gas constant, and C_L is a constant that depends upon the species involved. For water, $L/\mathscr{R} = 6062$ K and $C_L = 1.14 \times 10^{13}$ g cm^{-1} s^{-2} [76]. We can compare this pressure to the actual partial pressure of vapor in the disk. Using water with molecular weight $\mu_{\rm H_2O} = 18$ as an example, if the surface density of vapor is Σ_v, the mid-plane pressure is,

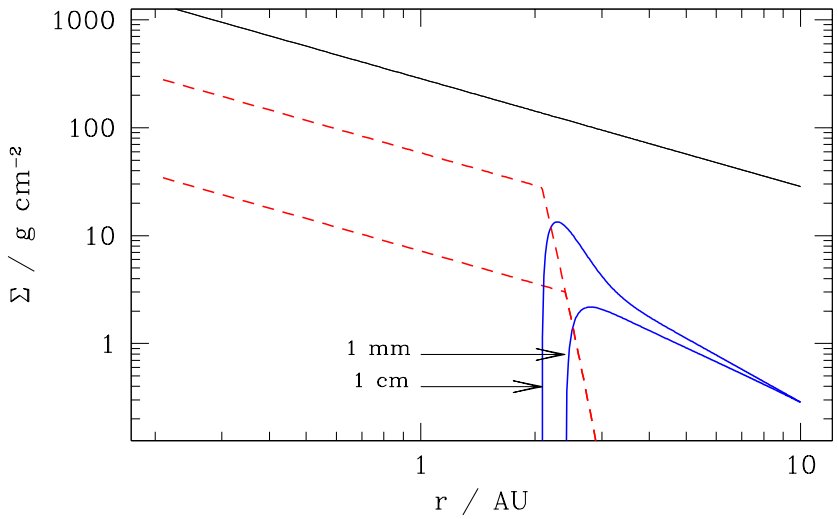

Fig. 28 Example steady-state profiles of gas (upper solid line), radially drifting icy particles (solid blue lines) and water vapor (red dashed lines) in a turbulent protoplanetary disk. The assumed disk model has an accretion rate of $10^{-8}\ M_\odot\ \mathrm{yr}^{-1}$, a temperature $T = 150(r/3\ \mathrm{AU})^{-1/2}$, and an α parameter of 5×10^{-3}. The ratio of the turbulent diffusivity to the turbulent viscosity is taken to be unity, and the concentration of icy solids is set (arbitrarily) to be 10^{-2} at 10 AU. The rapid radial drift of cm-sized particles leads to a high concentration of water vapor in the inner disk. Outward diffusion and re-condensation of this vapor — assumed here to form particles of a single fixed size — leads to an enhancement of solids just outside the snow line [317]. Note also the more elementary conclusion that the vapor concentration in the inner disk is a direct probe of the mass flux of radially drifting solids encountering the snow line.

$$P_v = \frac{1}{\sqrt{2\pi}} \frac{\Sigma_v}{h} \frac{k_B T}{\mu_{\mathrm{H_2O}} m_H}. \tag{233}$$

If $P_v < P_{\mathrm{eq}}$ water ice will sublimate, whereas if $P_v > P_{\mathrm{eq}}$ vapor will condense into solid form. For small particles whose sizes are measured in mm or cm sublimation is rapid [76], and hence to a reasonable approximation sublimation and condensation processes act to maintain the vapor pressure close to the equilibrium value.

The large value of $L/\mathscr{R}$ implies that the snow line is a sharply defined transition within the disk. At 150 K, the characteristic temperature interval over which the equilibrium vapor pressure varies, $P_{\mathrm{eq}}/(\mathrm{d}P_{\mathrm{eq}}/\mathrm{d}T)$, is just a few Kelvin. If sublimation of icy particles that drift through the snow line is fast, this has the consequence of imposing a sharp radial gradient in water vapor concentration at the snow line which, in a turbulent disk, will in turn result in a diffusive outward flux of vapor (equation 211). Re-condensation of the vapor can then lead to an enhancement of the solid surface density immediately outside the snow line.

Stevenson & Lunine [317] proposed that a vapor diffusion / condensation cycle of this type could enhance the surface density of ice enough to promote the rapid for-

mation of Jupiter's core. The strength of the effect depends upon the size of the icy solids drifting in toward the snow line, and upon what is assumed about processes including disk turbulence, condensation and coagulation / fragmentation. Figure 28 shows the results of a particularly simple calculation (after [81, 76]), which assumes that vapor condenses (or, condenses and rapidly coagulates) into solid particles of a single size that *matches* the size of icy solids drifting in from larger radii. For the adopted disk model, mm-sized icy solids have relatively low drift velocities, and these particles sublimate into vapor without generating any local enhancement in the surface density of solids. Larger cm-sized particles, conversely, are enhanced by a factor of several outside the snow line as a consequence of the diffusive transport of vapor followed by condensation. Surface density enhancements of this magnitude could be important, particularly in models where planetesimal formation depends upon the disk locally exceeding a threshold value of metallicity (as is the case for the streaming instability, see §6.3, [165]).

Ros & Johansen [296] investigated a related possibility. Instead of assuming that vapor condenses into new particles (or, on to very small grains released when aggregates break up at the snow line), they modeled the growth of pre-existing solids as vapor condenses on to their surfaces. A simple collisional argument gives the growth rate due to vapor condensation / sublimation as,

$$\frac{\mathrm{d}m}{\mathrm{d}t} = 4\pi s^2 v_{\mathrm{th}} \rho_v \left(1 - \frac{P_{\mathrm{eq}}}{P_v}\right), \tag{234}$$

for a particle of mass m and radius s, surrounded by vapor of density ρ_v and thermal speed v_{th}. (As noted by Supulver & Lin [319], this is not an exact expression [143].) Using a Monte Carlo approach, Ros & Johansen [296] found that condensation on to particle surfaces could provide an efficient growth mechanism up to sizes of the order of 10 cm. This could aid planetesimal formation by boosting the stopping time of particles into the range preferred by the streaming instability [67]. Moreover, by removing mass from the directly observable mm-size regime, condensation-driven growth could suppress the mm and sub-mm flux from disks in the vicinity of ice lines [355].

The aforementioned physics affects only trace components of the disk — the icy solids and the resulting vapor. It is easy, however, to contemplate feedback processes that couple the evolution of solids at ice lines to the bulk of the gas disk. At a minimum the opacity will vary depending upon the radial distribution of solids. Beyond that, we have already noted that the efficiency of angular momentum transport (in MHD models) is expected to be a function of the local ionization state, and that the ionization balance is affected by the abundance of small grains. Kretke & Lin [185] suggested that the enhanced abundance of solids near the snow line would act to suppress the rate of angular momentum transport, and that this could lead to the formation of a local pressure maximum that would act to trap particles (producing, in principle, a positive feedback loop). This argument (which has been invoked in some models of collisional growth [63]) is highly plausible, though the breadth and complexity of the physics involved makes quantitative investigation challenging.

Although I have focused here on the snow line, analogous considerations carry over to other ice lines. The CO ice line corresponds to a temperature of $T = 17-19$ K [54], and is somewhat more complicated to model because the CO is typically mixed with N_2 and water ices. The silicate "ice line" (or sublimation front) could also be important, since it lies at radii where a high fraction of stars are observed to host short-period planetary systems.

7.2 Particle traps

In a disk with a monotonically declining pressure profile, radial drift is always inward. More generally, however, aerodynamic drift is directed toward pressure maxima, and can be outward if there is a local pressure maximum within the disk. This possibility was recognized in a prescient paper by Whipple [349], who appealed to it as part of a model for the formation of comets[12]. The tendency for solids to be aerodynamically enhanced in the vicinity of pressure maxima is often described as particle "trapping", though this term is somewhat misleading; in a turbulent disk small particles are at most temporarily detained by pressure maxima rather than being permanently trapped.

The effect of local pressure maxima on the radial distribution of solids can be derived, in the limit where the solids remain a trace contaminant, following the methods described in §6.1.1 and §6.1.2. For an axisymmetric disk with an arbitrary mid-plane pressure profile, the radial velocity v_r of particles under the action of aerodynamic forces remains as given by equation (208), with the parameter η describing the deviation from Keplerian velocity becoming [322],

$$\eta = -\left(\frac{h}{r}\right)^2 \left[\frac{\mathrm{d}\ln\Sigma}{\mathrm{d}\ln r} + (q-3)\right]. \tag{235}$$

In this formula q is defined as the local power-law index describing the flaring of the disk,

$$\frac{h}{r} \propto r^{q-1}, \tag{236}$$

such that a non-flaring disk has $q = 1$. In axisymmetry and steady-state, equations (210) and (211) can be immediately integrated to give,

$$r(F_{\rm diff} + F_{\rm adv}) = k, \tag{237}$$

where the diffusive and advective fluxes are,

[12] Quoting from his paper, "should it be possible for a toroid of higher density to occur in the Solar nebula, the growing planetesimals would be drawn toward it from the inside as well as from the outside...".

$$F_{\rm diff} = -D\Sigma \frac{\rm d}{{\rm d}r}\left(\frac{\Sigma_d}{\Sigma}\right),$$
$$F_{\rm adv} = \Sigma_d v_r, \tag{238}$$

and the constant k is just the radial flux of solid material. Written out explicitly, the concentration of particles $f \equiv \Sigma_d/\Sigma$ obeys a first-order differential equation,

$$\frac{{\rm d}f}{{\rm d}r} - \frac{v_r}{D} f = \frac{k}{D\Sigma}\frac{1}{r}. \tag{239}$$

Analytic solutions to this equation are possible for simple choices of v_r, D and Σ. A straightforward quadrature gives the solution for the concentration profile given more realistic choices of these functions.

Figure 29 shows an illustrative numerical solution to equation (239). For this example, we have modeled a trap by assuming (arbitrarily) that the viscosity in the gas disk is reduced across a moderately narrow annulus. The lower viscosity leads to a higher surface density, producing a pressure maximum which in turn concentrates particles. The concentration effect is strongly size-dependent. Small particles (in this example those with radii of 0.1 mm and 1 mm) have a radial velocity that is similar to that of the gas, and are largely unaffected by the pressure maximum. Larger cm-sized particles, on the other hand, have a larger magnitude of radial drift, and can be strongly concentrated at the location of the pressure maximum. The enhancement in the local particle density can reach several orders of magnitude, depending both on the particle size and on the "strength" (radial width and amplitude) of the pressure maximum within the gas disk.

As should be obvious from the preceding discussion, in a turbulent disk (and ignoring particle feedback on the gas) it is *always* possible to find a steady-state solution for the radial particle concentration in which the particle mass flux is a constant at all radii. Physically, this is because particles accumulate near pressure maxima until the radial gradient in concentration becomes large enough for turbulent diffusion to allow them to leak out [343, 360]. Pressure maxima only act as a "filter" [290], *permanently* removing large particles from the inward radial drift flow, when additional physical effects are included [360]. If the local concentration of large particles becomes large enough, for example, planetesimal formation [137] could cause some fraction of the solid material to drop out of the radial flow.

A number of physical effects have been identified that could lead to the formation of local pressure maxima within protoplanetary disks. These include the exterior edges of planet-carved gaps [259, 290, 360], the outer edges of cavities created by photoevaporation (§8.1, [4]), and a photoelectric heating instability that may operate in gas-poor systems (primarily debris disks) [53, 222]. Spiral arms in self-gravitating disks [292, 123] and the inner edges of dead zones [221] can also concentrate solids via closely related physical processes, though these environments typically involve

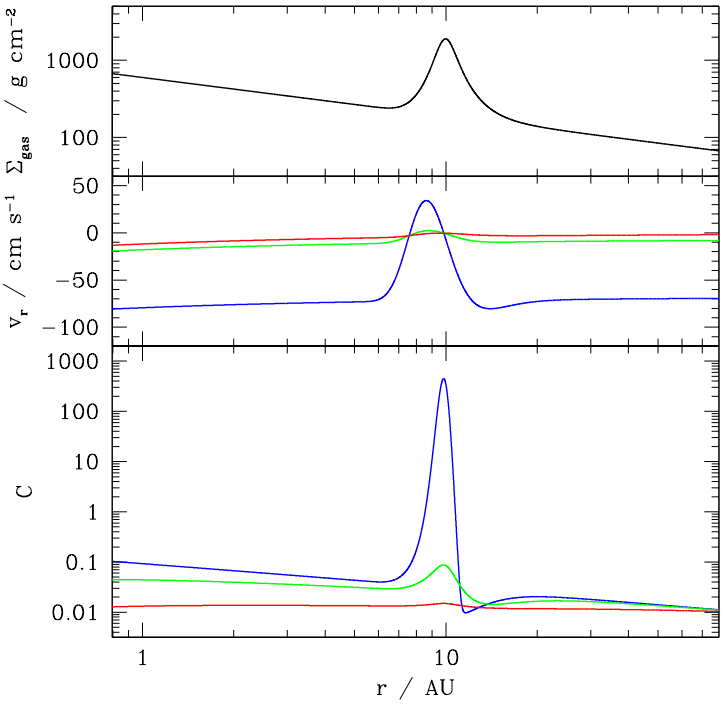

Fig. 29 The steady-state radial distribution of solids in a turbulent disk with an axisymmetric local pressure maximum (a particle "trap"). Upper panel: the surface density of the gas. Middle panel: the radial velocity of 0.1 mm (red), 1 mm (green) and 1 cm (blue) particles. The smallest particles have a radial velocity that is almost indistinguishable from that of the gas, while the larger particles experience rapid radial drift that can be outward near the location of the pressure maximum. Lower panel: the concentration $C = \Sigma_d/\Sigma_{\rm gas}$, normalized to an arbitrary value of 10^{-2} at 100 AU. The assumed disk model for this calculation has $\dot{M} = 10^{-8}\,M_\odot$ yr^{-1}, $M_* = M_\odot$, $h/r = 0.5$, $\alpha = 10^{-3}$ and $D = \nu$ (c.f. equation 212). The trap is modeled as a gaussian-shaped reduction in α to a minimum of 10^{-4}, with a width of $4h$. The particles are assumed to be spherical, with a material density of 1 g cm^{-3}, and to follow the Epstein drag law.

significant non-axisymmetry. With the exception of self-gravity, these possible locations for pressure maxima either form at specific places within the disk (e.g. at the inner dead zone edge, defined by a characteristic mid-plane temperature), or at a time after when we expect planets to have formed (during photoevaporative disk clearing, or in *responsе* to pre-existing massive planets). It is possible, however, for the turbulence within the gas disk to be generically unstable to the formation of pressure maxima within zonal flows. This would be interesting because it would imply the (possibly transient) existence of multiple particle traps within the disk, that could play a role in early-stage planet formation [271].

7.3 Zonal flows

It is evident from equation (12) that an equilibrium can be set up in which radial forces from a complex pressure profile (that may include local pressure maxima) are balanced by radial variations in azimuthal velocity. In a local description (equation 127, but here ignoring magnetic fields) the balance is between the pressure gradient term $\nabla P/\rho$ and that describing the Coriolis force $2\Omega_0 \times \mathbf{v}$. When these terms balance, such that

$$\frac{\mathrm{d}P}{\mathrm{d}x} = 2\Omega_0 \rho v_y, \tag{240}$$

the system is said to be in *geostrophic balance* (here x is the radial direction, and y the azimuthal). The pressure gradient is compensated by variations in the orbital velocity, creating *zonal flows* analogous to the banded structure of winds in giant planet atmospheres.

A disk zonal flow is an equilibrium solution to the fluid equations, but that equilibrium may not be stable. Too pronounced a deviation from Keplerian rotation results in a shear profile that is unstable to Rossby wave instability [212]. We will discuss this instability, which is similar to Kelvin-Helmholtz instability, in §7.5. Even if the rotation profile is stable, the diffusive nature of a classical viscosity (equation 51) would tend to erase any small-scale perturbations in the pressure that are sourced from surface density fluctuations. Persistent zonal flows are thus not expected in classical disk theory. They have been observed, however, in local numerical simulations of MHD turbulent disks [164]. The key to their formation appears to be the ability of MHD disk turbulence to generate large-scale structure in the magnetic field [309], which could be viewed as an inverse cascade of turbulent power. The details of how and when zonal flows form are not entirely clear, though Johansen et al. [164] describe a simplified dynamical model in which large-scale variations in the Maxwell stress lead first to azimuthal velocity perturbations and thence to axisymmetric structure in the pressure and density.

The lifetime and radial scale of zonal flows in protoplanetary disks depend upon the same factors that determine the properties of MHD disk turbulence more generally (§4.4.4), namely the strength of non-ideal terms in the induction equation and the presence of net vertical magnetic field. In ideal MHD, lifetimes of tens of orbital periods and radial scales of the order of 10 h appear to be typical [164, 309], though these results require a double dose of caveats — first because the inferred scales are not much smaller than the size of the local simulation domains used, and second because they are large enough that curvature terms neglected in local models may be important. Nonetheless, the amplitude, scale and lifetime of zonal flows under ideal MHD conditions plausibly lead to strong local enhancements in the dust to gas ratio for particles with stopping times $\tau_s \sim 0.1 - 1$ [92]. The presence of net vertical fields substantially enhances the amplitude of zonal flows [34].

Zonal flows are also found in MHD disk simulations that include ambipolar diffusion, and can be comparable in amplitude to the ideal MHD case if the net field is sufficient to stimulate a significant $\alpha \sim 10^{-2}$ [306]. However, both inferences from local simulations [306], and explicit tracking of particles in global simulations

[362], suggest that zonal flows in the outer regions of protoplanetary disks, where ambipolar diffusion dominates, have properties close to the boundary beyond which strong particle enhancement would be expected.

In summary, zonal flows are likely to be present in the inner disk, where ideal MHD is a good approximation, though these flows would only strongly influence the dynamics of relatively large solid particles. In the outer disk, where ambipolar diffusion is important and even mm-sized particles have significant stopping times, zonal flows could introduce observable large-scale axisymmetric structure and may contribute to particle concentration. In the Hall-dominates regime that prevails around 1 AU theoretical expectations are less clear. Extremely strong zonal structures were observed in local vertically unstratified Hall-MHD simulations [189], whereas comparable stratified runs instead led to large-scale Maxwell stress [195]. It is therefore unclear whether there are circumstances in which zonal flows on AU-scales could contribute to particle concentration and planetesimal formation.

7.4 Vortices

Few issues in planet formation are as long-debated as the possible role of vortices. Very general arguments suggest that large-scale vortices could be present in protoplanetary disks and play an important role in planetesimal formation. We note, first, that disks are (approximately) two dimensional fluid systems, that in contrast to three dimensional systems support an inverse cascade of turbulent energy toward large scales [181]. Second, for a barotropic disk (i.e. $P = P(\rho)$ only) the vortensity ω/ρ is conserved (equation 113). Taken together, these properties imply that vortices within disks have the potential to form persistent long-lived structures. Indeed, simulations of strictly two dimensional flows show that disks seeded with small-scale vorticity perturbations evolve to form a small number of large and persistent anticyclonic vortices [124, 167]. Anticyclonic vortices are high pressure regions that attract marginally coupled solids [44, 325], potentially catalyzing the subsequent formation of planetesimals. Even absent planetesimal formation, the natural tendency of vortices to form large-scale non-axisymmetric dust features makes it tempting to identify them with observed disk asymmetries [339].

The basic properties of disk vortices are well-established. What is much trickier is to determine (1) whether vortices form spontaneously in disks or only *after* planet formation (for the reasons already mentioned, spontaneous vortex formation generally requires non-barotropic processes), and (2) whether three dimensional instabilities and / or particle feedback are fatal impediments to their survival. Observations as well as theory are probably needed to resolve these issues.

7.4.1 The Kida solution

The magnitude of the vorticity in a strictly Keplerian disk is $\omega_K = -(3/2)\Omega_K$. A vortex can be modeled as a spatially localized elliptical perturbation, within which the vorticity $\omega = \omega_K + \omega_v$, with ω_v a constant. Other types of vortex are possible, but rather remarkably this type can be described by an exact non-linear solution [173] that is useful for both analytic and numerical studies.

The Kida solution [173] describes a vortex within a shearing-sheet approximation to disk flow. Following Lesur & Papaloizou [198] we define a cartesian co-ordinate system (x,y) that is centered at radius r_0 and which co-rotates with the background disk flow at angular velocity $\Omega_K = \Omega_K(r_0)$,

$$\begin{aligned} x &= r_0\phi \\ y &= -(r - r_0). \end{aligned} \tag{241}$$

Kida considered time-dependent vortex solutions, but here we will worry only about vortices that are steady[13]. Time-independent solutions are possible if the semi-major axis of the vortex is aligned with the azimuthal direction (x in the shearing sheet model), and the vorticity perturbation satisfies,

$$\frac{\omega_v}{\omega_K} = \frac{1}{\chi}\left(\frac{\chi+1}{\chi-1}\right). \tag{242}$$

Here $\chi = a/b$ is the aspect ratio of the vortex, which forms an elliptical patch with semi-major axis a and semi-minor axis b. The right-hand-side is evidently positive, which implies that the only steady Kida vortices in Keplerian disks are anticyclonic (with ω_v having the opposite sign to Ω_K).

The complete Kida solution is written in terms of a streamfunction ψ in an elliptic co-ordinate systems (μ,ν), where,

$$\begin{aligned} x &= f\cosh(\mu)\cos(\nu), \\ y &= f\sinh(\mu)\sin(\nu), \end{aligned} \tag{243}$$

and $f = a\sqrt{(\chi^2-1)/\chi^2}$. The solution can be split into a core and an exterior part,

$$\begin{aligned} \psi_{\rm core} &= -\frac{3\Omega_K f^2}{4(\chi-1)}\left[\chi^{-1}\cosh^2(\mu)\cos^2(\nu) + \chi\sinh^2(\mu)\sin^2(\nu)\right], \\ \psi_{\rm ext} &= -\frac{3\Omega_K f^2}{8(\chi-1)^2}\left[1 + 2(\mu-\mu_0) + 2(\chi-1)^2\sinh^2(\mu)\sin^2(\nu)\right. \\ &\qquad \left. + \frac{\chi-1}{\chi+1}\exp[-2(\mu-\mu_0)]\cos(2\nu)\right], \end{aligned} \tag{244}$$

[13] For a derivation of the steady Kida solution, see e.g. the appendix of Chavanis [73].

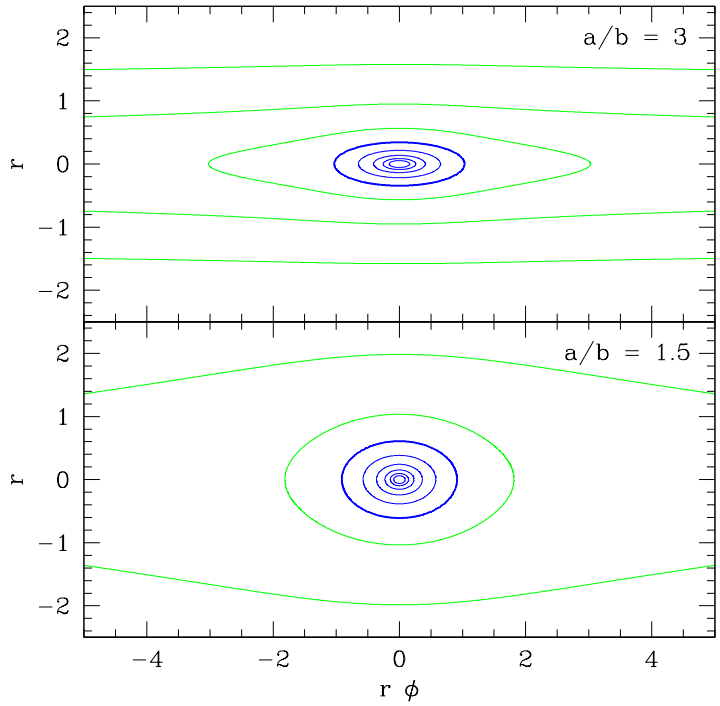

Fig. 30 Contours of the Kida vortex streamfunction $\psi(x,y)$ are shown for different values of the vortex aspect ratio $\chi \equiv a/b$. Within the vortex core, delineated by the bold contour, the streamlines defined by the solution are elliptical, with fixed aspect ratio. Outside the core, the vortex merges smoothly into the background shear flow of the disk.

which match at $\mu = \mu_0 = \tanh^{-1}(\chi^{-1})$. The cartesian velocity field is then given by $v_x = -\partial\psi/\partial y$, $v_y = \partial\psi/\partial x$. In general the cartesian representation of the velocity has no simple form, but within the core it is,

$$v_{x,\mathrm{core}} = \frac{3\Omega_K \chi}{2(\chi-1)} y,$$
$$v_{y,\mathrm{core}} = -\frac{3\Omega_K}{2\chi(\chi-1)} x, \tag{245}$$

describing simple elliptical motion. Figure 30 shows the contours (logarithmically spaced) of the full streamfunction for Kida vortices of varying aspect ratio.

Barge & Sommeria [44] studied the trajectories of aerodynamically coupled solids that encounter vortices (using a different and approximate vortex model). The high pressure within anticyclonic vortex cores acts as an attractor for solids. The cross-section for capture is maximized for particles with dimensionless stopping time $\tau_s = 1$ [73]. Since vortices can potentially grow to have radial extents

$\Delta r \approx h$ (the supersonic velocity perturbations of larger vortices would radiate sound waves sapping their energy) a single large vortex can potentially trap a substantial mass of solids flowing radially toward it due to ordinary radial drift.

7.4.2 Stability of vortices

Although the geometry of protoplanetary disks is approximately two dimensional, the fact that disk vortices are limited in radial size to $\Delta r \approx h$ means that they are three dimensional objects that notice the vertical stratification. Barranco & Marcus [46] and Shen et al. [304], using three dimensional simulations, found that mid-plane vortices that would be highly stable in 2D are rapidly destroyed by three dimensional instabilities. The origin of these observed instabilities, at least in part, appears to be the *elliptical instability* [172], which occurs whenever there is a resonance between the vortex rotation period and inertial waves within the disk. In a disk environment, Lesur & Papaloizou [198] find that purely gaseous vortices are unstable for almost all choices of the vortex aspect ratio and degree of vertical stratification, though these parameters strongly affect the linear growth time of the instability. The instability that afflicts 3D vortices, however, is typically slow-growing and of small radial scale. Numerically this makes studies of vortex survival particularly challenging. Physically it means that the questions of vortex formation and vortex survival are closely linked, except perhaps at very large radii (where "primordial vortices" might persist for interesting periods of time) the vortex population in a disk is expected to reflect an equilibrium between formation and destruction processes.

A significant loading of solids will also impact vortex longevity, generally for the worse. Railton & Papaloizou [286] studied the stability of generalized Kida vortices, containing both gas and dust in the limit of strongly aerodynamically coupled particles. They found that these configurations were vulnerable to parametric instabilities in the same way as gas-only vortices. This is consistent with a wide range of other analytic and numerical work [72, 154, 117], which suggests that dust to gas ratios in the range between 0.1 and 1 are sufficient to imperil the survival of disk vortices. This limitation may not, however, preclude vortices playing a role in planet formation. If we assume that there is a continual source of vorticity within the disk, then vortex particle concentration up to $\rho_p \sim \rho_g$ could be sufficient to initiate planetesimal formation via a variation of the streaming instability [282].

Observations have identified a number of systems (primarily transition disks) that show a non-axisymmetric distribution of sub-mm emission [69, 157, 339], consistent with that expected if aerodynamically coupled solids are accumulating in a vortex [361]. The putative vortices in these examples may all be *caused* by planets. It would be interesting to ask whether useful constraints on vortices could be derived from observations of the *most-axisymmetric* disks, where there is no independent suspicion that planets already exist.

7.5 Rossby wave instability

The Rossby wave instability (RWI) [212, 202, 201] is a well-characterized mechanism for producing vortices within protoplanetary disks. The RWI is a linear instability that grows whenever there is "sufficiently sharp" radial structure in the disk. Specifically, for a two dimensional disk model with angular velocity $\Omega(r)$, vertically integrated pressure $P(r)$, and adiabatic index γ, we define the entropy S and epicyclic frequency κ via,

$$S = \frac{P}{\Sigma^\gamma},$$
$$\kappa^2 = \frac{1}{r^3}\frac{\partial}{\partial r}(r^4\Omega^2). \tag{246}$$

In terms of these quantities, the stability of the disk to the RWI is determined by the radial profile of a generalized potential vorticity,

$$\mathscr{L}(r) = \frac{\kappa^2}{2\Omega\Sigma} \times S^{-2/\gamma}. \tag{247}$$

A necessary condition for RWI is that $\mathscr{L}$ have an extremum. A precise sufficient condition is not known, but variations in the potential vorticity of the order of 10% over radial scales $\approx h$ appear to be enough to trigger instability, which leads to the formation of anticyclonic vortices on time scales that can be rapid — of the order of $0.1\Omega^{-1}$ [202]. The instability, which can be understood in terms of the local trapping of waves in the vicinity of the vortensity perturbation [125, 337], has similarities to the Papaloizou-Pringle [264] instability of accretion tori. The RWI is essentially a two dimensional instability [232, 205], though the vortices that it forms are as vulnerable to unrelated three dimensional instabilities as any others.

We have already remarked that the edges of dead zones (and ice lines [185]) are places where local pressure maxima may form. The RWI criterion (equation 247) is not necessarily satisfied at every local pressure maximum, but it is nonetheless true that dead zone edges are plausible locations where the RWI may occur. Hydrodynamic models [340, 154, 220], and MHD simulations that include Ohmic diffusion as a simple model of dead zones [223, 103, 224, 106], support this expectation, and show that the radial disk structure introduced by dead zones is likely to be unstable to the RWI and subsequent formation of vortices. The vortices in turn act as sites of particle concentration [220]. Depending upon the radii involved, a single vortex generated by the RWI may have a lifetime that is very short as compared to the disk lifetime (this will be particularly true at the inner edge of the dead zone). However, in this scenario fresh generations of vortices may be expected to form as long as the non-ideal disk physics that sustains the RWI-unstable dead zone structure persists.

A second location where RWI may occur is at the edge of a gap created dynamically by a massive planet [179, 90]. Figure 31 shows the evolution of a disk in a two-dimensional simulation of this scenario. The formation of a massive planet creates an approximately axisymmetric gap within the disk, whose edges can be

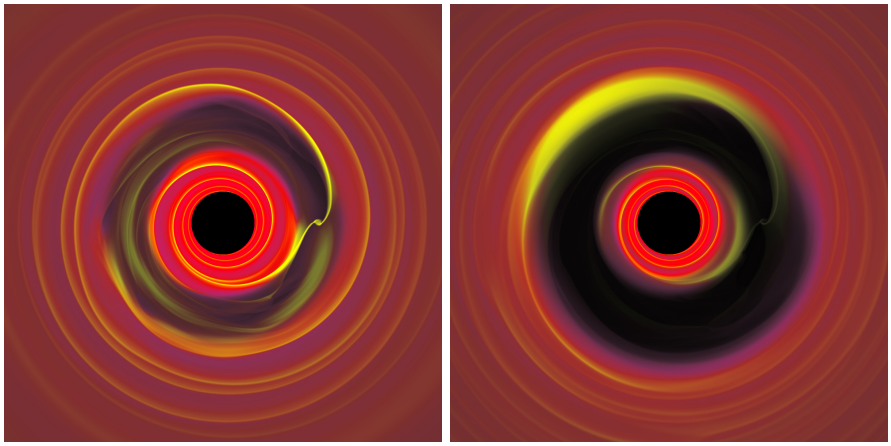

Fig. 31 Snapshots showing the hydrodynamic evolution of an almost inviscid disk containing a massive planet [17]. The planet rapidly clears an annular gap within the disk, whose edge is unstable to the generation of vortices. The system then evolves through a phase when the outer gap edge hosts a single large vortex, which can be an efficient trap for solid particles. The disk has $\alpha = 10^{-4}$ and $h/r = 0.05$ at the location of the planet, which has a mass ratio to the star of 5×10^{-3}.

unstable to the RWI. The vortices that are generated fairly rapidly merge, creating a single large vortex at either edge of the gap then can subsequently trap particles. This process works best if the disk in the vicinity of the planet's orbit has a low viscosity (roughly $\alpha \sim 10^{-3}$ or lower), and is at least partially a transient effect — the vortices form during the phase when the planet accretes its gaseous envelope. For these reasons, observable structure from planet-initiated vortices is likely to be easiest to see in the outer disk, where ambipolar diffusion damps turbulence [308] and the absolute lifetime of a single generation of vortices against disruptive instabilities is long. The particles trapped efficiently in the outer disk include those with $s \sim$ mm that can be seen in sub-mm observations of protoplanetary disks [363, 361].

8 Disk dispersal

There is not obviously any leading order mystery as to where the gas in protoplanetary disks goes to. If we divide the mean disk mass estimated from sub-mm studies in Taurus ($M_d \sim 5 \times 10^{-3}\ M_\odot$ [8]) by the median accretion rate ($\dot{M} \sim 10^{-8}\ M_\odot\ \mathrm{yr}^{-1}$ [135]) estimated in the same region, we obtain a characteristic evolution timescale of 0.5 Myr. The lifetime of detectable disks might be expected to be a small multiple of this timescale — say a few Myr — which is indeed what is observed [147].

The above exercise establishes that, from a purely observational perspective, most or all of the gas in protoplanetary disks *could* be lost via accretion on to the star. Beyond that, it proves nothing. Disk mass estimates and measurements of stellar ac-

cretion rates are subject to uncertainties, which when combined probably allow us to shift the inferred characteristic lifetime by an order of magnitude in either direction. In particular, if disk masses are systematically *under-estimated* from sub-mm continuum observations (because of particle growth to sizes too large to contribute to the sub-mm opacity) the characteristic lifetime could approach or exceed the observed one, challenging the view that most of the gas is accreted.

The next order observational diagnostic probes the time-dependence of the decay of disk signatures. Here a puzzle does emerge. The classical disk evolution equation (52) admits a self-similar solution [219] that ought to approximate the evolution at sufficiently late times. For a disk with a viscosity that scales with radius as $\nu \propto r^{\gamma}$, the late-time evolution of the surface density close to the star is predicted to follow (e.g. [15]),

$$\Sigma \propto t^{-(5/2-\gamma)/(2-\gamma)}. \tag{248}$$

If $\gamma = 1$, for example, as would be the case for a disk with a steady-state surface density profile $\Sigma \propto r^{-1}$, then the predicted late-time decay goes as $t^{-3/2}$. This is relatively slow, and would probably lead to a population of stars with weak disk signatures (in gas and dust tracers) that are not observed (for a review of these observational arguments, see Alexander et al. [3]). One might argue, of course, that this is an illusory problem that we have created for ourselves by placing unwarranted faith in the validity of classical viscous disk theory. A resolution along these lines is possible. More commonly, however, the discrepancy between the simple theory and observations is taken to imply that some distinct process acts to rapidly disperse the disk and terminate accretion. Photoevaporation is the leading candidate, on account both of robust theoretical estimates that suggest it should be important, and observations that are consistent with photoevaporation occurring in some relatively extreme situations.

8.1 Photoevaporation

Disk photoevaporation is a purely hydrodynamic process that occurs when molecular gas in the disk is dissociated or ionized by high energy (UV or X-ray) photons. If the gas is heated sufficiently to become unbound, it accelerates away from the disk under the influence of pressure gradient forces to form a thermally driven wind. Early models for photoevaporative flows were developed in the 1980s by Bally & Scoville [43] in the context of massive stars surrounded by neutral disks, and in more quantitative detail by Begelman et al. [48] who studied X-ray heated disks around compact objects. The essential physics is thus very well-established. We will begin by considering how photoevaporation works if the disk is exposed to extreme ultraviolet (EUV) photons that have sufficient energy ($h\nu > 13.6$ eV) to ionize hydrogen. This is probably *not* the dominant driver of photoevaporation from protoplanetary disks around low mass stars, but it is amenable to an analytic treatment that exposes the main principles [151].

8.1.1 Thermal winds from disks

We consider a disk whose surfaces are illuminated by a source of high energy photons, that may come either from the central star or from other luminous stars within a cluster. The radiation heats a surface layer of the disk to a temperature T, with a sound speed c_s. A characteristic scale r_g (the "gravitational radius") can be defined by asking where the sound speed equal the local Keplerian velocity,

$$r_g = \frac{GM_*}{c_s^2}. \tag{249}$$

Noting that the thermal energy per particle is $\sim k_B T$, the radius r_g is approximately equivalent to the smallest radius where the *total* energy of the gas in the heated surface layer (i.e. thermal plus gravitational) is zero. For radii $r > r_g$ the total energy is positive, and it is energetically possible for the surface gas to flow away in a thermal wind.

This is all quite rough, and we should really consider both the hydrodynamic structure of the wind (which is similar to the textbook example of a Parker wind [345]) and the role of rotation [204]. Doing so results in an improved estimate of the critical radius beyond which a thermal wind is launched, which scales with but is significantly smaller than r_g,

$$r_c \approx 0.2\frac{GM_*}{c_s^2} \approx 1.8\left(\frac{M_*}{M_\odot}\right)\left(\frac{c_s}{10\text{ km s}^{-1}}\right)^{-2}\text{ AU}. \tag{250}$$

We have picked 10 km s^{-1} as a fiducial sound speed because this is approximately the sound speed in EUV-ionized gas, which has a temperature near 10^4 K. X-rays or far ultraviolet (FUV) photons (those with 6 eV $< h\nu <$ 13.6 eV that dissociate but do not ionize hydrogen) heat the surface to lower temperatures — more like 10^3 K — resulting in correspondingly larger critical radii.

Interior to r_g the hot gas is bound, and unless some other process intervenes (such as a stellar wind or an MHD disk wind) it will form a static isothermal atmosphere with a scale height that varies with radius as $h \propto r^{3/2}$ (see §2.1.1). Outside r_g it will flow away, at a speed of the order of the sound speed. In the case of EUV illumination the hot and ionized surface layer is separated from the underlying cool gas by a sharp ionization front, which gives a clearly defined "base" to the wind. If the number density at the base is n_0, we expect a mass loss rate per unit area of the disk that is given by,

$$\dot{\Sigma}_w \simeq 2\mu m_H n_0 c_s, \tag{251}$$

up to factors of order unity that depend again on the detailed hydrodynamic structure of the flow. In the EUV case the mass loss profile due to photoevaporation is then determined by the radial scaling of the base density $n_0(r)$. Noting that the integrated mass loss rate is just,

$$\dot{M}_w = \int_{r_c}^{r_{\rm out}} 2\pi r \dot{\Sigma}_w \mathrm{d}r, \tag{252}$$

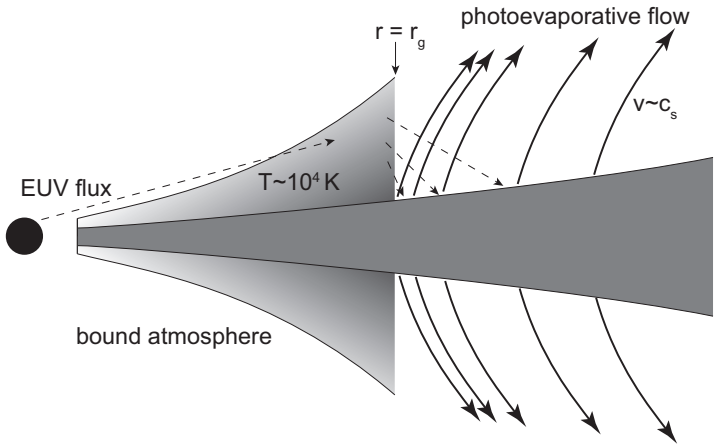

Fig. 32 Illustration of the simplest model of internal photoevaporation driven by extreme ultraviolet (EUV) radiation (based on the "weak stellar wind" case from Hollenbach et al. [151]). Stellar EUV radiation ionizes and heats the surface layers of the disk. Where the thermal energy of the surface layer remains small compared to the binding energy, the hot gas forms a bound atmosphere. At larger radii, where the gas is more weakly bound, the hot gas flows away in a thermally driven wind. Details of the radiative transfer and heating processes differ depending upon the nature of the high energy radiation, but a qualitatively similar scenario applies also to X-ray and FUV-driven photoevaporation.

we conclude that if $n_0(r)$ declines more steeply that r^{-2} the mass loss is predominantly from the inner disk (near r_c), whereas a shallower profile leads to most of the mass being lost from the outer disk.

Actually finding $n_0(r)$ for photoevaporation driven by EUV radiation from the central star requires the solution of a radiative transfer problem, whose geometry is illustrated in Figure 32. The base density is determined by equating the rate of ionization to that of recombination, which occurs at a rate per unit volume $\alpha n_e n_p$ with α, the recombination co-efficient, given by $\alpha \approx 3 \times 10^{-13}$. The main difficulty is determining the radial scaling of the ionization rate. This in principle has two components, a "direct" flux from the star and a "diffuse" field that originates from the fraction (about one third) of recombinations within the bound atmosphere that go to the ground state and hence regenerate an ionizing photon. Hollenbach et al. [151] presented analytic and approximate numerical solutions to the radiative transfer problem that imply $n_0(r) \propto r^{-5/2}$, and this scaling has been widely adopted in subsequent work. Important features of the Hollenbach et al. solution have been verified in more detailed radiation hydrodynamic simulations (including the $\Phi^{1/2}$ of the mass loss with the ionizing photon flux [293]), though the slope of $n_0(r)$ at $r > r_g$ remains to be confirmed (indeed, a recent radiative transfer calculation is inconsistent with the canonical slope [324]).

8.1.2 Drivers of photoevaporation

Photoevaporation driven by a photon flux of EUV radiation from the central star Φ is estimated to result in a mass loss rate [107, 3],

$$\dot{M}_w \simeq 1.6 \times 10^{-10} \left(\frac{M_*}{M_\odot}\right)^{1/2} \left(\frac{\Phi}{10^{41}\ \mathrm{s}^{-1}}\right)^{1/2} M_\odot \mathrm{yr}^{-1}, \tag{253}$$

provided that the disk is present and optically thick at all radii. The dominant uncertainty in applying this estimate to specific systems comes from lack of knowledge of Φ, which can be constrained but which remains hard to pin down precisely [5, 265]. For low mass stars ($M \leq M_\odot$) reasonable estimates imply that EUV photoevaporation rates are negligible when compared to the median accretion rate of T Tauri stars [135], but large enough to matter for disk dispersal if no stronger mass loss processes are operative. (EUV photon fluxes are of course vastly larger for massive stars, for which the theory was originally developed.)

Low mass pre-main-sequence stars are strong emitters of FUV and X-ray radiation [110, 274, 132]. The FUV luminosity has a base level that is set by chromospheric activity, on top of which there is a potentially much larger component from accretion [155]. The X-ray luminosity scales linearly with the bolometric luminosity, $\log(L_X/L_{\mathrm{bol}}) = -3.6$ [274], but with a large scatter. Qualitatively, these photons affect the disk in the same way as the EUV. The surfaces of the disk are heated, albeit to a somewhat lower temperature than the 10^4 K that is characteristic of HII regions, and where this heating results in unbound gas a wind ensues. Quantitatively, the main difference is that X-ray and FUV heated layers are not separated from the cool underlying disk by any analog of a sharp ionization front, and this makes modeling of FUV and X-ray photoevaporation more difficult. State of the art calculations [128, 256, 255], however, suggest that X-rays and FUV radiation drive mass loss rates that are substantially higher than the EUV prediction — with values of the order of $10^{-8}\ M_\odot\ \mathrm{yr}^{-1}$ being possible — with X-rays likely dominating in the inner region.

8.1.3 Disk evolution including photoevaporation

Including photoevaporation in classical viscous models for disk evolution is particularly simple, because thermal winds exert no torque on the disk (equation 63). The rate and radial dependence of the mass loss, moreover, is primarily a function of the spectral energy distribution of the irradiation. This may depend upon the stellar accretion rate (if the FUV luminosity is an important driver of photoevaporation) but it is not coupled at leading order to details of the disk structure[14]. These properties mean that disks evolving under the joint action of viscosity and photoevaporation

[14] In more detail, however, the grain population within the disk will affect the absorption of high energy photons and hence the local mass loss rate [129].

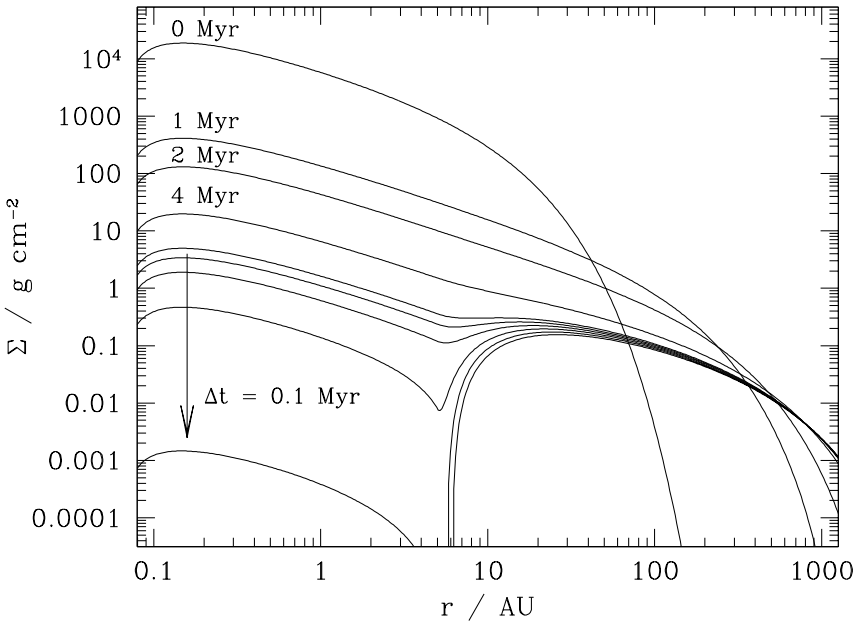

Fig. 33 An illustrative calculation of disk evolution including photoevaporative mass loss. The model plotted is based on a disk with $\nu \propto r$, and wind mass loss that scales as $\dot{\Sigma}_w \propto r^{-5/2}$ outside 5 AU. The disk displays the two time scale evolutionary behavior that is reasonably generic to internal photoevaporation models, with a long period of slow "viscous" evolution being followed by rapid inside-out dispersal.

exhibit two distinct phases of evolution, an early phase in which viscosity dominates and a short subsequent phase in which the wind results in rapid disk dispersal [80].

Figure 33, based on the original calculations by Clarke et al. [80], shows how a disk evolves under the action of viscosity and EUV photoevaporation from the central star. In addition to the two time scale evolutionary behavior, the concentration of EUV mass loss toward the inner disk leads to a characteristic radial structure of disk dispersal. As the disk accretion rate drops, photoevaporation first dominates the evolution near to the innermost radius where mass loss is possible (in the illustrated example, this is taken to be 5 AU). A gap opens at this location, separating the inner disk (with a short viscous time scale) from the outer disk (where the viscous time scale is much longer). The inner disk then drains on to the star, stellar accretion ceases, and the disk is dispersed from the inside-out. The final dispersal is rapid, because the formation of a hole in the disk allows EUV [6] or X-ray [257] radiation to directly illuminate the inner edge of the disk, which typically accelerates mass loss. The dust to gas ratio in whatever is left of the disk increases during the dispersal phase [327, 4, 129]. Although the details depend on the radial profile of the photoevaporative wind, broadly similar evolution is predicted in most models [127].

The observed lifetimes of disks are broadly consistent with theoretically estimates that are based on "best-guess" values of photoevaporative mass loss rates [22].

There is no universal form describing how the action of photoevaporation cuts off accretion in the inner disk. For simple models of EUV photoevaporation, however, it can be shown that the inner accretion rate $\dot{M}(t)$ is related to the accretion rate $\dot{M}_{\rm SS}$ that would be predicted by a self-similar model [219] without mass loss via [298],

$$\dot{M} = \left[1 - \left(\frac{t}{t_0}\right)^{3/2}\right] \dot{M}_{\rm SS}, \tag{254}$$

where t_0 is the time at which accretion ceases. This formula is derived for a specific viscosity law ($\nu \propto r$) and photoevaporation model, but provides a qualitative idea of how the inner disk drains under more general circumstances.

The inside-out character of photoevaporative dispersal applies only in the limit where radiation from the central star is dominant. In sufficiently rich stellar clusters, photoevaporation due to intense FUV radiation fields from other (massive) stars is more important. Unlike in the case of central star photoevaporation, for which the observational evidence is indirect [3], photoevaporative flows driven by external UV fields can sometimes be seen directly, most spectacularly in the core of the Orion Nebula [42]. Adams et al. [1] and Clarke [77] have modeled the evolution of viscous disks under external photoevaporation, and shown that it results in destruction of the disk from the outside-in. For the fraction of stars that form in such clusters, this process evidently limits the time over which gas-rich disks would be present on scales comparable to the Solar System's Kuiper Belt.

8.2 MHD winds

The theoretical and observational arguments for photoevaporation being an important component of disk evolution are strong, but it is not proven that other processes do not also contribute to disk dispersal. The obvious alternate candidate is MHD winds, which are likely to be present if mature disks retain a dynamically significant net magnetic field (see the discussion in §4.4.4). MHD disk winds have obvious qualitative differences from their photoevaporative cousins,

- Their strength depends upon the disk's net flux, rather than on the stellar radiation field.
- They can be accelerated from arbitrarily small radii, where even EUV-ionized gas would be bound, with a velocity proportional to the Keplerian velocity at the magnetic field footpoint.
- The local mass loss rate is (roughly) expected to scale with the disk surface density, rather than being (approximately) a constant independent of the underlying column.
- Predominantly neutral or molecular gas can, at least in principle, be accelerated (though it might subsequently be dissociated or ionized by stellar radiation).

If MHD disk winds are sufficiently strong, they can affect disk dispersal via some combination of mass and angular momentum loss. The resultant evolution can be quite similar to the photoevaporative case. In particular, if mass rather than angular momentum loss is dominant, Suzuki et al. [321] showed that MHD winds lead to the formation of a shallow surface density profile at small radii and, eventually, an expanding inner hole. In the opposite limit where angular momentum loss is strong (and mass loss negligible) Armitage et al. [19] suggested that dispersal could occur through the late onset of magnetic braking. Whether this is possible depends entirely on how the mass to flux ratio of the disk changes over time, and hence on the uncertain question of how net flux is transported and lost (§3.5.1).

It is highly likely that some level of net magnetic field threads disks whose surfaces are heated to $c_s > v_K$ by high energy radiation, leading to hybrid MHD / photoevaporative winds. There has been some work studying how MHD and line-driven winds interact [280], but rather little is known of the observational or theoretical consequences of hybrid wind models in the protoplanetary disk context.

Acknowledgements My work on protoplanetary disk physics and planet formation has been supported by the National Science Foundation, by NASA under the Origins of Solar Systems and Astrophysics Theory programs, and by the Space Telescope Science Institute. I acknowledge the hospitality of the IIB at the University of Liverpool, where much of this chapter was written.

References

1. Adams, F.C., Hollenbach, D., Laughlin, G., Gorti, U.: Photoevaporation of Circumstellar Disks Due to External Far-Ultraviolet Radiation in Stellar Aggregates. ApJ, **611**, 360–379 (2004). DOI 10.1086/421989
2. Alencar, S.H.P., Teixeira, P.S., Guimarães, M.M., McGinnis, P.T., Gameiro, J.F., Bouvier, J., Aigrain, S., Flaccomio, E., Favata, F.: Accretion dynamics and disk evolution in NGC 2264: a study based on CoRoT photometric observations. A&A, **519**, A88 (2010). DOI 10.1051/0004-6361/201014184
3. Alexander, R., Pascucci, I., Andrews, S., Armitage, P., Cieza, L.: The Dispersal of Protoplanetary Disks. Protostars and Planets VI pp. 475–496 (2014)
4. Alexander, R.D., Armitage, P.J.: Dust dynamics during protoplanetary disc clearing. MNRAS, **375**, 500–512 (2007). DOI 10.1111/j.1365-2966.2006.11341.x
5. Alexander, R.D., Clarke, C.J., Pringle, J.E.: Constraints on the ionizing flux emitted by T Tauri stars. MNRAS, **358**, 283–290 (2005). DOI 10.1111/j.1365-2966.2005.08786.x
6. Alexander, R.D., Clarke, C.J., Pringle, J.E.: Photoevaporation of protoplanetary discs - I. Hydrodynamic models. MNRAS, **369**, 216–228 (2006). DOI 10.1111/j.1365-2966.2006.10293.x
7. ALMA Partnership, Brogan, C.L., Pérez, L.M., Hunter, T.R., Dent, W.R.F., Hales, A.S., Hills, R.E., Corder, S., Fomalont, E.B., Vlahakis, C., Asaki, Y., Barkats, D., Hirota, A., Hodge, J.A., Impellizzeri, C.M.V., Kneissl, R., Liuzzo, E., Lucas, R., Marcelino, N., Matsushita, S., Nakanishi, K., Phillips, N., Richards, A.M.S., Toledo, I., Aladro, R., Broguiere, D., Cortes, J.R., Cortes, P.C., Espada, D., Galarza, F., Garcia-Appadoo, D., Guzman-

Ramirez, L., Humphreys, E.M., Jung, T., Kameno, S., Laing, R.A., Leon, S., Marconi, G., Mignano, A., Nikolic, B., Nyman, L.A., Radiszcz, M., Remijan, A., Rodón, J.A., Sawada, T., Takahashi, S., Tilanus, R.P.J., Vila Vilaro, B., Watson, L.C., Wiklind, T., Akiyama, E., Chapillon, E., de Gregorio-Monsalvo, I., Di Francesco, J., Gueth, F., Kawamura, A., Lee, C.F., Nguyen Luong, Q., Mangum, J., Pietu, V., Sanhueza, P., Saigo, K., Takakuwa, S., Ubach, C., van Kempen, T., Wootten, A., Castro-Carrizo, A., Francke, H., Gallardo, J., Garcia, J., Gonzalez, S., Hill, T., Kaminski, T., Kurono, Y., Liu, H.Y., Lopez, C., Morales, F., Plarre, K., Schieven, G., Testi, L., Videla, L., Villard, E., Andreani, P., Hibbard, J.E., Tatematsu, K.: The 2014 ALMA Long Baseline Campaign: First Results from High Angular Resolution Observations toward the HL Tau Region. ApJL, **808**, L3 (2015). DOI 10.1088/2041-8205/808/1/L3

8. Andrews, S.M., Williams, J.P.: Circumstellar Dust Disks in Taurus-Auriga: The Submillimeter Perspective. ApJ, **631**, 1134–1160 (2005). DOI 10.1086/432712
9. Andrews, S.M., Wilner, D.J., Hughes, A.M., Qi, C., Dullemond, C.P.: Protoplanetary Disk Structures in Ophiuchus. ApJ, **700**, 1502–1523 (2009). DOI 10.1088/0004-637X/700/2/1502
10. Andrews, S.M., Wilner, D.J., Hughes, A.M., Qi, C., Rosenfeld, K.A., Öberg, K.I., Birnstiel, T., Espaillat, C., Cieza, L.A., Williams, J.P., Lin, S.Y., Ho, P.T.P.: The TW Hya Disk at 870 μm: Comparison of CO and Dust Radial Structures. ApJ, **744**, 162 (2012). DOI 10.1088/0004-637X/744/2/162
11. Armitage, P.J.: Magnetic cycles and photometric variability of T Tauri stars. MNRAS, **274**, 1242–1248 (1995)
12. Armitage, P.J.: Turbulence and Angular Momentum Transport in a Global Accretion Disk Simulation. ApJL, **501**, L189–L192 (1998). DOI 10.1086/311463
13. Armitage, P.J.: Magnetic activity in accretion disc boundary layers. MNRAS, **330**, 895–900 (2002). DOI 10.1046/j.1365-8711.2002.05152.x
14. Armitage, P.J.: Lecture notes on the formation and early evolution of planetary systems. ArXiv Astrophysics e-prints (2007)
15. Armitage, P.J.: Astrophysics of Planet Formation (2010)
16. Armitage, P.J.: Dynamics of Protoplanetary Disks. ARA&A, **49**, 195–236 (2011). DOI 10.1146/annurev-astro-081710-102521
17. Armitage, P.J.: A Trap for Planet Formation. Science **340**, 1179–1180 (2013). DOI 10.1126/science.1239404
18. Armitage, P.J., Livio, M., Pringle, J.E.: Episodic accretion in magnetically layered protoplanetary discs. MNRAS, **324**, 705–711 (2001). DOI 10.1046/j.1365-8711.2001.04356.x
19. Armitage, P.J., Simon, J.B., Martin, R.G.: Two Timescale Dispersal of Magnetized Protoplanetary Disks. ApJL, **778**, L14 (2013). DOI 10.1088/2041-8205/778/1/L14
20. Artymowicz, P., Lubow, S.H.: Mass Flow through Gaps in Circumbinary Disks. ApJL, **467**, L77 (1996). DOI 10.1086/310200
21. Audard, M., Ábrahám, P., Dunham, M.M., Green, J.D., Grosso, N., Hamaguchi, K., Kastner, J.H., Kóspál, Á., Lodato, G., Romanova, M.M., Skinner, S.L., Vorobyov, E.I., Zhu, Z.: Episodic Accretion in Young Stars. Protostars and Planets VI pp. 387–410 (2014)
22. Bae, J., Hartmann, L., Zhu, Z., Gammie, C.: The Long-term Evolution of Photoevaporating Protoplanetary Disks. ApJ, **774**, 57 (2013). DOI 10.1088/0004-637X/774/1/57
23. Bae, J., Hartmann, L., Zhu, Z., Gammie, C.: Variable Accretion Outbursts in Protostellar Evolution. ApJ, **764**, 141 (2013). DOI 10.1088/0004-637X/764/2/141
24. Bae, J., Hartmann, L., Zhu, Z., Nelson, R.P.: Accretion Outbursts in Self-gravitating Protoplanetary Disks. ApJ, **795**, 61 (2014). DOI 10.1088/0004-637X/795/1/61
25. Bai, X.N.: Magnetorotational-instability-driven Accretion in Protoplanetary Disks. ApJ, **739**, 50 (2011). DOI 10.1088/0004-637X/739/1/50
26. Bai, X.N.: Wind-driven Accretion in Protoplanetary Disks. II. Radial Dependence and Global Picture. ApJ, **772**, 96 (2013). DOI 10.1088/0004-637X/772/2/96
27. Bai, X.N.: Hall-effect-Controlled Gas Dynamics in Protoplanetary Disks. I. Wind Solutions at the Inner Disk. ApJ, **791**, 137 (2014). DOI 10.1088/0004-637X/791/2/137
28. Bai, X.N.: Hall Effect Controlled Gas Dynamics in Protoplanetary Disks. II. Full 3D Simulations toward the Outer Disk. ApJ, **798**, 84 (2015). DOI 10.1088/0004-637X/798/2/84

29. Bai, X.N., Goodman, J.: Heat and Dust in Active Layers of Protostellar Disks. ApJ, **701**, 737–755 (2009). DOI 10.1088/0004-637X/701/1/737
30. Bai, X.N., Stone, J.M.: Dynamics of Solids in the Midplane of Protoplanetary Disks: Implications for Planetesimal Formation. ApJ, **722**, 1437–1459 (2010). DOI 10.1088/0004-637X/722/2/1437
31. Bai, X.N., Stone, J.M.: The Effect of the Radial Pressure Gradient in Protoplanetary Disks on Planetesimal Formation. ApJL, **722**, L220–L223 (2010). DOI 10.1088/2041-8205/722/2/L220
32. Bai, X.N., Stone, J.M.: Effect of Ambipolar Diffusion on the Nonlinear Evolution of Magnetorotational Instability in Weakly Ionized Disks. ApJ, **736**, 144 (2011). DOI 10.1088/0004-637X/736/2/144
33. Bai, X.N., Stone, J.M.: Wind-driven Accretion in Protoplanetary Disks. I. Suppression of the Magnetorotational Instability and Launching of the Magnetocentrifugal Wind. ApJ, **769**, 76 (2013). DOI 10.1088/0004-637X/769/1/76
34. Bai, X.N., Stone, J.M.: Magnetic Flux Concentration and Zonal Flows in Magnetorotational Instability Turbulence. ApJ, **796**, 31 (2014). DOI 10.1088/0004-637X/796/1/31
35. Bakes, E.L.O., Tielens, A.G.G.M.: The photoelectric heating mechanism for very small graphitic grains and polycyclic aromatic hydrocarbons. ApJ, **427**, 822–838 (1994). DOI 10.1086/174188
36. Balbus, S.A.: Magnetohydrodynamics of Protostellar Disks, pp. 237–282 (2011)
37. Balbus, S.A., Hawley, J.F.: A powerful local shear instability in weakly magnetized disks. I - Linear analysis. II - Nonlinear evolution. ApJ, **376**, 214–233 (1991). DOI 10.1086/170270
38. Balbus, S.A., Hawley, J.F.: Instability, turbulence, and enhanced transport in accretion disks. Reviews of Modern Physics **70**, 1–53 (1998). DOI 10.1103/RevModPhys.70.1
39. Balbus, S.A., Hawley, J.F., Stone, J.M.: Nonlinear Stability, Hydrodynamical Turbulence, and Transport in Disks. ApJ, **467**, 76 (1996). DOI 10.1086/177585
40. Balbus, S.A., Papaloizou, J.C.B.: On the Dynamical Foundations of α Disks. ApJ, **521**, 650–658 (1999). DOI 10.1086/307594
41. Balbus, S.A., Terquem, C.: Linear Analysis of the Hall Effect in Protostellar Disks. ApJ, **552**, 235–247 (2001). DOI 10.1086/320452
42. Bally, J., O'Dell, C.R., McCaughrean, M.J.: Disks, Microjets, Windblown Bubbles, and Outflows in the Orion Nebula. AJ, **119**, 2919–2959 (2000). DOI 10.1086/301385
43. Bally, J., Scoville, N.Z.: Structure and evolution of molecular clouds near H II regions. II - The disk constrained H II region, S106. ApJ, **255**, 497–509 (1982). DOI 10.1086/159850
44. Barge, P., Sommeria, J.: Did planet formation begin inside persistent gaseous vortices? A&A, **295**, L1–L4 (1995)
45. Barker, A.J., Ogilvie, G.I.: Hydrodynamic instability in eccentric astrophysical discs. MNRAS, **445**, 2637–2654 (2014). DOI 10.1093/mnras/stu1939
46. Barranco, J.A., Marcus, P.S.: Three-dimensional Vortices in Stratified Protoplanetary Disks. ApJ, **623**, 1157–1170 (2005). DOI 10.1086/428639
47. Baruteau, C., Meru, F., Paardekooper, S.J.: Rapid inward migration of planets formed by gravitational instability. MNRAS, **416**, 1971–1982 (2011). DOI 10.1111/j.1365-2966.2011.19172.x
48. Begelman, M.C., McKee, C.F., Shields, G.A.: Compton heated winds and coronae above accretion disks. I Dynamics. ApJ, **271**, 70–88 (1983). DOI 10.1086/161178
49. Bell, K.R., Cassen, P.M., Klahr, H.H., Henning, T.: The Structure and Appearance of Protostellar Accretion Disks: Limits on Disk Flaring. ApJ, **486**, 372–387 (1997)
50. Bell, K.R., Lin, D.N.C.: Using FU Orionis outbursts to constrain self-regulated protostellar disk models. ApJ, **427**, 987–1004 (1994). DOI 10.1086/174206
51. Belyaev, M.A., Rafikov, R.R., Stone, J.M.: Angular Momentum Transport by Acoustic Modes Generated in the Boundary Layer. I. Hydrodynamical Theory and Simulations. ApJ, **770**, 67 (2013). DOI 10.1088/0004-637X/770/1/67
52. Belyaev, M.A., Rafikov, R.R., Stone, J.M.: Angular Momentum Transport by Acoustic Modes Generated in the Boundary Layer. II. Magnetohydrodynamic Simulations. ApJ, **770**, 68 (2013). DOI 10.1088/0004-637X/770/1/68

53. Besla, G., Wu, Y.: Formation of Narrow Dust Rings in Circumstellar Debris Disks. ApJ, **655**, 528–540 (2007). DOI 10.1086/509495
54. Bisschop, S.E., Fraser, H.J., Öberg, K.I., van Dishoeck, E.F., Schlemmer, S.: Desorption rates and sticking coefficients for CO and N_2 interstellar ices. A&A, **449**, 1297–1309 (2006). DOI 10.1051/0004-6361:20054051
55. Bjorkman, J.E., Wood, K.: Radiative Equilibrium and Temperature Correction in Monte Carlo Radiation Transfer. ApJ, **554**, 615–623 (2001). DOI 10.1086/321336
56. Blaes, O.M., Balbus, S.A.: Local shear instabilities in weakly ionized, weakly magnetized disks. ApJ, **421**, 163–177 (1994). DOI 10.1086/173634
57. Blandford, R.D., Payne, D.G.: Hydromagnetic flows from accretion discs and the production of radio jets. MNRAS, **199**, 883–903 (1982)
58. Blum, J., Wurm, G.: The Growth Mechanisms of Macroscopic Bodies in Protoplanetary Disks. ARA&A, **46**, 21–56 (2008). DOI 10.1146/annurev.astro.46.060407.145152
59. Bonnell, I., Bastien, P.: A binary origin for FU Orionis stars. ApJL, **401**, L31–L34 (1992). DOI 10.1086/186663
60. Bouvier, J., Alencar, S.H.P., Harries, T.J., Johns-Krull, C.M., Romanova, M.M.: Magnetospheric Accretion in Classical T Tauri Stars. Protostars and Planets V pp. 479–494 (2007)
61. Bouvier, J., Cabrit, S., Fernandez, M., Martin, E.L., Matthews, J.M.: Coyotes-I - the Photometric Variability and Rotational Evolution of T-Tauri Stars. A&A, **272**, 176 (1993)
62. Bouvier, J., Matt, S.P., Mohanty, S., Scholz, A., Stassun, K.G., Zanni, C.: Angular Momentum Evolution of Young Low-Mass Stars and Brown Dwarfs: Observations and Theory. Protostars and Planets VI pp. 433–450 (2014)
63. Brauer, F., Henning, T., Dullemond, C.P.: Planetesimal formation near the snow line in MRI-driven turbulent protoplanetary disks. A&A, **487**, L1–L4 (2008). DOI 10.1051/0004-6361:200809780
64. Burke, J.R., Hollenbach, D.J.: The gas-grain interaction in the interstellar medium - Thermal accommodation and trapping. ApJ, **265**, 223–234 (1983). DOI 10.1086/160667
65. Cannizzo, J.K.: The Accretion Disk Limit Cycle Model: Toward an Understanding of the Long-Term Behavior of SS Cygni. ApJ, **419**, 318 (1993). DOI 10.1086/173486
66. Cao, X., Spruit, H.C.: Instability of an accretion disk with a magnetically driven wind. A&A, **385**, 289–300 (2002). DOI 10.1051/0004-6361:20011818
67. Carrera, D., Johansen, A., Davies, M.B.: How to form planetesimals from mm-sized chondrules and chondrule aggregates. A&A, **579**, A43 (2015). DOI 10.1051/0004-6361/201425120
68. Casassus, S., Marino, S., Perez, S., Roman, P., Dunhill, A., Armitage, P., Cuadra, J., Wootten, A., van der Plas, G., Cieza, L., Moral, V., Christiaens, V., Montesinos, M.: Accretion kinematics through the warped transition disk in HD142527 from resolved CO(6-5) observations. ArXiv e-prints (2015)
69. Casassus, S., van der Plas, G., M, S.P., Dent, W.R.F., Fomalont, E., Hagelberg, J., Hales, A., Jordán, A., Mawet, D., Ménard, F., Wootten, A., Wilner, D., Hughes, A.M., Schreiber, M.R., Girard, J.H., Ercolano, B., Canovas, H., Román, P.E., Salinas, V.: Flows of gas through a protoplanetary gap. Nature, **493**, 191–194 (2013). DOI 10.1038/nature11769
70. Cha, S.H., Nayakshin, S.: A numerical simulation of a 'Super-Earth' core delivery from 100 to 8 au. MNRAS, **415**, 3319–3334 (2011). DOI 10.1111/j.1365-2966.2011.18953.x
71. Chandrasekhar, S.: Hydrodynamic and hydromagnetic stability (1961)
72. Chang, P., Oishi, J.S.: On the Stability of Dust-laden Protoplanetary Vortices. ApJ, **721**, 1593–1602 (2010). DOI 10.1088/0004-637X/721/2/1593
73. Chavanis, P.H.: Trapping of dust by coherent vortices in the solar nebula. A&A, **356**, 1089–1111 (2000)
74. Chiang, E., Youdin, A.N.: Forming Planetesimals in Solar and Extrasolar Nebulae. Annual Review of Earth and Planetary Sciences **38**, 493–522 (2010). DOI 10.1146/annurev-earth-040809-152513
75. Chiang, E.I., Goldreich, P.: Spectral Energy Distributions of T Tauri Stars with Passive Circumstellar Disks. ApJ, **490**, 368–376 (1997)

76. Ciesla, F.J., Cuzzi, J.N.: The evolution of the water distribution in a viscous protoplanetary disk. Icarus, **181**, 178–204 (2006). DOI 10.1016/j.icarus.2005.11.009
77. Clarke, C.J.: The photoevaporation of discs around young stars in massive clusters. MNRAS, **376**, 1350–1356 (2007). DOI 10.1111/j.1365-2966.2007.11547.x
78. Clarke, C.J.: Pseudo-viscous modelling of self-gravitating discs and the formation of low mass ratio binaries. MNRAS, **396**, 1066–1074 (2009). DOI 10.1111/j.1365-2966.2009.14774.x
79. Clarke, C.J., Armitage, P.J., Smith, K.W., Pringle, J.E.: Magnetically modulated accretion in T Tauri stars. MNRAS, **273**, 639–642 (1995)
80. Clarke, C.J., Gendrin, A., Sotomayor, M.: The dispersal of circumstellar discs: the role of the ultraviolet switch. MNRAS, **328**, 485–491 (2001). DOI 10.1046/j.1365-8711.2001.04891.x
81. Clarke, C.J., Pringle, J.E.: The diffusion of contaminant through an accretion disc. MNRAS, **235**, 365–373 (1988)
82. Clarke, C.J., Syer, D.: Low-mass companions to T Tauri stars: a mechanism for rapid-rise FU Orionis outbursts. MNRAS, **278**, L23–L27 (1996)
83. Cleeves, L.I., Bergin, E.A., Qi, C., Adams, F.C., Öberg, K.I.: Constraining the X-Ray and Cosmic-Ray Ionization Chemistry of the TW Hya Protoplanetary Disk: Evidence for a Sub-interstellar Cosmic-Ray Rate. ApJ, **799**, 204 (2015). DOI 10.1088/0004-637X/799/2/204
84. Cody, A.M., Stauffer, J., Baglin, A., Micela, G., Rebull, L.M., Flaccomio, E., Morales-Calderón, M., Aigrain, S., Bouvier, J., Hillenbrand, L.A., Gutermuth, R., Song, I., Turner, N., Alencar, S.H.P., Zwintz, K., Plavchan, P., Carpenter, J., Findeisen, K., Carey, S., Terebey, S., Hartmann, L., Calvet, N., Teixeira, P., Vrba, F.J., Wolk, S., Covey, K., Poppenhaeger, K., Günther, H.M., Forbrich, J., Whitney, B., Affer, L., Herbst, W., Hora, J., Barrado, D., Holtzman, J., Marchis, F., Wood, K., Medeiros Guimarães, M., Lillo Box, J., Gillen, E., McQuillan, A., Espaillat, C., Allen, L., D'Alessio, P., Favata, F.: CSI 2264: Simultaneous Optical and Infrared Light Curves of Young Disk-bearing Stars in NGC 2264 with CoRoT and Spitzer — Evidence for Multiple Origins of Variability. AJ, **147**, 82 (2014). DOI 10.1088/0004-6256/147/4/82
85. Cossins, P., Lodato, G., Clarke, C.: The effects of opacity on gravitational stability in protoplanetary discs. MNRAS, **401**, 2587–2598 (2010). DOI 10.1111/j.1365-2966.2009.15835.x
86. Cossins, P., Lodato, G., Clarke, C.J.: Characterizing the gravitational instability in cooling accretion discs. MNRAS, **393**, 1157–1173 (2009). DOI 10.1111/j.1365-2966.2008.14275.x
87. Curry, C., Pudritz, R.E.: On the Global Stability of Magnetized Accretion Disks. II. Vertical and Azimuthal Magnetic Fields. ApJ, **453**, 697 (1995). DOI 10.1086/176431
88. D'Angelo, C.R., Spruit, H.C.: Episodic accretion on to strongly magnetic stars. MNRAS, **406**, 1208–1219 (2010). DOI 10.1111/j.1365-2966.2010.16749.x
89. Davis, S.W., Stone, J.M., Pessah, M.E.: Sustained Magnetorotational Turbulence in Local Simulations of Stratified Disks with Zero Net Magnetic Flux. ApJ, **713**, 52–65 (2010). DOI 10.1088/0004-637X/713/1/52
90. de Val-Borro, M., Artymowicz, P., D'Angelo, G., Peplinski, A.: Vortex generation in protoplanetary disks with an embedded giant planet. A&A, **471**, 1043–1055 (2007). DOI 10.1051/0004-6361:20077169
91. Desch, S.J.: Linear Analysis of the Magnetorotational Instability, Including Ambipolar Diffusion, with Application to Protoplanetary Disks. ApJ, **608**, 509–525 (2004). DOI 10.1086/392527
92. Dittrich, K., Klahr, H., Johansen, A.: Gravoturbulent Planetesimal Formation: The Positive Effect of Long-lived Zonal Flows. ApJ, **763**, 117 (2013). DOI 10.1088/0004-637X/763/2/117
93. D'Orazio, D.J., Haiman, Z., MacFadyen, A.: Accretion into the central cavity of a circumbinary disc. MNRAS, **436**, 2997–3020 (2013). DOI 10.1093/mnras/stt1787
94. Draine, B.T.: Photoelectric heating of interstellar gas. ApJS, **36**, 595–619 (1978). DOI 10.1086/190513
95. Draine, B.T., Roberge, W.G., Dalgarno, A.: Magnetohydrodynamic shock waves in molecular clouds. ApJ, **264**, 485–507 (1983). DOI 10.1086/160617

96. Draine, B.T., Sutin, B.: Collisional charging of interstellar grains. ApJ, **320**, 803–817 (1987). DOI 10.1086/165596
97. Dubrulle, B., Morfill, G., Sterzik, M.: The dust subdisk in the protoplanetary nebula. Icarus, **114**, 237–246 (1995). DOI 10.1006/icar.1995.1058
98. Eckhardt, B., Schneider, T.M., Hof, B., Westerweel, J.: Turbulence Transition in Pipe Flow. Annual Review of Fluid Mechanics **39**, 447–468 (2007). DOI 10.1146/annurev.fluid.39.050905.110308
99. Edlund, E.M., Ji, H.: Nonlinear stability of laboratory quasi-Keplerian flows. Phys. Rev. E, **89**(2), 021004 (2014). DOI 10.1103/PhysRevE.89.021004
100. Ercolano, B., Barlow, M.J., Storey, P.J.: The dusty MOCASSIN: fully self-consistent 3D photoionization and dust radiative transfer models. MNRAS, **362**, 1038–1046 (2005). DOI 10.1111/j.1365-2966.2005.09381.x
101. Ercolano, B., Glassgold, A.E.: X-ray ionization rates in protoplanetary discs. MNRAS, **436**, 3446–3450 (2013). DOI 10.1093/mnras/stt1826
102. Espaillat, C., Muzerolle, J., Najita, J., Andrews, S., Zhu, Z., Calvet, N., Kraus, S., Hashimoto, J., Kraus, A., D'Alessio, P.: An Observational Perspective of Transitional Disks. Protostars and Planets VI pp. 497–520 (2014)
103. Faure, J., Fromang, S., Latter, H., Meheut, H.: Vortex cycles at the inner edges of dead zones in protoplanetary disks. A&A, **573**, A132 (2015). DOI 10.1051/0004-6361/201424162
104. Federrath, C., Banerjee, S.: The density structure and star formation rate of non-isothermal polytropic turbulence. MNRAS, **448**, 3297–3313 (2015). DOI 10.1093/mnras/stv180
105. Fleming, T., Stone, J.M.: Local Magnetohydrodynamic Models of Layered Accretion Disks. ApJ, **585**, 908–920 (2003). DOI 10.1086/345848
106. Flock, M., Ruge, J.P., Dzyurkevich, N., Henning, T., Klahr, H., Wolf, S.: Gaps, rings, and non-axisymmetric structures in protoplanetary disks. From simulations to ALMA observations. A&A, **574**, A68 (2015). DOI 10.1051/0004-6361/201424693
107. Font, A.S., McCarthy, I.G., Johnstone, D., Ballantyne, D.R.: Photoevaporation of Circumstellar Disks around Young Stars. ApJ, **607**, 890–903 (2004). DOI 10.1086/383518
108. Forgan, D., Rice, K.: Stellar encounters in the context of outburst phenomena. MNRAS, **402**, 1349–1356 (2010). DOI 10.1111/j.1365-2966.2009.15974.x
109. Forgan, D., Rice, K., Cossins, P., Lodato, G.: The nature of angular momentum transport in radiative self-gravitating protostellar discs. MNRAS, **410**, 994–1006 (2011). DOI 10.1111/j.1365-2966.2010.17500.x
110. France, K., Schindhelm, E., Bergin, E.A., Roueff, E., Abgrall, H.: High-resolution Ultraviolet Radiation Fields of Classical T Tauri Stars. ApJ, **784**, 127 (2014). DOI 10.1088/0004-637X/784/2/127
111. Frank, J., King, A., Raine, D.J.: Accretion Power in Astrophysics: Third Edition (2002)
112. Fricke, K.: Instabilität stationärer Rotation in Sternen. Zeitschrift für Astrophysik, **68**, 317 (1968)
113. Fromang, S.: MRI-driven angular momentum transport in protoplanetary disks. In: P. Hennebelle, C. Charbonnel (eds.) EAS Publications Series, *EAS Publications Series*, vol. 62, pp. 95–142 (2013). DOI 10.1051/eas/1362004
114. Fromang, S., Latter, H., Lesur, G., Ogilvie, G.I.: Local outflows from turbulent accretion disks. A&A, **552**, A71 (2013). DOI 10.1051/0004-6361/201220016
115. Fromang, S., Papaloizou, J.: Dust settling in local simulations of turbulent protoplanetary disks. A&A, **452**, 751–762 (2006). DOI 10.1051/0004-6361:20054612
116. Fu, R.R., Weiss, B.P., Lima, E.A., Harrison, R.J., Bai, X.N., Desch, S.J., Ebel, D.S., Suavet, C., Wang, H., Glenn, D., Le Sage, D., Kasama, T., Walsworth, R.L., Kuan, A.T.: Solar nebula magnetic fields recorded in the semarkona meteorite. Science (2014). DOI 10.1126/science.1258022. URL `http://www.sciencemag.org/content/early/2014/11/12/science.1258022.abstract`
117. Fu, W., Li, H., Lubow, S., Li, S., Liang, E.: Effects of Dust Feedback on Vortices in Protoplanetary Disks. ApJL, **795**, L39 (2014). DOI 10.1088/2041-8205/795/2/L39

118. Galvagni, M., Hayfield, T., Boley, A., Mayer, L., Roškar, R., Saha, P.: The collapse of protoplanetary clumps formed through disc instability: 3D simulations of the pre-dissociation phase. MNRAS, **427**, 1725–1740 (2012). DOI 10.1111/j.1365-2966.2012.22096.x
119. Gammie, C.F.: Layered Accretion in T Tauri Disks. ApJ, **457**, 355 (1996). DOI 10.1086/176735
120. Gammie, C.F.: Instabilities in Circumstellar Discs. In: J.A. Sellwood, J. Goodman (eds.) Astrophysical Discs - an EC Summer School, *Astronomical Society of the Pacific Conference Series*, vol. 160, p. 122 (1999)
121. Gammie, C.F.: Nonlinear Outcome of Gravitational Instability in Cooling, Gaseous Disks. ApJ, **553**, 174–183 (2001). DOI 10.1086/320631
122. Garaud, P., Lin, D.N.C.: The Effect of Internal Dissipation and Surface Irradiation on the Structure of Disks and the Location of the Snow Line around Sun-like Stars. ApJ, **654**, 606–624 (2007). DOI 10.1086/509041
123. Gibbons, P.G., Mamatsashvili, G.R., Rice, W.K.M.: Planetesimal formation in self-gravitating discs - the effects of particle self-gravity and back-reaction. MNRAS, **442**, 361–371 (2014). DOI 10.1093/mnras/stu809
124. Godon, P., Livio, M.: The Formation and Role of Vortices in Protoplanetary Disks. ApJ, **537**, 396–404 (2000). DOI 10.1086/309019
125. Goldreich, P., Goodman, J., Narayan, R.: The stability of accretion tori. I - Long-wavelength modes of slender tori. MNRAS, **221**, 339–364 (1986)
126. Goldreich, P., Schubert, G.: Differential Rotation in Stars. ApJ, **150**, 571 (1967). DOI 10.1086/149360
127. Gorti, U., Dullemond, C.P., Hollenbach, D.: Time Evolution of Viscous Circumstellar Disks due to Photoevaporation by Far-Ultraviolet, Extreme-Ultraviolet, and X-ray Radiation from the Central Star. ApJ, **705**, 1237–1251 (2009). DOI 10.1088/0004-637X/705/2/1237
128. Gorti, U., Hollenbach, D.: Photoevaporation of Circumstellar Disks By Far-Ultraviolet, Extreme-Ultraviolet and X-Ray Radiation from the Central Star. ApJ, **690**, 1539–1552 (2009). DOI 10.1088/0004-637X/690/2/1539
129. Gorti, U., Hollenbach, D., Dullemond, C.P.: The Impact of Dust Evolution and Photoevaporation on Disk Dispersal. ApJ, **804**, 29 (2015). DOI 10.1088/0004-637X/804/1/29
130. Grady, C.A., Muto, T., Hashimoto, J., Fukagawa, M., Currie, T., Biller, B., Thalmann, C., Sitko, M.L., Russell, R., Wisniewski, J., Dong, R., Kwon, J., Sai, S., Hornbeck, J., Schneider, G., Hines, D., Moro Martín, A., Feldt, M., Henning, T., Pott, J.U., Bonnefoy, M., Bouwman, J., Lacour, S., Mueller, A., Juhász, A., Crida, A., Chauvin, G., Andrews, S., Wilner, D., Kraus, A., Dahm, S., Robitaille, T., Jang-Condell, H., Abe, L., Akiyama, E., Brandner, W., Brandt, T., Carson, J., Egner, S., Follette, K.B., Goto, M., Guyon, O., Hayano, Y., Hayashi, M., Hayashi, S., Hodapp, K., Ishii, M., Iye, M., Janson, M., Kandori, R., Knapp, G., Kudo, T., Kusakabe, N., Kuzuhara, M., Mayama, S., McElwain, M., Matsuo, T., Miyama, S., Morino, J.I., Nishimura, T., Pyo, T.S., Serabyn, G., Suto, H., Suzuki, R., Takami, M., Takato, N., Terada, H., Tomono, D., Turner, E., Watanabe, M., Yamada, T., Takami, H., Usuda, T., Tamura, M.: Spiral Arms in the Asymmetrically Illuminated Disk of MWC 758 and Constraints on Giant Planets. ApJ, **762**, 48 (2013). DOI 10.1088/0004-637X/762/1/48
131. Gressel, O., Turner, N.J., Nelson, R.P., McNally, C.P.: Global Simulations of Protoplanetary Disks With Ohmic Resistivity and Ambipolar Diffusion. ApJ, **801**, 84 (2015). DOI 10.1088/0004-637X/801/2/84
132. Güdel, M., Briggs, K.R., Arzner, K., Audard, M., Bouvier, J., Feigelson, E.D., Franciosini, E., Glauser, A., Grosso, N., Micela, G., Monin, J.L., Montmerle, T., Padgett, D.L., Palla, F., Pillitteri, I., Rebull, L., Scelsi, L., Silva, B., Skinner, S.L., Stelzer, B., Telleschi, A.: The XMM-Newton extended survey of the Taurus molecular cloud (XEST). A&A, **468**, 353–377 (2007). DOI 10.1051/0004-6361:20065724
133. Guilet, J., Ogilvie, G.I.: Transport of magnetic flux and the vertical structure of accretion discs - I. Uniform diffusion coefficients. MNRAS, **424**, 2097–2117 (2012). DOI 10.1111/j.1365-2966.2012.21361.x

134. Guilet, J., Ogilvie, G.I.: Global evolution of the magnetic field in a thin disc and its consequences for protoplanetary systems. MNRAS, **441**, 852–868 (2014). DOI 10.1093/mnras/stu532
135. Gullbring, E., Hartmann, L., Briceño, C., Calvet, N.: Disk Accretion Rates for T Tauri Stars. ApJ, **492**, 323–341 (1998). DOI 10.1086/305032
136. Hōshi, R.: Accretion Model for Outbursts of Dwarf Nova. Progress of Theoretical Physics **61**, 1307–1319 (1979). DOI 10.1143/PTP.61.1307
137. Haghighipour, N., Boss, A.P.: On Pressure Gradients and Rapid Migration of Solids in a Nonuniform Solar Nebula. ApJ, **583**, 996–1003 (2003). DOI 10.1086/345472
138. Haisch Jr., K.E., Lada, E.A., Lada, C.J.: Disk Frequencies and Lifetimes in Young Clusters. ApJL, **553**, L153–L156 (2001). DOI 10.1086/320685
139. Hartmann, L., Kenyon, S.J.: The FU Orionis Phenomenon. ARA&A, **34**, 207–240 (1996). DOI 10.1146/annurev.astro.34.1.207
140. Hawley, J.F., Gammie, C.F., Balbus, S.A.: Local Three-dimensional Magnetohydrodynamic Simulations of Accretion Disks. ApJ, **440**, 742 (1995). DOI 10.1086/175311
141. Hawley, J.F., Stone, J.M.: Nonlinear Evolution of the Magnetorotational Instability in Ion-Neutral Disks. ApJ, **501**, 758–771 (1998). DOI 10.1086/305849
142. Hayashi, C.: Structure of the Solar Nebula, Growth and Decay of Magnetic Fields and Effects of Magnetic and Turbulent Viscosities on the Nebula. Progress of Theoretical Physics Supplement **70**, 35–53 (1981). DOI 10.1143/PTPS.70.35
143. Haynes, D.R., Tro, N.J., George, S.M.: Condensation and evaporation of H_2O on ice surfaces. Journal of Physical Chemistry **96**, 8502–8509 (1992)
144. Henning, T., Semenov, D.: Chemistry in Protoplanetary Disks. Chemical Reviews **113**, 9016–9042 (2013). DOI 10.1021/cr400128p
145. Herbig, G.H.: Eruptive phenomena in early stellar evolution. ApJ, **217**, 693–715 (1977). DOI 10.1086/155615
146. Herbig, G.H.: History and Spectroscopy of EXor Candidates. AJ, **135**, 637–648 (2008). DOI 10.1088/0004-6256/135/2/637
147. Hernández, J., Hartmann, L., Megeath, T., Gutermuth, R., Muzerolle, J., Calvet, N., Vivas, A.K., Briceño, C., Allen, L., Stauffer, J., Young, E., Fazio, G.: A Spitzer Space Telescope Study of Disks in the Young σ Orionis Cluster. ApJ, **662**, 1067–1081 (2007). DOI 10.1086/513735
148. Hillenbrand, L.A., Findeisen, K.P.: A Simple Calculation in Service of Constraining the Rate of FU Orionis Outburst Events from Photometric Monitoring Surveys. ArXiv e-prints (2015)
149. Hirose, S., Blaes, O., Krolik, J.H., Coleman, M.S.B., Sano, T.: Convection Causes Enhanced Magnetic Turbulence in Accretion Disks in Outburst. ApJ, **787**, 1 (2014). DOI 10.1088/0004-637X/787/1/1
150. Hirose, S., Turner, N.J.: Heating and Cooling Protostellar Disks. ApJL, **732**, L30 (2011). DOI 10.1088/2041-8205/732/2/L30
151. Hollenbach, D., Johnstone, D., Lizano, S., Shu, F.: Photoevaporation of disks around massive stars and application to ultracompact H II regions. ApJ, **428**, 654–669 (1994). DOI 10.1086/174276
152. Ilgner, M., Nelson, R.P.: On the ionisation fraction in protoplanetary disks. I. Comparing different reaction networks. A&A, **445**, 205–222 (2006). DOI 10.1051/0004-6361:20053678
153. Illarionov, A.F., Sunyaev, R.A.: Why the Number of Galactic X-ray Stars Is so Small? A&A, **39**, 185 (1975)
154. Inaba, S., Barge, P.: Dusty Vortices in Protoplanetary Disks. ApJ, **649**, 415–427 (2006). DOI 10.1086/506427
155. Ingleby, L., Calvet, N., Hernández, J., Briceño, C., Espaillat, C., Miller, J., Bergin, E., Hartmann, L.: Evolution of X-ray and Far-ultraviolet Disk-dispersing Radiation Fields. AJ, **141**, 127 (2011). DOI 10.1088/0004-6256/141/4/127
156. Inutsuka, S.i., Sano, T.: Self-sustained Ionization and Vanishing Dead Zones in Protoplanetary Disks. ApJL, **628**, L155–L158 (2005). DOI 10.1086/432796
157. Isella, A., Pérez, L.M., Carpenter, J.M., Ricci, L., Andrews, S., Rosenfeld, K.: An Azimuthal Asymmetry in the LkHα 330 Disk. ApJ, **775**, 30 (2013). DOI 10.1088/0004-637X/775/1/30

158. Jacquet, E., Balbus, S., Latter, H.: On linear dust-gas streaming instabilities in protoplanetary discs. MNRAS, **415**, 3591–3598 (2011). DOI 10.1111/j.1365-2966.2011.18971.x
159. Jin, L.: Damping of the Shear Instability in Magnetized Disks by Ohmic Diffusion. ApJ, **457**, 798 (1996). DOI 10.1086/176774
160. Johansen, A., Blum, J., Tanaka, H., Ormel, C., Bizzarro, M., Rickman, H.: The Multifaceted Planetesimal Formation Process. Protostars and Planets VI pp. 547–570 (2014)
161. Johansen, A., Klahr, H., Henning, T.: High-resolution simulations of planetesimal formation in turbulent protoplanetary discs. A&A, **529**, A62 (2011). DOI 10.1051/0004-6361/201015979
162. Johansen, A., Oishi, J.S., Mac Low, M.M., Klahr, H., Henning, T., Youdin, A.: Rapid planetesimal formation in turbulent circumstellar disks. Nature, **448**, 1022–1025 (2007). DOI 10.1038/nature06086
163. Johansen, A., Youdin, A.: Protoplanetary Disk Turbulence Driven by the Streaming Instability: Nonlinear Saturation and Particle Concentration. ApJ, **662**, 627–641 (2007). DOI 10.1086/516730
164. Johansen, A., Youdin, A., Klahr, H.: Zonal Flows and Long-lived Axisymmetric Pressure Bumps in Magnetorotational Turbulence. ApJ, **697**, 1269–1289 (2009). DOI 10.1088/0004-637X/697/2/1269
165. Johansen, A., Youdin, A., Mac Low, M.M.: Particle Clumping and Planetesimal Formation Depend Strongly on Metallicity. ApJL, **704**, L75–L79 (2009). DOI 10.1088/0004-637X/704/2/L75
166. Johnson, B.M., Gammie, C.F.: Nonlinear Outcome of Gravitational Instability in Disks with Realistic Cooling. ApJ, **597**, 131–141 (2003). DOI 10.1086/378392
167. Johnson, B.M., Gammie, C.F.: Vortices in Thin, Compressible, Unmagnetized Disks. ApJ, **635**, 149–156 (2005). DOI 10.1086/497358
168. Kamp, I., Dullemond, C.P.: The Gas Temperature in the Surface Layers of Protoplanetary Disks. ApJ, **615**, 991–999 (2004). DOI 10.1086/424703
169. Kamp, I., van Zadelhoff, G.J.: On the gas temperature in circumstellar disks around A stars. A&A, **373**, 641–656 (2001). DOI 10.1051/0004-6361:20010629
170. Keith, S.L., Wardle, M.: Accretion in giant planet circumplanetary discs. MNRAS, **440**, 89–105 (2014). DOI 10.1093/mnras/stu245
171. Kenyon, S.J., Hartmann, L.: Spectral energy distributions of T Tauri stars - Disk flaring and limits on accretion. ApJ, **323**, 714–733 (1987). DOI 10.1086/165866
172. Kerswell, R.R.: Elliptical instability. Annual Review of Fluid Mechanics **34**, 83–113 (2002). DOI 10.1146/annurev.fluid.34.081701.171829
173. Kida, S.: Motion of an elliptic vortex in a uniform shear flow. Journal of the Physical Society of Japan **50**, 3517–3520 (1981). DOI 10.1143/JPSJ.50.3517
174. King, A.R., Pringle, J.E., Livio, M.: Accretion disc viscosity: how big is alpha? MNRAS, **376**, 1740–1746 (2007). DOI 10.1111/j.1365-2966.2007.11556.x
175. Klahr, H.H., Bodenheimer, P.: Turbulence in Accretion Disks: Vorticity Generation and Angular Momentum Transport via the Global Baroclinic Instability. ApJ, **582**, 869–892 (2003). DOI 10.1086/344743
176. Kley, W., Lin, D.N.C.: The Structure of the Boundary Layer in Protostellar Disks. ApJ, **461**, 933 (1996). DOI 10.1086/177115
177. Kley, W., Nelson, R.P.: Planet-Disk Interaction and Orbital Evolution. ARA&A, **50**, 211–249 (2012). DOI 10.1146/annurev-astro-081811-125523
178. Koenigl, A.: Disk accretion onto magnetic T Tauri stars. ApJL, **370**, L39–L43 (1991). DOI 10.1086/185972
179. Koller, J., Li, H., Lin, D.N.C.: Vortices in the Co-orbital Region of an Embedded Protoplanet. ApJL, **596**, L91–L94 (2003). DOI 10.1086/379032
180. Königl, A., Salmeron, R.: The Effects of Large-Scale Magnetic Fields on Disk Formation and Evolution, pp. 283–352 (2011)
181. Kraichnan, R.H.: Inertial Ranges in Two-Dimensional Turbulence. Physics of Fluids **10**, 1417–1423 (1967). DOI 10.1063/1.1762301

182. Krasnopolsky, R., Li, Z.Y., Shang, H.: Disk Formation in Magnetized Clouds Enabled by the Hall Effect. ApJ, **733**, 54 (2011). DOI 10.1088/0004-637X/733/1/54
183. Kratter, K.M., Matzner, C.D., Krumholz, M.R., Klein, R.I.: On the Role of Disks in the Formation of Stellar Systems: A Numerical Parameter Study of Rapid Accretion. ApJ, **708**, 1585–1597 (2010). DOI 10.1088/0004-637X/708/2/1585
184. Kratter, K.M., Murray-Clay, R.A., Youdin, A.N.: The Runts of the Litter: Why Planets Formed Through Gravitational Instability Can Only Be Failed Binary Stars. ApJ, **710**, 1375–1386 (2010). DOI 10.1088/0004-637X/710/2/1375
185. Kretke, K.A., Lin, D.N.C.: Grain Retention and Formation of Planetesimals near the Snow Line in MRI-driven Turbulent Protoplanetary Disks. ApJL, **664**, L55–L58 (2007). DOI 10.1086/520718
186. Kuiper, G.P.: On the Origin of the Solar System. Proceedings of the National Academy of Science **37**, 1–14 (1951). DOI 10.1073/pnas.37.1.1
187. Kunz, M.W.: On the linear stability of weakly ionized, magnetized planar shear flows. MNRAS, **385**, 1494–1510 (2008). DOI 10.1111/j.1365-2966.2008.12928.x
188. Kunz, M.W., Balbus, S.A.: Ambipolar diffusion in the magnetorotational instability. MNRAS, **348**, 355–360 (2004). DOI 10.1111/j.1365-2966.2004.07383.x
189. Kunz, M.W., Lesur, G.: Magnetic self-organization in Hall-dominated magnetorotational turbulence. MNRAS, **434**, 2295–2312 (2013). DOI 10.1093/mnras/stt1171
190. Kurosawa, R., Romanova, M.M.: Spectral variability of classical T Tauri stars accreting in an unstable regime. MNRAS, **431**, 2673–2689 (2013). DOI 10.1093/mnras/stt365
191. Lai, D.: Magnetically Driven Warping, Precession, and Resonances in Accretion Disks. ApJ, **524**, 1030–1047 (1999). DOI 10.1086/307850
192. Larwood, J.D., Nelson, R.P., Papaloizou, J.C.B., Terquem, C.: The tidally induced warping, precession and truncation of accretion discs in binary systems: three-dimensional simulations. MNRAS, **282**, 597–613 (1996)
193. Lasota, J.P.: The disc instability model of dwarf novae and low-mass X-ray binary transients. New Astronomy Reviews, **45**, 449–508 (2001). DOI 10.1016/S1387-6473(01)00112-9
194. Lecar, M., Podolak, M., Sasselov, D., Chiang, E.: On the Location of the Snow Line in a Protoplanetary Disk. ApJ, **640**, 1115–1118 (2006). DOI 10.1086/500287
195. Lesur, G., Kunz, M.W., Fromang, S.: Thanatology in protoplanetary discs. The combined influence of Ohmic, Hall, and ambipolar diffusion on dead zones. A&A, **566**, A56 (2014). DOI 10.1051/0004-6361/201423660
196. Lesur, G., Longaretti, P.Y.: On the relevance of subcritical hydrodynamic turbulence to accretion disk transport. A&A, **444**, 25–44 (2005). DOI 10.1051/0004-6361:20053683
197. Lesur, G., Ogilvie, G.I.: On the angular momentum transport due to vertical convection in accretion discs. MNRAS, **404**, L64–L68 (2010). DOI 10.1111/j.1745-3933.2010.00836.x
198. Lesur, G., Papaloizou, J.C.B.: On the stability of elliptical vortices in accretion discs. A&A, **498**, 1–12 (2009). DOI 10.1051/0004-6361/200811577
199. Lesur, G., Papaloizou, J.C.B.: The subcritical baroclinic instability in local accretion disc models. A&A, **513**, A60 (2010). DOI 10.1051/0004-6361/200913594
200. Levin, Y.: Starbursts near supermassive black holes: young stars in the Galactic Centre, and gravitational waves in LISA band. MNRAS, **374**, 515–524 (2007). DOI 10.1111/j.1365-2966.2006.11155.x
201. Li, H., Colgate, S.A., Wendroff, B., Liska, R.: Rossby Wave Instability of Thin Accretion Disks. III. Nonlinear Simulations. ApJ, **551**, 874–896 (2001). DOI 10.1086/320241
202. Li, H., Finn, J.M., Lovelace, R.V.E., Colgate, S.A.: Rossby Wave Instability of Thin Accretion Disks. II. Detailed Linear Theory. ApJ, **533**, 1023–1034 (2000). DOI 10.1086/308693
203. Li, Z.Y., Banerjee, R., Pudritz, R.E., Jørgensen, J.K., Shang, H., Krasnopolsky, R., Maury, A.: The Earliest Stages of Star and Planet Formation: Core Collapse, and the Formation of Disks and Outflows. Protostars and Planets VI pp. 173–194 (2014)
204. Liffman, K.: The Gravitational Radius of an Irradiated Disk. Publications of the Astronomical Society of Australia, **20**, 337–339 (2003). DOI 10.1071/AS03019
205. Lin, M.K.: Non-barotropic Linear Rossby Wave Instability in Three-dimensional Disks. ApJ, **765**, 84 (2013). DOI 10.1088/0004-637X/765/2/84

206. Lin, M.K., Youdin, A.: Cooling Requirements for the Vertical Shear Instability in Protoplanetary Disks. ArXiv e-prints (2015)
207. Lodato, G., Clarke, C.J.: Massive planets in FU Orionis discs: implications for thermal instability models. MNRAS, **353**, 841–852 (2004). DOI 10.1111/j.1365-2966.2004.08112.x
208. Lodato, G., Pringle, J.E.: Warp diffusion in accretion discs: a numerical investigation. MNRAS, **381**, 1287–1300 (2007). DOI 10.1111/j.1365-2966.2007.12332.x
209. Lodato, G., Rice, W.K.M.: Testing the locality of transport in self-gravitating accretion discs. MNRAS, **351**, 630–642 (2004). DOI 10.1111/j.1365-2966.2004.07811.x
210. Lodato, G., Rice, W.K.M.: Testing the locality of transport in self-gravitating accretion discs - II. The massive disc case. MNRAS, **358**, 1489–1500 (2005). DOI 10.1111/j.1365-2966.2005.08875.x
211. Lodders, K.: Solar System Abundances and Condensation Temperatures of the Elements. ApJ, **591**, 1220–1247 (2003). DOI 10.1086/375492
212. Lovelace, R.V.E., Li, H., Colgate, S.A., Nelson, A.F.: Rossby Wave Instability of Keplerian Accretion Disks. ApJ, **513**, 805–810 (1999). DOI 10.1086/306900
213. Lovelace, R.V.E., Rothstein, D.M., Bisnovatyi-Kogan, G.S.: Advection/Diffusion of Large-Scale B Field in Accretion Disks. ApJ, **701**, 885–890 (2009). DOI 10.1088/0004-637X/701/2/885
214. Lubow, S.H., Martin, R.G., Nixon, C.: Tidal Torques on Misaligned Disks in Binary Systems. ApJ, **800**, 96 (2015). DOI 10.1088/0004-637X/800/2/96
215. Lubow, S.H., Ogilvie, G.I.: On the Tilting of Protostellar Disks by Resonant Tidal Effects. ApJ, **538**, 326–340 (2000). DOI 10.1086/309101
216. Lubow, S.H., Papaloizou, J.C.B., Pringle, J.E.: Magnetic field dragging in accretion discs. MNRAS, **267**, 235–240 (1994)
217. Lubow, S.H., Papaloizou, J.C.B., Pringle, J.E.: On the Stability of Magnetic Wind-Driven Accretion Discs. MNRAS, **268**, 1010 (1994)
218. Lynden-Bell, D.: On why discs generate magnetic towers and collimate jets. MNRAS, **341**, 1360–1372 (2003). DOI 10.1046/j.1365-8711.2003.06506.x
219. Lynden-Bell, D., Pringle, J.E.: The evolution of viscous discs and the origin of the nebular variables. MNRAS, **168**, 603–637 (1974)
220. Lyra, W., Johansen, A., Klahr, H., Piskunov, N.: Embryos grown in the dead zone. Assembling the first protoplanetary cores in low mass self-gravitating circumstellar disks of gas and solids. A&A, **491**, L41–L44 (2008). DOI 10.1051/0004-6361:200810626
221. Lyra, W., Johansen, A., Zsom, A., Klahr, H., Piskunov, N.: Planet formation bursts at the borders of the dead zone in 2D numerical simulations of circumstellar disks. A&A, **497**, 869–888 (2009). DOI 10.1051/0004-6361/200811265
222. Lyra, W., Kuchner, M.: Formation of sharp eccentric rings in debris disks with gas but without planets. Nature, **499**, 184–187 (2013). DOI 10.1038/nature12281
223. Lyra, W., Mac Low, M.M.: Rossby Wave Instability at Dead Zone Boundaries in Three-dimensional Resistive Magnetohydrodynamical Global Models of Protoplanetary Disks. ApJ, **756**, 62 (2012). DOI 10.1088/0004-637X/756/1/62
224. Lyra, W., Turner, N.J., McNally, C.P.: Rossby wave instability does not require sharp resistivity gradients. A&A, **574**, A10 (2015). DOI 10.1051/0004-6361/201424919
225. Marcus, P., Pei, S., Jiang, C.H., Barranco, J., Hassanzadeh, P., Lecoanet, D.: Zombie Vortex Instability I: A Purely Hydrodynamic Instability to Resurrect the Dead Zones of Protoplanetary Disks. ArXiv e-prints (2014)
226. Marley, M.S., Fortney, J.J., Hubickyj, O., Bodenheimer, P., Lissauer, J.J.: On the Luminosity of Young Jupiters. ApJ, **655**, 541–549 (2007). DOI 10.1086/509759
227. Martin, R.G., Livio, M.: On the evolution of the snow line in protoplanetary discs. MNRAS, **425**, L6–L9 (2012). DOI 10.1111/j.1745-3933.2012.01290.x
228. Martin, R.G., Lubow, S.H.: The Gravo-magneto Limit Cycle in Accretion Disks. ApJL, **740**, L6 (2011). DOI 10.1088/2041-8205/740/1/L6
229. Martin, R.G., Lubow, S.H.: Tidal truncation of circumplanetary discs. MNRAS, **413**, 1447–1461 (2011). DOI 10.1111/j.1365-2966.2011.18228.x

230. Martin, R.G., Lubow, S.H.: The gravo-magneto disc instability with a viscous dead zone. MNRAS, **437**, 682–689 (2014). DOI 10.1093/mnras/stt1917
231. Maslowe, S.A.: Critical layers in shear flows. Annual Review of Fluid Mechanics **18**, 405–432 (1986). DOI 10.1146/annurev.fl.18.010186.002201
232. Meheut, H., Casse, F., Varniere, P., Tagger, M.: Rossby wave instability and three-dimensional vortices in accretion disks. A&A, **516**, A31 (2010). DOI 10.1051/0004-6361/201014000
233. Meru, F., Bate, M.R.: Non-convergence of the critical cooling time-scale for fragmentation of self-gravitating discs. MNRAS, **411**, L1–L5 (2011). DOI 10.1111/j.1745-3933.2010.00978.x
234. Meyer, F., Meyer-Hofmeister, E.: On the Elusive Cause of Cataclysmic Variable Outbursts. A&A, **104**, L10 (1981)
235. Michael, S., Durisen, R.H., Boley, A.C.: Migration of Gas Giant Planets in Gravitationally Unstable Disks. ApJL, **737**, L42 (2011). DOI 10.1088/2041-8205/737/2/L42
236. Min, M., Dullemond, C.P., Kama, M., Dominik, C.: The thermal structure and the location of the snow line in the protosolar nebula: Axisymmetric models with full 3-D radiative transfer. Icarus, **212**, 416–426 (2011). DOI 10.1016/j.icarus.2010.12.002
237. Miranda, R., Lai, D.: Tidal Truncation of Inclined Circumstellar and Circumbinary Discs in Young Stellar Binaries. ArXiv e-prints (2015)
238. Morbidelli, A., Chambers, J., Lunine, J.I., Petit, J.M., Robert, F., Valsecchi, G.B., Cyr, K.E.: Source regions and time scales for the delivery of water to Earth. Meteoritics and Planetary Science **35**, 1309–1320 (2000). DOI 10.1111/j.1945-5100.2000.tb01518.x
239. Morfill, G.E.: Some cosmochemical consequences of a turbulent protoplanetary cloud. Icarus, **53**, 41–54 (1983). DOI 10.1016/0019-1035(83)90019-2
240. Muranushi, T., Okuzumi, S., Inutsuka, S.i.: Interdependence of Electric Discharge and Magnetorotational Instability in Protoplanetary Disks. ApJ, **760**, 56 (2012). DOI 10.1088/0004-637X/760/1/56
241. Nakagawa, Y., Sekiya, M., Hayashi, C.: Settling and growth of dust particles in a laminar phase of a low-mass solar nebula. Icarus, **67**, 375–390 (1986). DOI 10.1016/0019-1035(86)90121-1
242. Nayakshin, S., Lodato, G.: Fu Ori outbursts and the planet-disc mass exchange. MNRAS, **426**, 70–90 (2012). DOI 10.1111/j.1365-2966.2012.21612.x
243. Nelson, R.P., Gressel, O., Umurhan, O.M.: Linear and non-linear evolution of the vertical shear instability in accretion discs. MNRAS, **435**, 2610–2632 (2013). DOI 10.1093/mnras/stt1475
244. Nesvorný, D., Youdin, A.N., Richardson, D.C.: Formation of Kuiper Belt Binaries by Gravitational Collapse. AJ, **140**, 785–793 (2010). DOI 10.1088/0004-6256/140/3/785
245. Nixon, C., King, A.: Warp propagation in astrophysical discs. ArXiv e-prints (2015)
246. Nixon, C.J., Pringle, J.E.: The observable effects of tidally induced warps in protostellar discs. MNRAS, **403**, 1887–1893 (2010). DOI 10.1111/j.1365-2966.2010.16331.x
247. Ogilvie, G.I.: The non-linear fluid dynamics of a warped accretion disc. MNRAS, **304**, 557–578 (1999). DOI 10.1046/j.1365-8711.1999.02340.x
248. Ogilvie, G.I.: Non-linear fluid dynamics of eccentric discs. MNRAS, **325**, 231–248 (2001). DOI 10.1046/j.1365-8711.2001.04416.x
249. Ogilvie, G.I., Latter, H.N.: Local and global dynamics of warped astrophysical discs. MNRAS, **433**, 2403–2419 (2013). DOI 10.1093/mnras/stt916
250. Ogilvie, G.I., Livio, M.: Launching of Jets and the Vertical Structure of Accretion Disks. ApJ, **553**, 158–173 (2001). DOI 10.1086/320637
251. Ogilvie, G.I., Pringle, J.E.: The non-axisymmetric instability of a cylindrical shear flow containing an azimuthal magnetic field. MNRAS, **279**, 152–164 (1996)
252. Oppenheimer, M., Dalgarno, A.: The Fractional Ionization in Dense Interstellar Clouds. ApJ, **192**, 29–32 (1974). DOI 10.1086/153030
253. Ormel, C.W., Cuzzi, J.N.: Closed-form expressions for particle relative velocities induced by turbulence. A&A, **466**, 413–420 (2007). DOI 10.1051/0004-6361:20066899

254. Owen, J.E., Armitage, P.J.: Importance of thermal diffusion in the gravomagnetic limit cycle. MNRAS, **445**, 2800–2809 (2014). DOI 10.1093/mnras/stu1928
255. Owen, J.E., Clarke, C.J., Ercolano, B.: On the theory of disc photoevaporation. MNRAS, **422**, 1880–1901 (2012). DOI 10.1111/j.1365-2966.2011.20337.x
256. Owen, J.E., Ercolano, B., Clarke, C.J., Alexander, R.D.: Radiation-hydrodynamic models of X-ray and EUV photoevaporating protoplanetary discs. MNRAS, **401**, 1415–1428 (2010). DOI 10.1111/j.1365-2966.2009.15771.x
257. Owen, J.E., Hudoba de Badyn, M., Clarke, C.J., Robins, L.: Characterizing thermal sweeping: a rapid disc dispersal mechanism. MNRAS, **436**, 1430–1438 (2013). DOI 10.1093/mnras/stt1663
258. Paardekooper, S.J.: Numerical convergence in self-gravitating shearing sheet simulations and the stochastic nature of disc fragmentation. MNRAS, **421**, 3286–3299 (2012). DOI 10.1111/j.1365-2966.2012.20553.x
259. Paardekooper, S.J., Mellema, G.: Planets opening dust gaps in gas disks. A&A, **425**, L9–L12 (2004). DOI 10.1051/0004-6361:200400053
260. Paczynski, B.: A model of accretion disks in close binaries. ApJ, **216**, 822–826 (1977). DOI 10.1086/155526
261. Paczynski, B.: A model of selfgravitating accretion disk. Acta Astronomica, **28**, 91–109 (1978)
262. Papaloizou, J., Pringle, J.E.: Tidal torques on accretion discs in close binary systems. MNRAS, **181**, 441–454 (1977)
263. Papaloizou, J.C.B., Pringle, J.E.: The time-dependence of non-planar accretion discs. MNRAS, **202**, 1181–1194 (1983)
264. Papaloizou, J.C.B., Pringle, J.E.: The dynamical stability of differentially rotating discs with constant specific angular momentum. MNRAS, **208**, 721–750 (1984)
265. Pascucci, I., Ricci, L., Gorti, U., Hollenbach, D., Hendler, N.P., Brooks, K.J., Contreras, Y.: Low Extreme-ultraviolet Luminosities Impinging on Protoplanetary Disks. ApJ, **795**, 1 (2014). DOI 10.1088/0004-637X/795/1/1
266. Perez-Becker, D., Chiang, E.: Surface Layer Accretion in Conventional and Transitional Disks Driven by Far-ultraviolet Ionization. ApJ, **735**, 8 (2011). DOI 10.1088/0004-637X/735/1/8
267. Pessah, M.E., Psaltis, D.: The Stability of Magnetized Rotating Plasmas with Superthermal Fields. ApJ, **628**, 879–901 (2005). DOI 10.1086/430940
268. Petersen, M.R., Julien, K., Stewart, G.R.: Baroclinic Vorticity Production in Protoplanetary Disks. I. Vortex Formation. ApJ, **658**, 1236–1251 (2007). DOI 10.1086/511513
269. Petersen, M.R., Stewart, G.R., Julien, K.: Baroclinic Vorticity Production in Protoplanetary Disks. II. Vortex Growth and Longevity. ApJ, **658**, 1252–1263 (2007). DOI 10.1086/511523
270. Pfalzner, S.: Encounter-driven accretion in young stellar clusters - A connection to FUors? A&A, **492**, 735–741 (2008). DOI 10.1051/0004-6361:200810879
271. Pinilla, P., Birnstiel, T., Ricci, L., Dullemond, C.P., Uribe, A.L., Testi, L., Natta, A.: Trapping dust particles in the outer regions of protoplanetary disks. A&A, **538**, A114 (2012). DOI 10.1051/0004-6361/201118204
272. Popham, R., Narayan, R., Hartmann, L., Kenyon, S.: Boundary Layers in Pre-Main-Sequence Accretion Disks. ApJL, **415**, L127 (1993). DOI 10.1086/187049
273. Preibisch, T., Kim, Y.C., Favata, F., Feigelson, E.D., Flaccomio, E., Getman, K., Micela, G., Sciortino, S., Stassun, K., Stelzer, B., Zinnecker, H.: The Origin of T Tauri X-Ray Emission: New Insights from the Chandra Orion Ultradeep Project. ApJS, **160**, 401–422 (2005). DOI 10.1086/432891
274. Preibisch, T., Kim, Y.C., Favata, F., Feigelson, E.D., Flaccomio, E., Getman, K., Micela, G., Sciortino, S., Stassun, K., Stelzer, B., Zinnecker, H.: The Origin of T Tauri X-Ray Emission: New Insights from the Chandra Orion Ultradeep Project. ApJS, **160**, 401–422 (2005). DOI 10.1086/432891
275. Pringle, J.E.: Soft X-ray emission from dwarf novae. MNRAS, **178**, 195–202 (1977)
276. Pringle, J.E.: Accretion discs in astrophysics. ARA&A, **19**, 137–162 (1981). DOI 10.1146/annurev.aa.19.090181.001033

277. Pringle, J.E.: The properties of external accretion discs. MNRAS, **248**, 754–759 (1991)
278. Pringle, J.E.: A simple approach to the evolution of twisted accretion discs. MNRAS, **258**, 811–818 (1992)
279. Pringle, J.E., King, A.: Astrophysical Flows (2007)
280. Proga, D.: Winds from Accretion Disks Driven by Radiation and Magnetocentrifugal Force. ApJ, **538**, 684–690 (2000). DOI 10.1086/309154
281. Qi, C., Öberg, K.I., Wilner, D.J., D'Alessio, P., Bergin, E., Andrews, S.M., Blake, G.A., Hogerheijde, M.R., van Dishoeck, E.F.: Imaging of the CO Snow Line in a Solar Nebula Analog. Science **341**, 630–632 (2013). DOI 10.1126/science.1239560
282. Raettig, N., Klahr, H., Lyra, W.: Particle Trapping and Streaming Instability in Vortices in Protoplanetary Disks. ApJ, **804**, 35 (2015). DOI 10.1088/0004-637X/804/1/35
283. Raettig, N., Lyra, W., Klahr, H.: A Parameter Study for Baroclinic Vortex Amplification. ApJ, **765**, 115 (2013). DOI 10.1088/0004-637X/765/2/115
284. Rafikov, R.R.: Properties of Gravitoturbulent Accretion Disks. ApJ, **704**, 281–291 (2009). DOI 10.1088/0004-637X/704/1/281
285. Rafikov, R.R.: Viscosity Prescription for Gravitationally Unstable Accretion Disks. ApJ, **804**, 62 (2015). DOI 10.1088/0004-637X/804/1/62
286. Railton, A.D., Papaloizou, J.C.B.: On the local stability of vortices in differentially rotating discs. MNRAS, **445**, 4409–4426 (2014). DOI 10.1093/mnras/stu2060
287. Rebusco, P., Umurhan, O.M., Kluźniak, W., Regev, O.: Global transient dynamics of three-dimensional hydrodynamical disturbances in a thin viscous accretion disk. Physics of Fluids **21**(7), 076,601 (2009). DOI 10.1063/1.3167411
288. Rice, W.K.M., Armitage, P.J., Bate, M.R., Bonnell, I.A.: The effect of cooling on the global stability of self-gravitating protoplanetary discs. MNRAS, **339**, 1025–1030 (2003). DOI 10.1046/j.1365-8711.2003.06253.x
289. Rice, W.K.M., Armitage, P.J., Mamatsashvili, G.R., Lodato, G., Clarke, C.J.: Stability of self-gravitating discs under irradiation. MNRAS, **418**, 1356–1362 (2011). DOI 10.1111/j.1365-2966.2011.19586.x
290. Rice, W.K.M., Armitage, P.J., Wood, K., Lodato, G.: Dust filtration at gap edges: implications for the spectral energy distributions of discs with embedded planets. MNRAS, **373**, 1619–1626 (2006). DOI 10.1111/j.1365-2966.2006.11113.x
291. Rice, W.K.M., Lodato, G., Armitage, P.J.: Investigating fragmentation conditions in self-gravitating accretion discs. MNRAS, **364**, L56–L60 (2005). DOI 10.1111/j.1745-3933.2005.00105.x
292. Rice, W.K.M., Lodato, G., Pringle, J.E., Armitage, P.J., Bonnell, I.A.: Accelerated planetesimal growth in self-gravitating protoplanetary discs. MNRAS, **355**, 543–552 (2004). DOI 10.1111/j.1365-2966.2004.08339.x
293. Richling, S., Yorke, H.W.: Photoevaporation of protostellar disks. II. The importance of UV dust properties and ionizing flux. A&A, **327**, 317–324 (1997)
294. Robitaille, T.P.: HYPERION: an open-source parallelized three-dimensional dust continuum radiative transfer code. A&A, **536**, A79 (2011). DOI 10.1051/0004-6361/201117150
295. Romanova, M.M., Ustyugova, G.V., Koldoba, A.V., Lovelace, R.V.E.: MRI-driven accretion on to magnetized stars: global 3D MHD simulations of magnetospheric and boundary layer regimes. MNRAS, **421**, 63–77 (2012). DOI 10.1111/j.1365-2966.2011.20055.x
296. Ros, K., Johansen, A.: Ice condensation as a planet formation mechanism. A&A, **552**, A137 (2013). DOI 10.1051/0004-6361/201220536
297. Rosenfeld, K.A., Andrews, S.M., Hughes, A.M., Wilner, D.J., Qi, C.: A Spatially Resolved Vertical Temperature Gradient in the HD 163296 Disk. ApJ, **774**, 16 (2013). DOI 10.1088/0004-637X/774/1/16
298. Ruden, S.P.: Evolution of Photoevaporating Protoplanetary Disks. ApJ, **605**, 880–891 (2004). DOI 10.1086/382524
299. Rybicki, G.B., Lightman, A.P.: Radiative processes in astrophysics (1979)
300. Sano, T., Inutsuka, S.i.: Saturation and Thermalization of the Magnetorotational Instability: Recurrent Channel Flows and Reconnections. ApJL, **561**, L179–L182 (2001). DOI 10.1086/324763

301. Sano, T., Stone, J.M.: The Effect of the Hall Term on the Nonlinear Evolution of the Magnetorotational Instability. I. Local Axisymmetric Simulations. ApJ, **570**, 314–328 (2002). DOI 10.1086/339504
302. Sano, T., Stone, J.M.: The Effect of the Hall Term on the Nonlinear Evolution of the Magnetorotational Instability. II. Saturation Level and Critical Magnetic Reynolds Number. ApJ, **577**, 534–553 (2002). DOI 10.1086/342172
303. Shakura, N.I., Sunyaev, R.A.: Black holes in binary systems. Observational appearance. A&A, **24**, 337–355 (1973)
304. Shen, Y., Stone, J.M., Gardiner, T.A.: Three-dimensional Compressible Hydrodynamic Simulations of Vortices in Disks. ApJ, **653**, 513–524 (2006). DOI 10.1086/508980
305. Shu, F., Najita, J., Ostriker, E., Wilkin, F., Ruden, S., Lizano, S.: Magnetocentrifugally driven flows from young stars and disks. 1: A generalized model. ApJ, **429**, 781–796 (1994). DOI 10.1086/174363
306. Simon, J.B., Armitage, P.J.: Efficiency of Particle Trapping in the Outer Regions of Protoplanetary Disks. ApJ, **784**, 15 (2014). DOI 10.1088/0004-637X/784/1/15
307. Simon, J.B., Bai, X.N., Armitage, P.J., Stone, J.M., Beckwith, K.: Turbulence in the Outer Regions of Protoplanetary Disks. II. Strong Accretion Driven by a Vertical Magnetic Field. ApJ, **775**, 73 (2013). DOI 10.1088/0004-637X/775/1/73
308. Simon, J.B., Bai, X.N., Stone, J.M., Armitage, P.J., Beckwith, K.: Turbulence in the Outer Regions of Protoplanetary Disks. I. Weak Accretion with No Vertical Magnetic Flux. ApJ, **764**, 66 (2013). DOI 10.1088/0004-637X/764/1/66
309. Simon, J.B., Beckwith, K., Armitage, P.J.: Emergent mesoscale phenomena in magnetized accretion disc turbulence. MNRAS, **422**, 2685–2700 (2012). DOI 10.1111/j.1365-2966.2012.20835.x
310. Simon, J.B., Hawley, J.F.: Viscous and Resistive Effects on the Magnetorotational Instability with a Net Toroidal Field. ApJ, **707**, 833–843 (2009). DOI 10.1088/0004-637X/707/1/833
311. Simon, J.B., Lesur, G., Kunz, M.W., Armitage, P.J.: Magnetically driven accretion in protoplanetary discs. ArXiv e-prints (2015)
312. Smak, J.: Eruptive binaries. XI - Disk-radius variations in U GEM. Acta Astronomica, **34**, 93–96 (1984)
313. Spruit, H.C.: Magnetohydrodynamic jets and winds from accretion disks. In: R.A.M.J. Wijers, M.B. Davies, C.A. Tout (eds.) NATO Advanced Science Institutes (ASI) Series C, *NATO Advanced Science Institutes (ASI) Series C*, vol. 477, pp. 249–286 (1996)
314. Steiman-Cameron, T.Y., Durisen, R.H., Boley, A.C., Michael, S., McConnell, C.R.: Convergence Studies of Mass Transport in Disks with Gravitational Instabilities. II. The Radiative Cooling Case. ApJ, **768**, 192 (2013). DOI 10.1088/0004-637X/768/2/192
315. Steinacker, J., Baes, M., Gordon, K.D.: Three-Dimensional Dust Radiative Transfer*. ARA&A, **51**, 63–104 (2013). DOI 10.1146/annurev-astro-082812-141042
316. Stepinski, T.F.: Generation of dynamo magnetic fields in the primordial solar nebula. Icarus, **97**, 130–141 (1992). DOI 10.1016/0019-1035(92)90062-C
317. Stevenson, D.J., Lunine, J.I.: Rapid formation of Jupiter by diffuse redistribution of water vapor in the solar nebula. Icarus, **75**, 146–155 (1988). DOI 10.1016/0019-1035(88)90133-9
318. Stoll, M.H.R., Kley, W.: Vertical shear instability in accretion disc models with radiation transport. A&A, **572**, A77 (2014). DOI 10.1051/0004-6361/201424114
319. Supulver, K.D., Lin, D.N.C.: Formation of Icy Planetesimals in a Turbulent Solar Nebula. Icarus, **146**, 525–540 (2000). DOI 10.1006/icar.2000.6418
320. Suzuki, T.K., Inutsuka, S.i.: Disk Winds Driven by Magnetorotational Instability and Dispersal of Protoplanetary Disks. ApJL, **691**, L49–L54 (2009). DOI 10.1088/0004-637X/691/1/L49
321. Suzuki, T.K., Muto, T., Inutsuka, S.i.: Protoplanetary Disk Winds via Magnetorotational Instability: Formation of an Inner Hole and a Crucial Assist for Planet Formation. ApJ, **718**, 1289–1304 (2010). DOI 10.1088/0004-637X/718/2/1289
322. Takeuchi, T., Lin, D.N.C.: Radial Flow of Dust Particles in Accretion Disks. ApJ, **581**, 1344–1355 (2002). DOI 10.1086/344437

323. Takeuchi, T., Okuzumi, S.: Radial Transport of Large-scale Magnetic Fields in Accretion Disks. II. Relaxation to Steady States. ApJ, **797**, 132 (2014). DOI 10.1088/0004-637X/797/2/132
324. Tanaka, K.E.I., Nakamoto, T., Omukai, K.: Photoevaporation of Circumstellar Disks Revisited: The Dust-free Case. ApJ, **773**, 155 (2013). DOI 10.1088/0004-637X/773/2/155
325. Tanga, P., Babiano, A., Dubrulle, B., Provenzale, A.: Forming Planetesimals in Vortices. Icarus, **121**, 158–170 (1996). DOI 10.1006/icar.1996.0076
326. Terquem, C., Papaloizou, J.C.B.: On the stability of an accretion disc containing a toroidal magnetic field. MNRAS, **279**, 767–784 (1996)
327. Throop, H.B., Bally, J.: Can Photoevaporation Trigger Planetesimal Formation? ApJL, **623**, L149–L152 (2005). DOI 10.1086/430272
328. Toomre, A.: On the gravitational stability of a disk of stars. ApJ, **139**, 1217–1238 (1964). DOI 10.1086/147861
329. Tout, C.A., Pringle, J.E.: Accretion disc viscosity - A simple model for a magnetic dynamo. MNRAS, **259**, 604–612 (1992)
330. Tsukamoto, Y., Iwasaki, K., Okuzumi, S., Machida, M.N., Inutsuka, S.: Bimodality of circumstellar disk evolution induced by Hall current. ArXiv e-prints (2015)
331. Tsukamoto, Y., Takahashi, S.Z., Machida, M.N., Inutsuka, S.: Effects of radiative transfer on the structure of self-gravitating discs, their fragmentation and the evolution of the fragments. MNRAS, **446**, 1175–1190 (2015). DOI 10.1093/mnras/stu2160
332. Turner, N.J., Benisty, M., Dullemond, C.P., Hirose, S.: Herbig Stars' Near-infrared Excess: An Origin in the Protostellar Disk's Magnetically Supported Atmosphere. ApJ, **780**, 42 (2014). DOI 10.1088/0004-637X/780/1/42
333. Turner, N.J., Drake, J.F.: Energetic Protons, Radionuclides, and Magnetic Activity in Protostellar Disks. ApJ, **703**, 2152–2159 (2009). DOI 10.1088/0004-637X/703/2/2152
334. Turner, N.J., Sano, T.: Dead Zone Accretion Flows in Protostellar Disks. ApJL, **679**, L131–L134 (2008). DOI 10.1086/589540
335. Turner, N.J., Sano, T., Dziourkevitch, N.: Turbulent Mixing and the Dead Zone in Protostellar Disks. ApJ, **659**, 729–737 (2007). DOI 10.1086/512007
336. Umebayashi, T., Nakano, T.: Effects of Radionuclides on the Ionization State of Protoplanetary Disks and Dense Cloud Cores. ApJ, **690**, 69–81 (2009). DOI 10.1088/0004-637X/690/1/69
337. Umurhan, O.M.: Potential vorticity dynamics in the framework of disk shallow-water theory. I. The Rossby wave instability. A&A, **521**, A25 (2010). DOI 10.1051/0004-6361/201015210
338. Urpin, V., Brandenburg, A.: Magnetic and vertical shear instabilities in accretion discs. MNRAS, **294**, 399 (1998). DOI 10.1046/j.1365-8711.1998.01118.x
339. van der Marel, N., van Dishoeck, E.F., Bruderer, S., Birnstiel, T., Pinilla, P., Dullemond, C.P., van Kempen, T.A., Schmalzl, M., Brown, J.M., Herczeg, G.J., Mathews, G.S., Geers, V.: A Major Asymmetric Dust Trap in a Transition Disk. Science **340**, 1199–1202 (2013). DOI 10.1126/science.1236770
340. Varnière, P., Tagger, M.: Reviving Dead Zones in accretion disks by Rossby vortices at their boundaries. A&A, **446**, L13–L16 (2006). DOI 10.1051/0004-6361:200500226
341. Velikhov, E.: Stability of an ideally conducting liquid flowing between rotating cylinders in a magnetic field. Zhur. Eksptl?. i Teoret. Fiz. **Vol: 36** (1959)
342. Vorobyov, E.I., Basu, S.: The Origin of Episodic Accretion Bursts in the Early Stages of Star Formation. ApJL, **633**, L137–L140 (2005). DOI 10.1086/498303
343. Ward, W.R.: Particle Filtering by a Planetary Gap. In: Lunar and Planetary Science Conference, *Lunar and Planetary Inst. Technical Report*, vol. 40, p. 1477 (2009)
344. Wardle, M.: The Balbus-Hawley instability in weakly ionized discs. MNRAS, **307**, 849–856 (1999). DOI 10.1046/j.1365-8711.1999.02670.x
345. Waters, T.R., Proga, D.: Parker winds revisited: an extension to disc winds. MNRAS, **426**, 2239–2265 (2012). DOI 10.1111/j.1365-2966.2012.21823.x
346. Weidenschilling, S.J.: Aerodynamics of solid bodies in the solar nebula. MNRAS, **180**, 57–70 (1977)

347. Weidenschilling, S.J.: The distribution of mass in the planetary system and solar nebula. Astrophysics and Space Science, **51**, 153–158 (1977). DOI 10.1007/BF00642464
348. Weingartner, J.C., Draine, B.T.: Photoelectric Emission from Interstellar Dust: Grain Charging and Gas Heating. ApJS, **134**, 263–281 (2001). DOI 10.1086/320852
349. Whipple, F.L.: On certain aerodynamic processes for asteroids and comets. In: A. Elvius (ed.) From Plasma to Planet, p. 211 (1972)
350. Yang, C.C., Johansen, A.: On the Feeding Zone of Planetesimal Formation by the Streaming Instability. ApJ, **792**, 86 (2014). DOI 10.1088/0004-637X/792/2/86
351. Youdin, A.N., Chiang, E.I.: Particle Pileups and Planetesimal Formation. ApJ, **601**, 1109–1119 (2004). DOI 10.1086/379368
352. Youdin, A.N., Goodman, J.: Streaming Instabilities in Protoplanetary Disks. ApJ, **620**, 459–469 (2005). DOI 10.1086/426895
353. Youdin, A.N., Lithwick, Y.: Particle stirring in turbulent gas disks: Including orbital oscillations. Icarus, **192**, 588–604 (2007). DOI 10.1016/j.icarus.2007.07.012
354. Youdin, A.N., Shu, F.H.: Planetesimal Formation by Gravitational Instability. ApJ, **580**, 494–505 (2002). DOI 10.1086/343109
355. Zhang, K., Blake, G.A., Bergin, E.A.: Evidence of Fast Pebble Growth Near Condensation Fronts in the HL Tau Protoplanetary Disk. ApJL, **806**, L7 (2015). DOI 10.1088/2041-8205/806/1/L7
356. Zhu, Z., Hartmann, L., Calvet, N., Hernandez, J., Muzerolle, J., Tannirkulam, A.K.: The Hot Inner Disk of FU Orionis. ApJ, **669**, 483–492 (2007). DOI 10.1086/521345
357. Zhu, Z., Hartmann, L., Gammie, C.: Long-term Evolution of Protostellar and Protoplanetary Disks. II. Layered Accretion with Infall. ApJ, **713**, 1143–1158 (2010). DOI 10.1088/0004-637X/713/2/1143
358. Zhu, Z., Hartmann, L., Gammie, C., McKinney, J.C.: Two-dimensional Simulations of FU Orionis Disk Outbursts. ApJ, **701**, 620–634 (2009). DOI 10.1088/0004-637X/701/1/620
359. Zhu, Z., Hartmann, L., Gammie, C.F., Book, L.G., Simon, J.B., Engelhard, E.: Long-term Evolution of Protostellar and Protoplanetary Disks. I. Outbursts. ApJ, **713**, 1134–1142 (2010). DOI 10.1088/0004-637X/713/2/1134
360. Zhu, Z., Nelson, R.P., Dong, R., Espaillat, C., Hartmann, L.: Dust Filtration by Planet-induced Gap Edges: Implications for Transitional Disks. ApJ, **755**, 6 (2012). DOI 10.1088/0004-637X/755/1/6
361. Zhu, Z., Stone, J.M.: Dust Trapping by Vortices in Transitional Disks: Evidence for Non-ideal Magnetohydrodynamic Effects in Protoplanetary Disks. ApJ, **795**, 53 (2014). DOI 10.1088/0004-637X/795/1/53
362. Zhu, Z., Stone, J.M., Bai, X.N.: Dust Transport in MRI Turbulent Disks: Ideal and Non-Ideal MHD With Ambipolar Diffusion. ApJ, **801**, 81 (2015). DOI 10.1088/0004-637X/801/2/81
363. Zhu, Z., Stone, J.M., Rafikov, R.R., Bai, X.n.: Particle Concentration at Planet-induced Gap Edges and Vortices. I. Inviscid Three-dimensional Hydro Disks. ApJ, **785**, 122 (2014). DOI 10.1088/0004-637X/785/2/122
364. Zweibel, E.G.: Ambipolar Diffusion, *Astrophysics and Space Science Library*, vol. 407, p. 285 (2015)